

Phenotypic variability in monogenic disorders involving skeletal malformations

Dissertation zur Erlangung des akademischen Grades des
Doktors der Naturwissenschaften (Dr. rer. nat.)

eingereicht im Fachbereich Biologie, Chemie, Pharmazie
der Freien Universität Berlin

vorgelegt von
Wibke Schwarzer
aus Baden-Baden

Juni 2010

Diese Dissertation wurde in der Zeit vom 15.05.2006 bis zum 30.04.2010 in der Arbeitsgruppe von Prof. Dr. Stefan Mundlos am MPI für Molekulare Genetik in Berlin angefertigt.

1. Gutachter: Prof. Dr. Stefan Mundlos

Max-Planck-Institut für Molekulare Genetik

Innstraße 73, 14195 Berlin

Tel.: 030/8413 1449

Email: mundlos@molgen.mpg.de

2. Gutachter: Prof. Dr. Wolfgang Schuster

Institut für Biologie

Freie Universität Berlin

Albrecht-Thaer-Weg 6 , 14195 Berlin

Tel.: 030/838 56797

Email: schuwowi@zedat.fu-berlin.de

Disputation am: 28.09.2010

“It is owing to wonder that people began to philosophize, and wonder remains the beginning of knowledge.”

Aristoteles

Selbstständigkeitserklärung

Hiermit erkläre ich, dass ich die vorliegende Arbeit selbst angefertigt und keine anderen, als die hier angegebenen Hilfsmittel verwendet habe. Ich versichere, dass ich diese Arbeit weder in dieser noch in einer anderen Form bei einer anderen Prüfungsbehörde eingereicht habe.

Berlin, den 03. Juni 2010

Wibke Schwarzer

Table of Content

1 Introduction	1
1.1 <i>ROR2</i> - the genetic cause for two developmental disorders	2
1.1.1 Receptor tyrosine kinase-like orphan receptor 2 (ROR2).....	2
1.1.2 Mutations in <i>ROR2</i> cause either Recessive Robinow Syndrome (RRS) or dominant Brachydactyly Type B1 (BDB1)	3
1.1.3 <i>Ror2</i> mouse models for RRS and BDB1	7
1.2 Split hand and foot malformation (SHFM).....	8
1.2.1 SHFM is a clinically variable and genetically heterogeneous disorder.....	8
1.2.2 Molecular pathogenesis of ectrodactylies	10
1.2.3 The <i>dactylaplasia</i> mouse - a model for human SHFM3	13
1.3 Thesis objectives	18
2 Material	19
2.1 Instruments.....	19
2.2 Chemicals.....	20
2.3 Buffers.....	20
2.4 Kits	20
2.5 Enzymes	21
2.6 Bacterial strains.....	21
2.7 Expression constructs and vectors	21
2.8 Primer	21
2.8.1 ROR2 mutagenesis primer	21
2.8.2 Primer for qPCR.....	22
2.8.3 Primer for probe amplification.....	22
2.8.4 Primer for microsatellite profiling.....	22
2.8.5 Primer for SNP profiling.....	23
2.9 Cultured cell lines	26
2.10 Antibodies	26
2.10.1 Primary antibodies.....	26
2.10.2 Secondary antibodies.....	27

2.11 Animals.....	27
2.12 Software.....	27
2.13 Internet resources.....	28
3 Methods.....	29
3.1 Molecular Biological Methods.....	29
3.1.1 DNA Isolation.....	29
3.1.2 RNA isolation.....	30
3.1.3 Generation of cDNA.....	30
3.1.4 Linear mRNA amplification.....	30
3.1.5 Polymerase chain reaction (PCR).....	31
3.1.6 DNA sequencing.....	36
3.2 Cell culture.....	37
3.2.1 Thawing of cells.....	37
3.2.2 Splitting of cells.....	37
3.2.3 Cryopreservation of cells.....	37
3.2.4 Cell number determination.....	38
3.2.5 Cell transfection.....	38
3.2.6 Generation of stable cell lines.....	38
3.2.7 Immunocytochemistry (ICC).....	39
3.2.8 Cell-surface protein biotinylation.....	39
3.3 Biochemical methods.....	40
3.3.1 Determination of protein concentration.....	40
3.3.2 SDS-PAGE.....	40
3.3.3 Western Blot (WB).....	41
3.4 Animal sample preparation.....	42
3.4.1 Embryo dissection.....	42
3.4.2 AER dissection.....	42
3.4.3 Skeletal preparations.....	42
3.5 Histology.....	43
3.5.1 Paraffin embedding and sectioning.....	43
3.5.2 Immunohistochemistry (IHC).....	43
3.5.3 RNA <i>In situ</i> hybridisation (ISH).....	44

3.6	Bioinformatics and data processing	46
3.6.1	SNP data and haplotype analysis	46
3.6.2	3D-reconstruction of embryonic limbs	47
4	Results	48
4.1	Molecular analysis of ROR2 mutations leading to dominant BDB1, recessive RRS and intermediary phenotypes	48
4.1.1	A novel recessive mutation in <i>ROR2</i> exhibiting features of RRS and severe brachydactyly	48
4.1.2	Exact copies of human ROR2 were generated for molecular analysis.....	49
4.1.3	Cellular distribution of wt ROR2 and the BDB1 and RRS mutations.....	50
4.1.4	Relative quantification of ROR2 protein at the plasma membrane	52
4.1.5	Additional quantification of protein levels reveal a gradient model for BDB1 versus RRS	55
4.1.6	An allelic series of <i>Ror2</i> mutations in the mouse confirms BDB1 versus RRS phenotype gradient	57
4.2	Mapping the modifier of dactylaplasia (<i>mdac</i>)	59
4.2.1	Genetic mapping reduces the <i>Mdac</i> interval to ~ 3 Mb	60
4.2.2	Analysis of haplotype structures refines the potential <i>mdac</i> region....	63
4.2.3	Genomic features of the <i>Mdac</i> region	67
4.3	Characterisation of mutational consequences leading to ectrodactyly in the dactylaplasia mouse	69
4.3.1	The defect in AER maintenance is caused by increased apoptosis.....	70
4.3.2	Expression analysis indicates deregulation of canonical Wnt-signalling in the mutant AER	73
5	Discussion.....	76
5.1	<i>ROR2</i> - the common genetic cause for two developmental disorders	76
5.1.1	Patients exhibiting intermediary phenotypes challenge the classical gain-of-function and loss-of function hypotheses	76
5.1.2	Trafficking defects of intracellular ROR2 mutants causes RRS.....	77
5.1.3	A gradient of <i>Ror2</i> protein stability and membrane localisation confers BDB1 or RRS phenotypes.....	79
5.1.4	Possible pathogenetic mechanisms leading to BDB1 and RRS.....	81

5.2	The modifier of dactylaplasia - a second locus defines a disease phenotype	83
5.2.1	The molecular effect exerted by <i>Mdac</i> provides cues for candidate search	84
5.2.2	Minimising the genomic interval of <i>Mdac</i> is a step towards elucidating its identity	85
5.2.3	The modifier of dactylaplasia: another MusD element?	87
5.3	From phenotype to genotype of Dactylaplasia mice	91
5.3.1	Many roads to destruction: deregulation of Wnt-signalling may eventually lead to Dactylaplasia	92
5.3.2	Dactylaplasia and human SHFM3 - a common genetic misregulation?	93
6	Summary	96
6.1	Summary in English	96
6.2	Deutsche Zusammenfassung	98
7	Literature	101
8	Indices	112
8.1	List of Figures	112
8.2	List of Tables	114
8.3	Abbreviations	115
9	Appendix	117
9.1	Acknowledgements	117
9.2	List of publications and congresses	119
9.3	Curriculum vitae	120

1 Introduction

The development of functional organisms from a single fertilised oocyte remains one of the greatest wonders in biology and life. As research in this field progresses, it becomes clear that a myriad of genes and environmental cues are necessary to control the complex processes of embryologic development. The role of a specific gene in this intricate network can be only determined, if its function is impaired and physiological consequences of this impairment are observed. Frequently, mutations in different genes contributing to a common molecular pathway lead to the same, or very similar phenotypic outcome. On the other hand, distinct mutations in one gene can sometimes result phenotypically different conditions. Hence, there is no one-to-one relationship between genes and congenital disorders. The situation is often further complicated by the influence of environmental factors and diverse genetic background, leading to a broad spectrum of clinical variability in monogenic Mendelian disorders.

In humans, congenital malformations arise with a frequency of approx. 3% in alive newborns. Most frequently the central nervous system is affected in approx. 1% of all newborns, closely followed by congenital heart defects with 0.8%. A further clinically relevant class of dysplasias comprise malformations of the skeleton. Although the individual abnormalities are rarely observed, combined they constitute the fourth largest group of congenital malformations. Skeletal dysplasias of the extremities in particular arise in approx. 0.1% of all newborns [1].

This dissertation is concerned with two cases, in which genetic aberrations lead to malformations of the skeleton. First, the question on how mutations in a single gene, *ROR2*, can give rise to two distinct developmental disorders is examined on a molecular level. Secondly, it is analysed how the phenotypic outcome of single gene mutations is affected by genetic background. A classical model for such modifier effects is the dactylaplasia mouse. A genomic feature, named *modifier of dactylaplasia (mdac)*, exists in the genomic background of several inbred mouse strains, which abrogates the phenotype completely and whose identity is narrowed down by genetic mapping. Furthermore, the molecular consequences of the mutation leading to ec-

trodactyly in dactylaplasia mice, the model for human split hand and foot malformation 3 (SHFM3), are investigated.

1.1 *ROR2* - the genetic cause for two developmental disorders

1.1.1 Receptor tyrosine kinase-like orphan receptor 2 (ROR2)

The human genome encodes 58 receptor tyrosine kinases (RTK) [2], a class of transmembrane receptors mediating intracellular response to extracellular growth factors, cytokines and hormones. RTKs are key regulators for many cellular processes including cell proliferation, migration, differentiation and apoptosis, and play important roles in development and cancer progression.

One member of this class of proteins is the receptor tyrosine kinase-like orphan receptor 2 (ROR2), which was initially identified in human neuroblastoma cells together with its closely related paralog ROR1 [3]. The denomination "orphan" in the name of ROR2 accounts for the former lack of knowledge about its ligands and signalling pathways. Recently, several studies established ROR2 as WNT-receptor, which predominantly binds WNT5A and plays a role in non-canonical Wnt-signalling [4-8]. Like all RTKs, ROR2 is composed of modular domains. The extracellular part of ROR2 consists of immunoglobulin-like, cysteine-rich and frizzled-like, and kringle domains; intracellularly, the tyrosine kinase domain is followed by a serine-proline-threonine rich region that is unique for the two proteins of the ROR family (Figure 1).

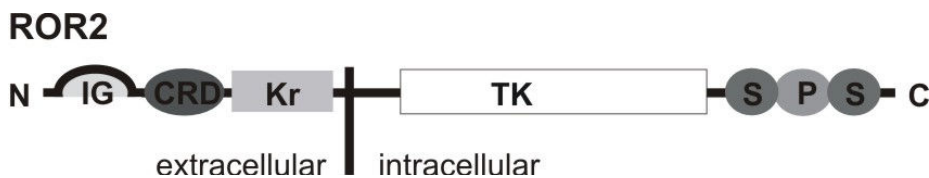


Figure 1: The molecular structure of ROR2.

Abbreviations of domains from N- to C-terminus: IG: immunoglobulin-like domain; CRD: cysteine-rich domain; Kr: Kringle domain; TK: tyrosine kinase; S: serine/threonine-rich domain; P proline-rich domain.

Studies in *Ror2*-deficient mice identified *Ror2* as regulator of several developmental processes including chondrogenesis, osteogenesis and heart development [9, 10].

Recently, *ROR2* gained importance in the field of oncology, where it has been shown to influence tumour invasiveness and malignancy in several types of cancers [11-14]. However, *ROR2* initially received most attention in human genetics. In 2000, several groups have independently shown, that mutations in *ROR2* lead to either recessive Robinow syndrome (RRS) [15, 16] or the dominant brachydactyly type B1 (BDB1) [17, 18]. These two developmental disorders and their molecular causes will be described in detail in the next sections.

1.1.2 Mutations in *ROR2* cause either Recessive Robinow Syndrome (RRS) or dominant Brachydactyly Type B1 (BDB1)

1.1.2.1 Clinical features of BDB1 and RRS

Brachydactyly is a developmental disorder referring to shortening of digits due to missing or shortened bones in hands and feet. It may occur as part of complex syndromes or as isolated trait. Depending on which skeletal elements are affected, isolated brachydactylies have been classified into 5 groups A-E, including further subtypes in group A and B [19]. The isolated brachydactyly type B1 (BDB1, OMIM 113000) is a dominant congenital disorder caused by mutations in *ROR2*.

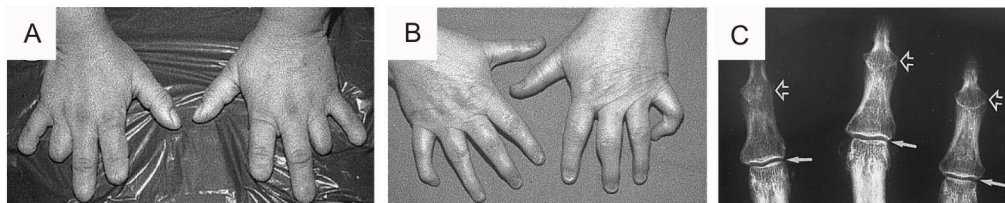


Figure 2: Clinical features of BDB1.

(A) Severe phenotype of BDB1. Note the complete absence of distal phalanges and nails in fingers 2-5. (B) Mild phenotype of BDB1, showing moderate hypoplasia of distal phalanges, normal nails, but distal symphalangism of fingers 2-5 and camptodactyly of finger 5. (C) X-ray showing distal part of fingers of BDB1 patient with mild phenotype. Note the symphalangism with fusion of distal and middle phalanges.

Adapted from [18].

It is characterised by hypoplasia and/or aplasia of distal phalanges in hands and feet resulting in an amputation-like phenotype (Figure 2). In less severe cases the distal phalanges may be present but they are frequently fused with the middle phalanges (distal symphalangism).

Robinow syndrome is a relative frequent congenital disorder with approx. 100 cases reported in literature. Both autosomal dominant (DRS, OMIM 180700) and autosomal recessive (RRS, OMIM 268310) forms of Robinow syndrome have been described, which show significant overlap in their phenotypes [20]. Although mutations in *ROR2* are known to be responsible for RRS for some time now, missense mutations in *WNT5A*, a *ROR2* ligand, were only recently discovered as genetic cause for dominant Robinow syndrome [21].

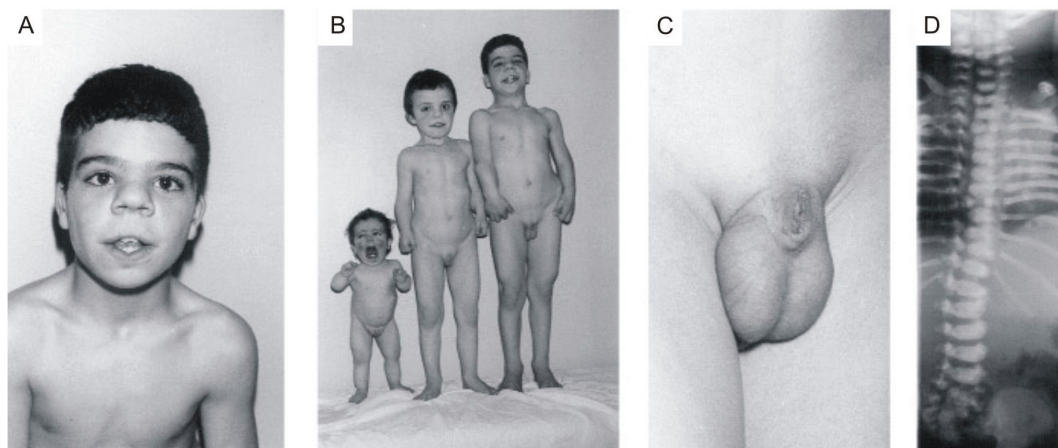


Figure 3: Clinical features of RRS.

(A) Facial appearance showing orbital hypertelorism, a broad nose, long philtrum, triangular mouth and frontal bossing. (B) Three affected members of a family. Note the mesomelic shortening of the limbs. (C) Micropenis. (D) X-ray showing vertebral and rib anomalies. The vertebral column is due to multiple hemivertebrae and the shape and number of the ribs are abnormal. Adapted from [15].

RRS is a complex congenital disorder with a multitude of clinical features, that may vary between patients. The most prominent and penetrant, however, are short stature, mesomelic limb shortening, hemivertebrae, genital hypoplasia and a characteristic facial dysmorphism (Figure 3) [22], also called "fetal face". In addition, many patients exhibit a very mild form of brachydactyly with shortened phalanges, which is distinct from the dominant BDB1. In a few cases in Turkey, RRS was observed in conjunction with split hand malformation and ectrodactyly [23].

1.1.2.2 Localisation and type of mutation decide on the phenotypic outcome

Several lines of evidence indicate that the recessive Robinow syndrome is due to a complete loss of function (LOF) of *ROR2*, whereas the dominant BDB1 is most likely caused by a gain of function (GOF) or dominant negative effect rather than simple haploinsufficiency. Heterozygous carriers of RRS mutations are phenotypically normal and individuals with a heterozygous chromosomal deletion involving *ROR2* show no hand phenotype [24].

Furthermore, localisation and type of mutation decide on the phenotypic outcome. RRS associated changes are scattered throughout the *ROR2* molecule consisting of missense mutations, or premature termination of the polypeptide chain at extracellular or intracellular positions [25] (Figure 4A). Chen et al. [26] have shown that proteins carrying missense mutations in the extracellular domains lead to intracellular retention. Although intracellular RRS mutations had not been assessed so far (except p.N620K), it can be assumed that all RRS associated *ROR2* mutations result in a LOF, presumably through protein degradation.

In contrast, all BDB1 associated changes known to date are frame shift and nonsense mutations that cluster in two mutational hot-spots located either immediately N-terminal or C-terminal of the tyrosine kinase domain (Figure 4B). While the mutations located N-terminal of the tyrosine kinase domain are small deletions or duplications resulting in frame shifts, nonsense as well as frame shift mutations have been reported in the C-terminal location. These mutations are predicted to lead to the expression of truncated proteins that always lack the C-terminal serine-proline-threonine rich region but may or may not contain the tyrosine kinase domain. Since BDB1 associated mutations are outside of important protein domains, it is possible that they escape protein quality control and may reach the plasma membrane in order to interfere with normal signalling. Their subcellular localisation, however, had not been investigated prior to this study.

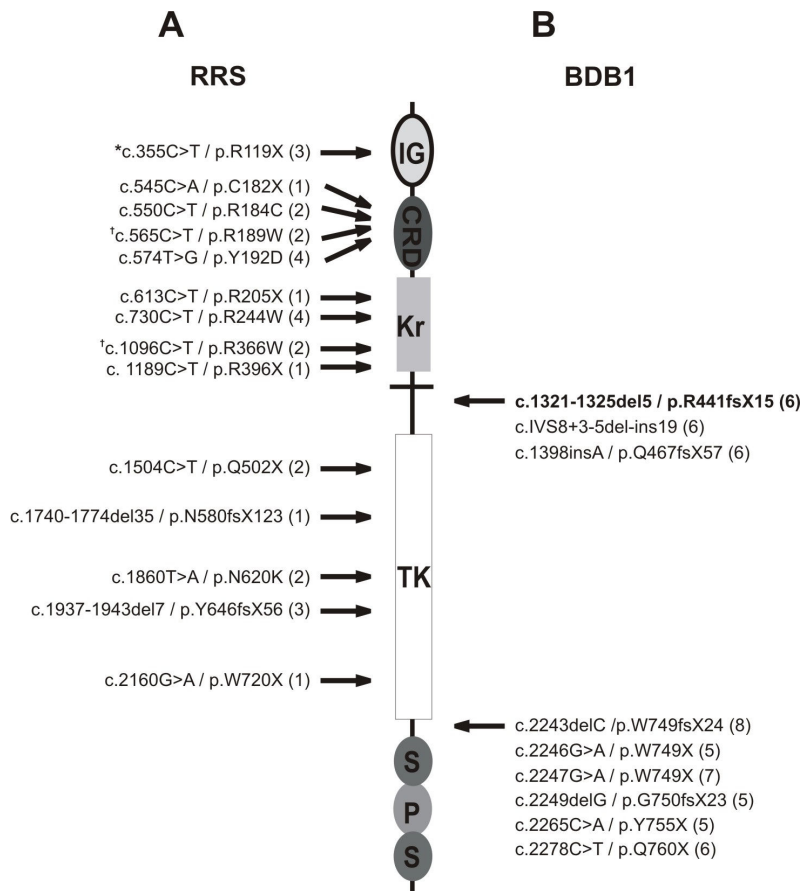


Figure 4: A selection of *ROR2* mutations leading to RRS and BDB1.

(A) RRS associated mutations are scattered throughout the entire protein. *: compound heterozygote with the mutation c.550C>T / p.R184C; †: present on the same allele; (1) [15]; (2) [16]; (3) [27]; (4) [28]. (B) BDB1 associated mutations cluster at two hotspots proximal and distal to the tyrosine kinase domain. The mutation for which a homozygous patient exists is depicted in bold. (5) [17]; (6) [18]; (7) [29]; (8) [30].

Interestingly, the phenotypic variability seen in BDB1 patients (1.1.2.1) also seems to correlate with the position of the mutation. C-terminal truncations result in a more severe phenotype (Figure 2A) than the N-terminal mutations (Figure 2B) [18]. The cause for this is so far unknown. In addition to these findings, Schwabe et al. published a patient homozygous for the C-terminal BDB1 mutation p.R441fsX15. Both parents exhibit a mild BDB1, whereas the homozygous child suffered from an extreme form of brachydactyly in conjunction with several RRS features (Figure 5), such as mesomelic limb shortening and vertebral segmentation defects. However, the patient lacks most of the typical craniofacial abnormalities and thus does not

suffer from classical RRS. How this overlap between the GOF malformation BDB1 and the LOF disorder RRS is possible could not be explained to date.

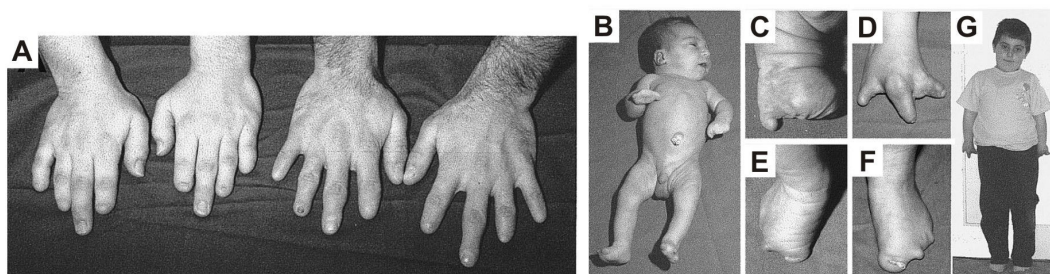


Figure 5: A patient homozygous for p.R441fxX15 shows severe brachydactyly in conjunction with RRS features.

(A) Hands of the parents with typical BDB1 phenotype (distal hypoplasia of phalanges 2, 4, and 5, nail dysplasia and distal symphalangism). (B) Presentation of the patient at birth. Corresponding pictures of the hands (C and D) and feet (E and F) demonstrate almost complete absence of phalanges and nails. (G) The patient at 7.5 years of age.

Adapted from [18].

1.1.3 *Ror2* mouse models for RRS and BDB1

Several different mouse strains with disrupted *Ror2* have been published to date. In 2000, Takeuchi et al. [9] presented mice completely lacking *Ror2* expression. These *Ror2*^{-/-} mice died just after birth, exhibiting dwarfism, severe cyanosis, and short limbs and tails. In addition, the mutants had cardiac septal defects, shortened facial structures, and fused and split vertebrae. Later, this mouse was discussed as model for recessive Robinow syndrome [31], since the phenotypes largely overlap and only subtle differences were observed.

Also in 2000, DeChiara et al. [10] published mice with a *lacZ* insertion proximal to the tyrosine kinase domain of *Ror2* (*Ror2*^{TMlacZ/TMlacZ}), thus resembling human mutations leading to mild dominant BDB1. However, these mice are phenotypically normal in the heterozygous state and the homozygous *Ror2*^{TMlacZ/TMlacZ} mutation largely mimics the phenotype of *Ror2*^{-/-}. Interestingly, they additionally lack the middle phalanges (p2), whereas *Ror2*^{-/-} mice only show shortened digits with all elements present. Hence, *Ror2*^{TMlacZ/TMlacZ} mice display a BDB-like phenotype in conjunction with RRS features.

In an attempt to model the BDB1 phenotype observed in humans, a *Ror2* mutant was created lacking the serine/threonine and proline-rich regions in the C-terminal part of *Ror2* resembling the stronger human mutation p.W749X (*Ror2*^{W749FLAG/W749FLAG} [32]). Unexpectedly, the heterozygous mice were normal and did not display brachydactyly. Homozygous *Ror2*^{W749FLAG/W749FLAG} mice are perinatally viable, lacked the middle phalanges and showed some RRS features (shortened limbs, craniofacial defects, spine phenotype), although in a significantly milder fashion than *Ror2*^{-/-} and *Ror2*^{TMlacZ/TMlacZ} mice.

In summary, both *Ror2*^{TMlacZ/TMlacZ} and *Ror2*^{W749FLAG/W749FLAG} mice exhibit intermediary phenotypes that are, to some degree, comparable to the phenotype of the homozygous patient for p.R441fsX15. The cause for the lack of limb phenotype in heterozygous mice is currently unknown.

1.2 Split hand and foot malformation (SHFM)

1.2.1 SHFM is a clinically variable and genetically heterogeneous disorder

Split hand and foot malformation (SHFM, also called ectrodactyly) is a limb malformation characterized by a deep median cleft in hands and feet due to the absence of the central rays, which occurs in approximately 1 of 18000 newborns [33]. SHFM may present with syndactyly, median clefts, and aplasia and/or hypoplasia of the phalanges, metacarpals and metatarsals. The severity of the phenotype is extremely variable, ranging from non-penetrance, syndactyly (Figure 6B) in mildly affected individuals to monodactyly (Figure 6D) or bidactyly (Figure 6C, lobster claw-like phenotype) in severe cases [34 and references therein]. Interestingly, this clinical variability not only exists between patients, but also between limbs of a single individual (Figure 6A).

In most cases, SHFM is inherited as an autosomal dominant trait with variable penetrance, although autosomal recessive [35] and X-linked forms [36] have been described. Similar to brachydactylies, SHFM can occur as isolated trait and has been described as feature in over 75 syndromes [34 and references therein]. The molecular causes for most of these syndromes are not yet known.

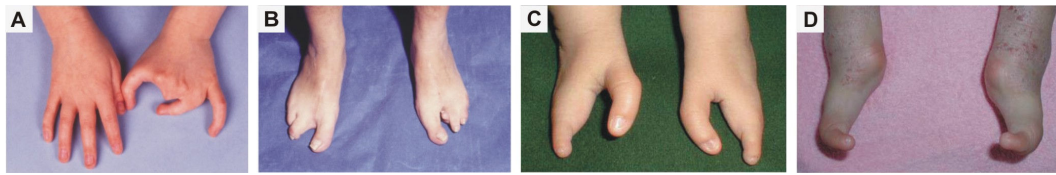


Figure 6: Clinical variability of ectrodactyly.

SHFM in hands (A) and with increasing severity in feet (B-D). Note the phenotypical variability in a single patient (A). Images adapted from [34, 37].

To date, six loci for isolated SHFM have been identified and several more have been suggested [33, 38]. For only two the causative genes could be determined so far. A homozygous mutation in *WNT10B* [39] was revealed in patients with an autosomal recessive form of SHFM (SHFM6, OMIM 601906) and mutations in the *TP63* gene can either cause isolated (SHFM4, OMIM 605289) or syndromic ectrodactyly [40-42]. Several cases of ectrodactyly have been associated with chromosomal aberrations at chromosome 7q21 (SHFM1, OMIM 183600) [43-48] and deletions on chromosome 2q31 (SHFM5, OMIM 606708) [49, 50]. SHFM2 (chromosome Xq26; OMIM 313350) is associated with X-chromosomal inheritance of ectrodactyly in a single family [36, 51, 52].

1.2.1.1 SHFM3 is caused by a tandem duplication at 10q24

The well studied locus for SHFM3 (OMIM 600095) was initially mapped to a large interval on chromosome 10q24-25 [53-56]. Detailed analyses identified large tandem duplications (~500 kb) in affected individuals [37, 57], with proximal and distal breakpoints clustering 160 kb and 60 kb, respectively. Lyle and colleagues [58] delineated this region further and identified a 325 kb duplication as minimal critical region (Figure 7). The maximal duplicated region contains at least 6 genes: *TLX1*, *LBX1*, *BTRC*, *POLL*, *DPCD* and *FBXW4*, however, the minimal duplication is restricted to *BTRC*, *POLL*, and *DPCD*. All distal breakpoints reside within *FBXW4*, resulting in an disrupted extra copy of this gene. Two studies attempted to elucidate the molecular consequences of the duplication via gene expression studies in blood or cultured patient cells [58, 59]. However, the results are contradictory, which is most likely due to the different cell systems employed.

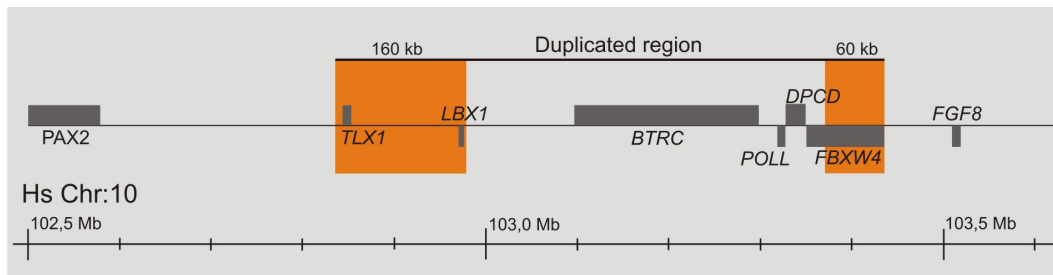


Figure 7: Localisation of the common duplicated region in SHFM3. Proximal and distal breakpoint clusters determined by Lyle et al. [58] are shaded in orange.

Until recently, SHFM3 was the only exclusive locus for isolated ectrodactyly, whereas for all other loci syndromic forms were described. In 2009, Dimitrov et al. [60] revealed a genomic rearrangement at 10q24 in patients with Distal limb deficiencies with micrognathia syndrome (OMIM 246560) with severe ectrodactyly. Interestingly, the duplications observed were essentially similar to those of isolated SHFM3, although they extended distally and resulted in a full duplication of *FBXW4*.

1.2.2 Molecular pathogenesis of ectrodactylies

Despite the heterogeneity of hereditary ectrodactylies, studies in mouse models suggest a common pathogenic mechanism leading to a split hand/foot phenotype. In all cases, ectrodactyly develops due to a failure to maintain median activity of the apical ectodermal ridge (AER).

1.2.2.1 Roles of the apical ectodermal ridge (AER) in early limb development

Outgrowth and patterning of the structurally complex limbs requires gradients from signalling molecules from all three spatial dimensions. Correspondingly, three signalling centres control patterning in one of the main axes of the limb: the apical ectodermal ridge (AER), the zone of polarizing activity (ZPA) and the non-AER ectoderm [reviewed in 61, 62, 63]. The AER is a specialised thickened ectoderm lining the distal edge of the limb bud that controls elongation in the proximo-distal axis from shoulder to finger. The ZPA is a group of mesodermal cells at the posterior border of the bud and controls patterning along the anterior-posterior axis from

thumb to little finger, whereas the non-AER ectoderm defines the pattern identity in the dorso-ventral axis from the back of the hand to the palm (Figure 8A).

The AER is induced from the underlying mesoderm of the emerging forelimb at stage E9.5. Initially, it comprises a relatively broad area of thickened ectoderm (Figure 8D), which becomes progressively compacted to give rise to a "mature" AER (Figure 8B, C, E) with a polystratified epithelial structure at stage E11.0 [64 and references therein]. At stage E13.0, the AER flattens and regresses completely, and no descendants of AER cells remain until birth [65]. In concordance with this dynamic morphology, both cell proliferation and apoptosis are concomitantly observed in the AER [66].

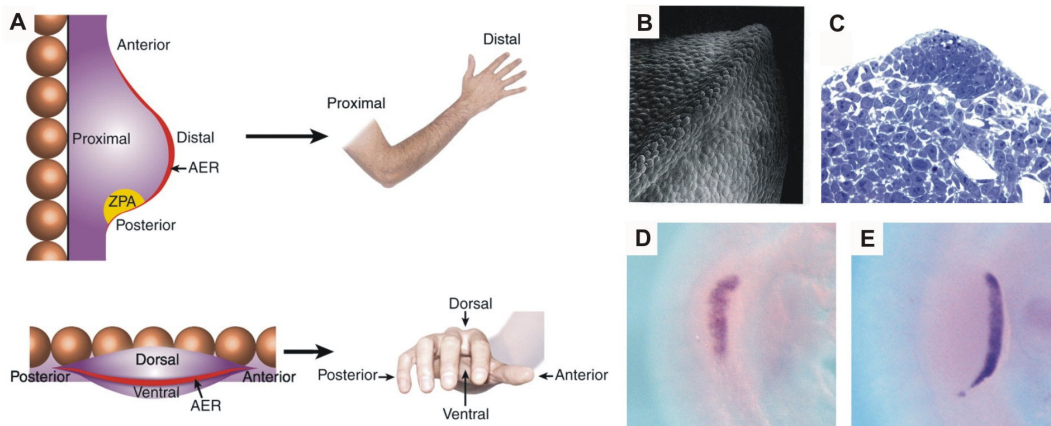


Figure 8: The AER contributes to the three dimensional development of the limb.

(A) Representations of the three primary axes of the developing limb and equivalent structures of the mature human limb. Adapted and from [62]. (B) Scanning electron micrograph showing the distinctive morphology of the AER (photograph: K. W. Tosney). (C) Longitudinal section through the distal tip of a mouse E10.5 forelimb. Note the polystratified epithelium [64]. *Fgf8* expression in the pre-AER (D) and mature AER(E).

The critical role of the AER in limb bud elongation was initially revealed by its removal from chick limb buds [67-69]. These experiments resulted in truncations of distal limb elements or the complete absence of the limbs, depending on the developmental stage at removal. The outgrowth is mediated by fibroblast growth factors (FGFs) secreted by the AER, which was proven by their ectopic application on limbs with removed AER. Several FGFs can rescue the truncations caused by AER removal and hence act as substitutes [70, 71]. In mouse, conditional ablation of the

FGFs in the AER showed that *Fgf8* is the only essential AER-FGF required for normal limb development [72, 73], while all other expressed FGFs (*Fgf4*, *Fgf9*, *Fgf17*) are individually and conjointly dispensable [74-77]. However, if these FGFs are ablated together with *Fgf8* in different combinations, the skeletal phenotypes increase in severity [77]. This indicates that the AER-FGFs have partially redundant functions.

One main function of FGF signalling is the maintenance of *Sonic Hedgehog* (*Shh*) expression in the zone of polarizing activity [75, 77, 78]. *Shh* is a secreted morphogen that acts as a key determinant in anterior-posterior patterning [79] and is in turn required for the maintenance of AER-FGF expression, hence establishing a positive feedback loop between the AER and ZPA.

1.2.2.2 AER maintenance

Interestingly, AER-FGFs play only a role in the functional, but not the structural maintenance of the AER, which is still present in all *Fgf-ko* mice [72, 77]. Both FGF-signalling and AER integrity depends on signals from the underlying mesoderm, namely *Fgf10* signalling and *Gremlin1* (*Grem1*) signalling, which is downstream of *Shh* signalling from the ZPA [80]. *Grem1*-deficient mice exhibit increased BMP signalling in the mesoderm perturbing normal AER morphology, which appears flattened and regresses [81, 82]. Hence, *Grem1* blocks the negative effects of bone morphogenic proteins (BMPs) on AER propagation and *Fgf8* expression [83].

In addition to signals from the mesoderm, continuous canonical WNT signalling from the ectoderm and the AER itself is required for AER maintenance. Conditional disruption of *β -catenin* (*β -cat*), an effector of canonical WNT signalling, in the pre-AER results in a loss of FGF8 expression. In addition, the AER is degraded due to increased apoptosis, in conjunction leading to severe truncations of the murine limbs [84].

An important protein involved in the pathogenesis of ectrodactylies, and hence in AER maintenance, is p63, a transcription factor homologous to p53 and p73. Mutations in *p63* have been shown to be responsible in isolated SHFM4 and numerous syndromes involving ectrodactyly, including Ectrodactyly-ectodermal dysplasia - tooth (ADULT, OMIM 103285) cleft lip/palate syndrome (EEC, OMIM 604292),

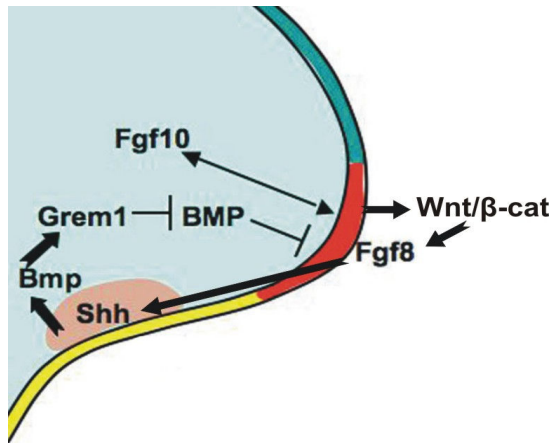


Figure 9: Signalling cascades in AER maintenance.

The arrows indicate induction and bars indicate repression. Red: AER, Pink: ZPA. See text for detailed description.

Adapted and modified from [63].

Limb mammary syndrome (LMS, OMIM 603543) and Acro-dermato-ungual-lacrimal syndrome [40, 42, 85]. Mice deficient for *p63* exhibit limb, craniofacial and ectodermal abnormalities, including the absence of stratified squamous epithelia and associated appendages [86, 87]. Therefore, *p63* is thought to preserve the proliferative activity in specialized ectodermal cells including the AER. The factors driving *p63* expression in the ectoderm and AER have not been elucidated in mammals, however, it was shown that *Dlx5/6* and *P-cadherin (CDH3)* are direct transcriptional targets of *p63* [88, 89]. *DLX5* and *DLX6* are candidate genes for SHFM1 and their double knock-out leads to ectrodactyly in mice [90, 91]. Mutations in *CDH3*, in turn, are responsible for the Ectodermal dysplasia-ectrodactyly-macular dystrophy (EEM, OMIM 225280) syndrome [89, 92]. The involvement *p63* and its downstream targets in various ectrodactyly syndromes implies a central role of this pathway in the pathogenesis of SHFM.

1.2.3 The *dactylaplasia* mouse - a model for human SHFM3

1.2.3.1 *Dac* mice are mutated at the SHFM3 syntenic region and display ectrodactyly

In the early 1970s, mice with a phenotype resembling human SHFM were observed in inbred mouse strains of the Jackson laboratory (Bar Harbor, Maine). Breeding tests revealed an autosomal semidominant pattern of inheritance, characterised by missing central digital rays in the heterozygous and monodactyly in the homozygous state (Figure 10) [93, 94]. Later, a second spontaneous mutation occurred at the

Jackson lab with an identical phenotype. Since the compound heterozygote was indistinguishable from either homozygote, the novel mutation revealed a second allele for *dactylaplasia*, which were subsequently named *Dac^{1J}* and *Dac^{2J}* [95].



Figure 10: Skeletal phenotype of the dactylaplasia mouse.

Alizarin red/Alcian blue staining of E18.5 forelimbs. Digits labelled anterior to posterior. Heterozygotes are phenotypically variable, but often lack the central phalanges, metatarsals and metacarpals. Homozygotes consistently show only one posterior digit. Figure adapted from [96].

The alleles were eventually mapped to reside within or in close proximity to the *Fbxw4* gene on chromosome 19, the syntenic region to the human SHFM3 locus, 10q24 [95]. In both cases, the mutations are caused by the independent insertion of early transposon (ETn) repeat elements, namely MusD elements (Figure 11) [95, 97]. The *Dac^{1J}* insertion was integrated 10 kb upstream of *Fbxw4* in antisense orientation, whereas the retrotransposable element causing *Dac^{2J}* integrated in intron 5 of *Fbxw4* in sense orientation, a position where many distal duplication breakpoints cluster in human SHFM3. Interestingly, the two MusD elements are 99.6% identical and each had 100% identical 5' and 3' long terminal repeats (LTRs) [97], a prerequisite for active transposition [98].

The consequences of the MusD insertions on *Fbxw4* expression were determined by Northern blot analysis on different tissue samples: brain, heart, liver kidney and spleen [95]. The *Dac^{1J}* insertion seemed to have no effect on *Fbxw4* transcription, since there was no change in transcript size (~2.8 kb) and abundance compared to

wild-type. In contrast, the *Dac*^{2J} insertion almost abolished *Fbxw4* transcription, producing low amounts of an abnormally large transcript (~9.5 kb).

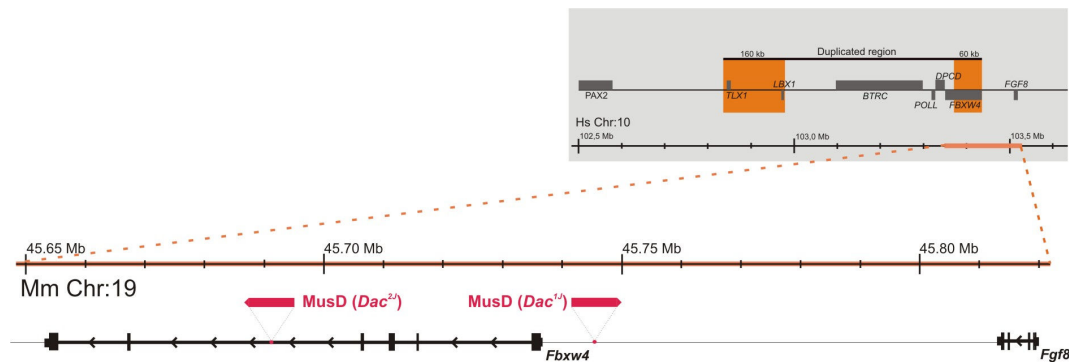


Figure 11: MusD insertions in the SHFM3 syntenic region.

The MusD elements integrated in chromosome 19, a region syntenic to the distal breakpoint cluster in human SHFM3. The *Dac*^{1J} insertion was integrated 10 kb upstream of *Fbxw4* in antisense orientation, whereas the retrotransposable element causing *Dac*^{2J} integrated in intron 5 of *Fbxw4* in sense orientation (red arrows).

In order to determine the cause for the semidominant pattern of inheritance, Sidow and colleagues [95] crossed the *Dac*^{1J} and *Dac*^{2J} strains to mice carrying a large deletion on chromosome 19 (*Krd*) that includes the *Dac* locus [99]. None of the *Krd*/+ progeny displayed a limb phenotype. This indicates that the phenotype of heterozygous *Dac* mice is not due to haploinsufficiency, but rather a gain-of-function or dominant negative effect.

1.2.3.2 *Dac* mice exhibit defects in AER maintenance

Embryologic analysis of the *Dac* phenotype revealed a defect in maintenance of the median AER. At stage E10.5, the AER morphology is relatively normal, but starts to degrade at stage E11.0. Only half a day later, the AER is completely absent from the central portion of the limb and is restricted to a small posterior region in homozygous animals. Ambiguous data for the cause of the degradation has been presented: Seto et al. [100] suggested that increased apoptosis leads to the loss of AER, whereas Crackower [96] and colleagues identified a lack of proliferation to be the cause.

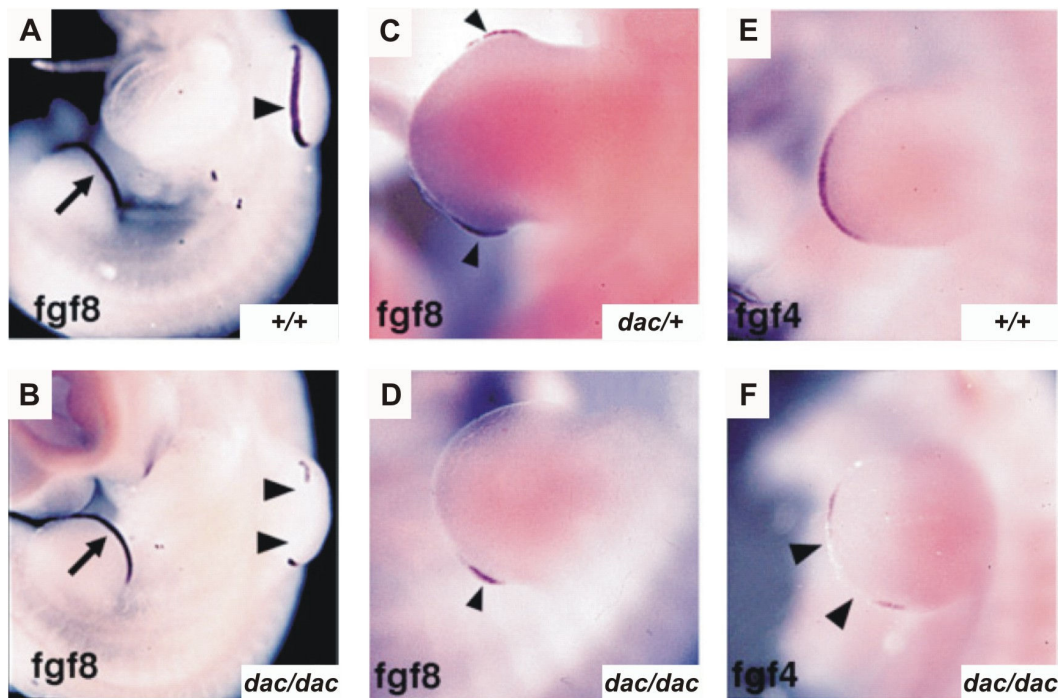


Figure 12 *In situ* hybridisation of *Fgf8* and *Fgf4* in *Dac* mutant limbs.

(A) *Fgf8* expression in wild-type limbs at stage E10.5, which is lost in the central part of the AER (B, arrows) in homozygous mutant limbs. At stage E11.0, *Fgf8* expression remains only in the very anterior and posterior regions in heterozygous mutants (C, arrows), and only in a posterior patch in homozygous animals (D, arrow). (E) *Fgf4* expression in wild-type limbs at stage E10.5, which is also lost in the central part of the AER (F, arrows) in homozygous mutant limbs. Figure adapted from [96].

Just prior to AER degradation commencing at stage E10.5, *Fgf8* expression is lost in the central part of the AER and only remains in structurally intact regions (Figure 12). Interestingly, *Fgf4* expression is also diminished [96], although it is normally upregulated upon loss of *Fgf8* [72]. At stage E10.5, *Msx1*, a downstream target of mesenchymal BMP signalling [101, 102], is the only analysed mesenchymal marker that is misregulated in *Dac* mice [95]. In contrast, *Shh*, *Bmp4*, and *Fgf10* show no difference in expression at the onset of losing *Fgf8* expression [96].

Despite these studies on gene expression in *Dac* limbs, there is no evidence in which structure the phenotype originates: the AER or its underlying mesenchyme. In dactylaplasia mice, no experiments on expression of the duplicated genes in human SHFM3 have yet been published and the molecular mechanism by which AER maintenance is disrupted in these mice still needs to be elucidated.

1.2.3.3 The modifier of *Dactylaplasia* (*mdac*) can suppress the *Dac* phenotype

A very interesting feature of the Dactylaplasia mice is the fact, that the manifestation of the *Dac* mutation is controlled by a second locus. Early breeding experiments with different inbred mouse strains resulted in either the expected heterozygous phenotype or a complete loss of the phenotype, depending on the inbred strain used [93]. Hence a modifier of *dactylaplasia* must exist in the genetic background of mouse strains, which is present in two alleles: a dominant allele inhibiting the development of the phenotype (*Mdac*) and a recessive allele allowing the phenotype to occur (*mdac*).

Mdac was initially mapped to a 27 Mb interval on chromosome 13 [94], which was recently refined to an area spanning 9.4 Mb [97]. A first study on the functional consequences of *Mdac* was published in 2007 [97]. Kano and colleagues could show, that the 5'LTRs of the MusD elements inserted in *Dac*^{1J} and *Dac*^{2J} are differentially methylated depending on the *Mdac/mdac* allele present. In case the recessive *mdac* allele is present, the 5'LTR is demethylated and abundant MusD transcripts were

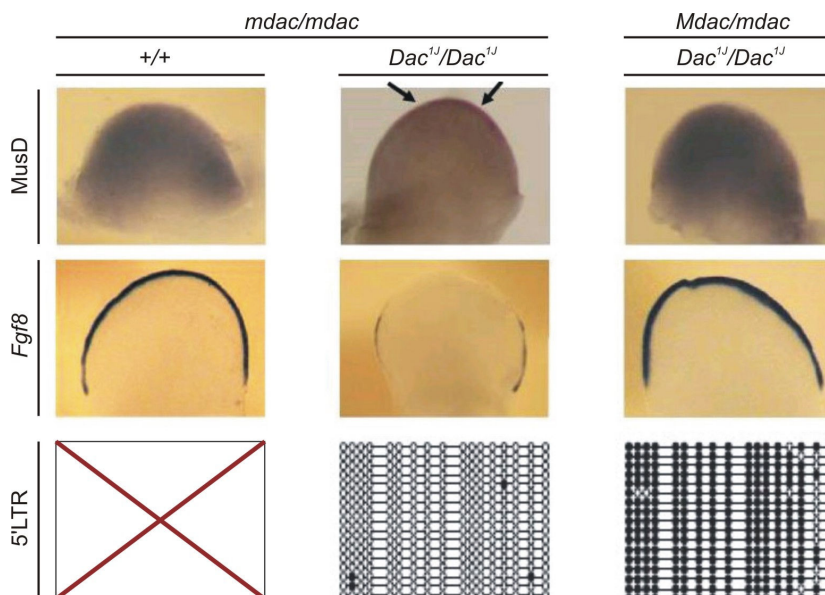


Figure 13: *Mdac* causes epigenetic modification of the integrated MusD element.

In situ hybridisation shows ectopic expression of MusD (arrows) and reduced *Fgf8* expression in the AER of homozygous *Dac*^{1J} mice at stage E10.5. This effect is abolished in mutants carrying *Mdac*, where the 5'LTR of the MusD element is methylated. Open circles: unmethylated CpGs, filled circles: methylated CpGs.

Figure adopted and modified from [97].

detected in the AER by *in situ* hybridisation (Figure 13). In contrast, the dominant *Mdac* allele caused heavy methylation of the 5'LTR and abolished the ectopic expression of MusD. These results indicate, that *Mdac* has a direct influence on the methylation status of the inserted MusD elements leading to dactylaplasia. Albeit this functional characterisation, no good *Mdac/mdac* candidate could yet be identified within its genomic interval.

1.3 Thesis objectives

During the course of this thesis, different sources for phenotypic variation in monogenic disorders leading to skeletal abnormalities were to be analysed. Different mutant alleles of *ROR2* lead to either recessive Robinow syndrome (RRS) or dominant Brachydactyly type B (BDB1). Generation of exact copies of selected mutant alleles should constitute a tool to examine the effects of these mutations on a cellular level. As central points, the underlying causes for phenotypic variability seen in BDB1 and the existence of phenotypes intermediate between BDB1 and RRS were to be analysed. The use of mouse models for BDB1 and RRS should deepen the understanding of the molecular mechanisms leading to these two congenital disorders and their intermediary phenotypes.

In addition to the allelic variability observed for *ROR2*, the effect of genetic background on the *Dactylaplasia* mutation was to be determined. The initial interval harbouring the *modifier of dactylaplasia* (*Mdac*) comprises 27 Mb on chromosome 13 and needed to be refined to clarify the identity of this genomic feature. Furthermore, genetic and pathophysiological consequences of the *Dactylaplasia* mutation had not been thoroughly investigated. Analyses of apoptosis and proliferation in the AER should clarify the cause for the AER degradation involved in this phenotype. Additionally, gene expression analyses by *in situ* hybridisation and RNAseq should shed light on genes and signalling pathways commonly misregulated in Dactylaplasia and SHFM3.

2 Material

2.1 Instruments

Centrifuges

Name	Supplier
Microtiterplate centrifuge 5416	Eppendorf
Microcentrifuge 5415 D	Eppendorf
Chilling centrifuge 5417 R	Eppendorf
Chilling centrifuge Sorvall RC-5	Thermo Electron

Thermo cyclers

Name	Supplier
GeneAmp PCR System 2700	Applied Biosystems
GeneAmp PCR System 2720	Applied Biosystems
GeneAmp PCR System 9700	Applied Biosystems
ABIPrism HT 7900 Realtime Cycler	Applied Biosystems

Microscopy

Name	Supplier
Microscope DMR	Leica
Camera AxioCam HRc	Zeiss
Microscope Axiovert 200M	Zeiss
ApoTome System	Zeiss
Camera AxioCam MRm	Zeiss
Stereo microscope MZ6	Leica
Stereo microscope MZ7-5	Leica
Camera AxioCam MRc5	Zeiss
Light source KL1500 LCD	Leica

Other

Name	Supplier
BioRobot M48 workstation	Invitrogen
Microtome Cool Cut HM355S	Microm
Embedding station EC 350-1&2	Microm
LAS-4000 Imaging System	Fuji

2.2 Chemicals

Unless denoted otherwise, all chemicals were supplied by Merck (Darmstadt), Sigma-Aldrich (Deisenhofen) and Roth (Karlsruhe).

2.3 Buffers

If not mentioned otherwise, all solutions were prepared according to Sambrooke, et al. 2001.

2.4 Kits

Name	Supplier
BCA Protein Assay Reagent Kit	Pierce
DIG RNA Labeling Kit	Roche
Epitect Bisulfite Kit	Qiagen
Gel-out Gel Extraction Kit	A&A Biotechnology
Invisorb Spin PCRapid PCR Purification	Invitex
MagAttract DNA Blood Mini Kit	Invitrogen
Plasmid DNA Mini Kit	A&A Biotechnology
Plasmid DNA Purification Kit Nucleobond AX	Machery - Nagel
RNeasy Micro Kit	Qiagen
Superscript II	Invitrogen
Superscript Double-Stranded cDNA Synthesis Kit	Invitrogen
T7 MEGAscript Kit	Ambion
TaqMan Reverse Transcription Reagents	Applied Biosystems

2.5 Enzymes

Restriction enzymes, ligases, polymerases and other DNA modifying enzymes were purchased from MBI Fermentas (St. Leon-Roth)

2.6 Bacterial strains

Name	Supplier
<i>E. coli</i> XL1 blue	Stratagene
<i>E. coli</i> Top10	Invitrogen

2.7 Expression constructs and vectors

Name	Supplier	Application
pcDNA3	Invitrogen	expression in mammalian cell systems
pcDNA5/FRT/TO	Invitrogen	genomic integration and inducible expression in mammalian cell systems
pOG44	Invitrogen	expression of Flp-recombinase
pTA-GFP	Dr. J. Hecht (Berlin)	subcloning of PCR products
pCS2/GAP43-GFP	Robertis [103]	expression of GFP targeted to the plasma membrane

2.8 Primer

All primer were purchased from Eurofins MWG Operon (Ebersberg).

2.8.1 ROR2 mutagenesis primer

Table 1: Mutagenesis primer to copy human mutations in ROR2

Name	5' – 3' sequence
hRor2_del1321-1325_F	ACAGCTGATGGCCTCGCCAGCC
hRor2_del1321-1325_R	CTGCGGTGTGGACGCAGATGCCTT
hRor2_C1324T_F	CACCGCAGCGGTGACAGCTGATGGCCTC
hRor2_C1324T_R	TGGACGCAGATGCCTTCTGCTTATTCCGGC
hRor2_1396insA_F	CCAAACTCAAAGAGATCAGCCTGTCTG
hRor2_1396insA_R	CCTGTTTGTGCTGGTTAATGAGGGG
hRor2_C1504T_F	GGAGCAGACCTAGGCTGTGGCCATCAA
hRor2_C1504T_R	CCCGGGGCAGGGCCGAACAGGT

hRor2_T1860A_F	ACCCGCAAAGTGCTAGTGTACGACAAG
hRor2_T1860A_R	GGCCAGGTCCTTGTGAACCACGT
hRor2_G2160A_F	GTCCCGCCTGAGTGTATGCCCTCATG
hRor2_G2160A_R	AGTCATCGGGGCAAGGCACCT
hRor2_G2246A_F	GCTCCGAGCCTAGGGCAACCTTTCCAA
hRor2_G2246A_R	CGGCTGTGGATGTCCTTGAAGCGG

2.8.2 Primer for qPCR

Table 2: qPCR primer for quantification of ROR2 expression in HEK293 cells

Name	5' – 3' sequence
rt-hROR2-F	CATGGCAGACAGGGCAGC
rt-hROR2-R	TTCTGTGTGTCATCAGCGCC
rt-hACTB-F	TCAAGATCATTGCTCCTCCTGAG
rt-hACTB-R	ACATCTGCTGGAAGGTGGACA

Table 3: qPCR primer for gene expression analysis in mouse AER

Name	5' – 3' sequence
rt-hRor2-F	CATGGCAGACAGGGCAGC
rt-hRor2-R	TTCTGTGTGTCATCAGCGCC
rt-hACTB-F	TCAAGATCATTGCTCCTCCTGAG
rt-hACTB-R	ACATCTGCTGGAAGGTGGACA

2.8.3 Primer for probe amplification

Table 4: Primer to amplify specific probes for *in situ* hybridisation

Name	5' – 3' sequence
rt-hRor2-F	CATGGCAGACAGGGCAGC
rt-hRor2-R	TTCTGTGTGTCATCAGCGCC
rt-hACTB-F	TCAAGATCATTGCTCCTCCTGAG
rt-hACTB-R	ACATCTGCTGGAAGGTGGACA

2.8.4 Primer for microsatellite profiling

Primer sequences were obtained from Mouse Genome Informatics (MGI) database. For cost-effective sequencing [104], the M13 recognition sequence was fused to the 5' end of the forward primers (denoted in small letters).

Table 5: Primer for microsatellite profiling of DAC vs, C57Bl/6 genomic information

Name	5' – 3' sequence
49.7Mb-10_M13F	tgtaaacgacggccagtAGTCCTGCCATTTGTCCTCTGACC
49.7Mb-10_R	ATGTCTTAGTCTCACATGCTGGGG
51.7Mb-139_M13F	tgtaaacgacggccagtAGAATAAGTCAAGGCTATGATGTGG
51.7Mb-139_R	TTGTTTGTGTTTGTGTTGAAGTAGAACG
52.9Mb-248_M13F	tgtaaacgacggccagtTAAAGTAGAAGGCAGCATGAGTG
52.9Mb-248_R	ACCCAAATGTTTTGGATCCA
54.4Mb-54_M13F	tgtaaacgacggccagtCCATGTTTTGAAGCCTGCTT
54.4Mb-54_R	GACATGGGGAACCTGTACCTCA
56.4Mb-13_M13F	tgtaaacgacggccagtCTGTGGTAAGTCCAGATTTG
56.4Mb-13_R	GGAAAGAGTAGGAAGATGCC
57.5Mb-65_M13F	tgtaaacgacggccagtAGCAACAAGTTCAGAATGATGC
57.5Mb-65_R	CCACATACAGCCACACATCTG
59.6Mb-186_M13F	tgtaaacgacggccagtGAAAGCCCTAGGGGAAGATG
59.6Mb-186_R	TGCAGTTTCTAAGGTTAAACTAAAGC
60.9Mb-318_M13F	tgtaaacgacggccagtCCAAATTCAAATACATACATACACA
60.9Mb-318_R	GCTTCAAATGCTCAAAGCC
63.3Mb-283_M13F	tgtaaacgacggccagtGGAAGCAGTCTCCTGCCTC
63.3Mb-283_R	GAGAGGTGGCACATGAGGTT
64.9Mb-310_M13F	tgtaaacgacggccagtCATTGTCTGGTGCCCTCC
64.9Mb-310_R	GAGCAAATAGTCTAGCCTGACTCC
67.6Mb-66_M13F	tgtaaacgacggccagtCTGCCCTGCTTGTTTGGG
67.6Mb-66_R	CCAACCTCAGCCATAAGACAG
69.1Mb-281_M13F	tgtaaacgacggccagtTGTCTAAGTGCACGTGGAGC
69.1Mb-281_R	ATGTGAATTGATTTTGTGGGC
71.7Mb-313_M13F	tgtaaacgacggccagtGCATGGATGTTAAACTAGTTGATG
71.7Mb-313_R	AAATCTCTACTTCAATTCAGTGTGTG
73.4Mb-11_M13F	tgtaaacgacggccagtCATGGCTCCTTTAACCTGTTT
73.4Mb-11_R	CAATGATTAACCTTGAAAAACA
75.3Mb-257_M13F	tgtaaacgacggccagtTCTAGTGCCTTGTAAGTTTCAACC
75.3Mb-257_R	CCAACGGAGAAAGAGTTGCT
77.2Mb-99_M13F	tgtaaacgacggccagtCAACAGGCAGATTTGGTGG
77.2Mb-99_R	TATAGTGGCAACTTTCAGATGGA

2.8.5 Primer for SNP profiling

SNPs, that are polymorphic between C57Bl/6 and DAC mice, were selected using the Mouse Phenome Database (MPD, Jackson Lab). Their surrounding sequences were extracted from the UCSC genome browser and primer for amplification were designed using VectorNTI (Invitrogen). Additionally, primer carrying the suffix

*SNP in their name were designed for single-base extension SNP-sequencing (3.1.6.3).

Table 6: Primer for SNP profiling

Name	5' – 3' sequence
60.6-rs29683016F	ATGGGAAAATATCAAGCAAGCCA
60.6-rs29683016R	AAAATGCACTCCAAGTGGAGCA
60.6-rs2968301SNP	AGTCCTGCCAGAATGCAAACCATCCAC
60.7-rs29636656F	CACCCACACAGACTTCTGCTG
60.7-rs29636656R	CCAGTTTGGATGTGGTCTGTCC
60.7-rs29636656SNP	CAGTCCTTGTGACATCACCTGGATGAC
60.9-rs13481840F	CTGGCCAATTGACAGGAAGAAA
60.9-rs13481840R	GGTGTTCATGTGTGATTAGTCGT
60.9-rs13481840SNP	CTCAAGTGTTCATTTTAGAATTAATC
61.2-rs29227798F	TCACTTACCCTTCCTTTGTATGGATAG
61.2-rs29227798R	TCTACTCATACCTAGTGGCCTCCATATT
61.2-rs29227798SNP	TGCAGGTTGTTGGTGCCAAGGAAAGACATTTAATT
61.353193F	CACCATTGAGAATGGCTAAGATCAA
61.353193R	CTCCCAACCTGACAAGCCAAAT
61.353193SNP	AGTGCTCGCCACCTTGAGCCTGACTTC
61.4-rs6280770F	CAGATCATCAGGACATTTCGAATCC
61.4-rs6280770R	GGAGTGGAAGAAAATGACCAACATATA
61.4-rs6280770SNP	AATGCCCTGCCATTGTGGAATGGGATT
61.5-rs13481856R	CCAATTTTACCCTTCTGTCCATAC
61.5-rs13481856SNP	TGCTACTTCTGATTTTTTTTCCAGACAGAAAGGCC
61.5-rs3089610F	GGTGGAAACATTCTTTGGATTCTT
61.5-rs3089610R	CTCATTTGTGGTTATTGACTTTACATGG
61.5-rs3089610SNP	TGCAGCTGTATGGGAACTCACCAGTCAACAACCTCC
61.6-rs29632065F	GAGAGAGAACTGTGTGTGAATAATGTG
61.6-rs29632065R	CATGGACTTAAAGTGAAGTGTGAATTCT
61.6-rs29632065SNP	ACTCTGATGGACATGGTCCAATCTCTG
61.780220F	GTAGTCTTCAACTCTTCATGGGTACAAA
61.780220R	CTGCATTCCTATGTTATGAACTTTTCAC
61.780220SNP	TGCCAGCTTCAGGAATAAGCTGTAAAT
61.927562F	CAACTTCTCTCAGGTCTGTTTAACAA
61.927562R	TTTGAGCAGCTCACTCTCCCAA
61.927562SNP	GCTGTTCCATCCCTTCTACCCTTTCCTTATTGATA
62.0-rs13477285F	GGAAGAACACGCCTCTCCTTCT
62.0-rs13477285R	CGGTTTTCTGATGTCGGTGTA
62.0-rs13477285SNP	CCTTCTCCTTGCTCCGCCCTCCTCC
61.780220F	GTAGTCTTCAACTCTTCATGGGTACAAA
61.780220R	CTGCATTCCTATGTTATGAACTTTTCAC
61.780220SNP	TGCCAGCTTCAGGAATAAGCTGTAAAT

62.2-rs29531590F	CCTGCTCCGGCCTAAAGATTTA
62.2-rs29531590R	GGGTGTGTATATGGTTTCATGCATG
62.2-rs29531590SNP	AACTCCTGGAGCTGCAGAGAAGACAAC
62.3-rs13481843F	AAAGGTTTTATCTGGGAACAACATG
62.3-rs13481843R	GCATTCTATTCATCTATCTCAGAGACG
62.3-rs13481843SNP	TATTCTATACAAACCAAGTAAAAAATTGAAAAAT
62.444317F	ATGTAGCATCTGTACATAGTTCCAAAAGG
62.444317R	GGTTTATTCAGGAAAGGAAAAGGAA
62.444317SNP	TTGTGGGTACACCTTCTACTCTTGGAC
62.512497F	TCCATTTTCCAAATATATGTGGTGG
62.512497R	GGCCACGTTTTTCATGTACAATTTT
62.512497SNP	ATTAATGTAAAATGCTTAATACATGG
62.6-rs33883575F	TCCCTGATGAACAAAGAATTTGAAC
62.6-rs33883575R	CAGAGGCAAGTGGATTTCTGAGTT
62.6-rs33883575SNP	GAGATGGACCTAGTGGCCATATTAATCAGGGTCGT
62.756908F	TTAGATGTGAGTTATAGGACCAGGGTAG
62.756908R	CATGTGACAGGAAGCAGTCATTAAT
62.756908SNP	CTTGTTATATTTCTGCCCTCCACCTACTTCTGAT
62.8-rs29233090F	GGTGCTGCACAGTGGACAAACT
62.8-rs29233090R	AGCTGTGGTTGGGCGTACCTAC
62.8-rs29233090SNP	CAGGATGATGCTTAGGGCTTACTGGCCAGTCAGTA
63.0-rs6255190F	ACAAACTGACACCCTCTAGGTTTCAT
63.0-rs6255190R	GCTTTTGCTTACACTGATCAATCAA
63.0-rs6255190SNP	AATCCAGTGAATTTTCATTTTCATGTGCACAATTCT
63.1-rs3654821F	GCAAAGGTCTGGGAGTGCATTT
63.1-rs3654821R	TCCTGTAGATGTCTAACTACTCAGCACTAG
63.1-rs3654821SNP	TTTTCTATACCACAGAGATGGCTTGAT
63.3-rs29552136F	GAGCAGGCTCCAGACACAAACT
63.3-rs29552136R	CTGTCATTAACACACAGCCTTCCT
63.3-rs29552136SNP	TTCTTGGAAGTGGCTCTATGCTAGCTC
63.4-rs3708089F	CTCCTGATTAGTTCAGGGACTGAATTC
63.4-rs3708089R	ATCCCCTTTGGAGATGATGGTC
63.4-rs3708089SNP	GGAGATCAAATATTACATCAGTGTAAG
63.5-rs29584348F	ACTGAATCTGGATTCATTACAATGCC
63.5-rs29584348R	GCTGTAAACAGGCATTTGATAAAGAGTA
63.5-rs29584348SNP	TCTAAGTCATCATCTTACTAATAGCTTCAAACAC
63.7-rs3726453F	TACCTTGCTATAATTAATGGCAGAAGTC
63.7-rs3726453R	ATTAACCACAATGACCATCCCC
63.7-rs3726453SNP	TGTAAGAATGCTTACCTCTGCTCTATG
63.8-rs29527548F	GGGAAAGACTGATAAACACAAATTCTC
63.8-rs29527548R	TGTCTGTCATCACCATGATTTACTTTC
63.8-rs29527548SNP	TTTCTTCTGAATCTGATGATGAGACAAAGGATCAC
63.9-rs29571510F	CACCAGCCATCCTGTGTCTGAC
63.9-rs29571510R	CACATAAACATGCTCCCAACGC
63.9-rs29571510SNP	ATGTCATCTGTATTGACAGGCCCTACTTTCCAGGA

64.3-rs3697016F	CCTGGGTTTGATCCTGAGTGCT
64.3-rs3697016R	AGAGGCCCTTTCAAGGAAAGAA
64.3-rs3697016SNP	GTCCTCCATGGACCGTGTGACAGTGTCTGGGACTG
64.5-rs29229374F	TATACAGTTTAGACAAGAGGACAAGAGAGC
64.5-rs29229374R	AGACACCAAGAATGGACTGGCA
64.5-rs29229374SNP	GATAGACTATGGCTTATTTCTTGTCTA
64.7-rs13481853F	CTTCTTCAATAGAAGTATTTCCCCATTC
64.7-rs13481853R	ATCGAACCCTACAGGACCAAG
64.7-rs13481853SNP	TTGAATTCTGGTATGATACATAAAGTG
64.8-rs29780588F	AGAGGAGTTGAAGCCAGAACAGC
64.8-rs29780588R	TGGATAGACAAATCACAGAGACAGGT
64.8-rs29780588SNP	TCAAAAGTAAAGCGGAGAGTGACTGAGTAAGTCAC

2.9 Cultured cell lines

Name	Origin
HEK293T	human embryonic keratinocytes
HEK293 Flp-In T-REx	human embryonic keratinocytes containing a single FRT site and expressing the Tet repressor (Invitrogen)
Cos-1	African green monkey kidney cell-line

2.10 Antibodies

2.10.1 Primary antibodies

Antigen	Source Animal	Supplier, cat.#	Application		
			WB	ICC	IHC
α Ror2	goat	R&D, AF2064	1:1000	1:500	
α BAP31	mouse	Alexis, ALX-804-601		1:500	
α GM130	mouse	BD, 610822		1:1000	
α H4B4	mouse	Develomenta Hybridoma Bank	Studies	1:500	
α Actin	rabbit	Sigma-Aldrich, A2066	1:1000		
α pan-cadherin	mouse	Abcam, ab6528	1:1000		

2.10.2 Secondary antibodies

Antigen	Conjugated	Supplier, cat.#	Application		
			WB	ICC	IHC
α goat	HRP	Calbiochem, 401515	1:8000		
α rabbit	HRP	Calbiochem, DC03L	1:1000		
α mouse	HRP	Calbiochem, DC08L	1:1000		
α goat	Alexa568	Invitrogen, A-11057		1:500	
α mouse	Alexa488	Invitrogen, A-11001		1:500	

2.11 Animals

Breeding and crossings were performed by Janine Wetzel and Maria Pohle in the animal facility of the institute under the direction of Ludger Hartmann.

- *Ror2*^{W749FLAG/W749FLAG} [32] was generated by A. Economidis and R. Raz (Regeneron Inc., Tarrytown, NY)
- *Ror2*^{-/-} [9] was provided by Y. Minami (Kobe University, Japan)
- SM/Ckc-*Fbxw4*^{Dac/J} [93] (hereafter named DAC), was purchased from the Jackson Laboratory (stock number: 000264)

2.12 Software

Program	Producer	Application
ABI PRISM GeneMapper Software	Applied Biosystems	analysis of SSLP and SNP data
Adobe Photoshop CS2	Adobe	image processing
AIDA Image Analyzer	Raytest	densitometric analysis of chemoluminescence
AxioVision Rel.4.8	Zeiss	microscopy, digital photography
CorelDRAW12	Corel	image processing
ImageJ	National Institutes of Health (NIH)	densitometric analysis of immunohistological sections
SDS 2.1	Applied Biosystems	analysis of qRT-PCR data
VectorNTI	Invitrogen	sequence analysis, primer design

2.13 Internet resources

Resource	Address
UCSC Genome Browser	http://genome.ucsc.edu/
Mouse Phenome Database (MPD, Jackson Lab)	http://www.jax.org/
Mouse Genome Informatics (MGI, Jackson Lab)	http://www.informatics.jax.org/
National Center of Biotechnology Information (NCBI)	http://www.ncbi.nlm.nih.gov/

3 Methods

3.1 Molecular Biological Methods

All classical molecular biological or microbiological experiments not described in this section were performed according to the handbooks “Molecular Cloning: A Laboratory Manual” (Sambrook, et al., 1989; [105]).

3.1.1 DNA Isolation

3.1.1.1 Isolation of Plasmid-DNA

Depending on the amount needed, plasmid-DNA was isolated with a Plasmid DNA Mini Kit (A&A Biotechnology, small scale) or the Nucleobond PC100 kit (Machery and Nagel, medium scale) according to the specifications of the manufacturer.

3.1.1.2 Isolation of Genomic DNA

Isolation of genomic DNA was necessary for determination of animal genotypes and the analysis of recombinational breakpoints in genetic mapping. These applications require varying levels of DNA purity and different isolation protocols.

3.1.1.2.1 Low purity genomic DNA isolation

For genotyping purposes, animal biopsies were digested overnight in 0.5ml SDS-buffer with 200 µg/ml proteinase K at 55°C. The following day, 0.25 ml 5M NaCl was added and incubated 10 min on a rocker at RT. The probes were subsequently placed on ice for 10 min, before spinning them for 10 min at 8000 rpm and 4°C. 500 µl supernatant were transferred into a new tube and 1 ml ice-cold ethanol was added. The samples were centrifuged again for 10 min at 13000 rpm and 4°C and the supernatant was discarded. The pellet was washed twice with 70% EtOH prior to dissolving the genomic DNA in an appropriate amount of ddH₂O.

SDS-buffer: 0.85% SDS, 17 mM EDTA, 170 mM NaCl, 17 mM Tris; pH 7.5

3.1.1.2.2 High purity genomic DNA isolation

For recombination and methylation analysis the DNA requires a higher purity as achieved with the conventional salting-out method. Here, the samples were digested as described above, followed by automated purification on the BioRobot M48 workstation using the MagAttract DNA Blood Mini Kit (both Invitrogen).

3.1.2 RNA isolation

Total RNA was isolated with 500µl peqGold TriFast (peqLab) according to specifications of the manufacturer. These include a chloroform extraction step, followed by isopropanol precipitation.

For very low starting amount of tissue (i.e. dissected AERs; 3.4.2), the samples were initially treated as described above. After chloroform extraction, total RNA was cleaned using RNeasy Micro Kit (Qiagen) columns according to the manufacturer and eluted with 12 µl nuclease-free water.

3.1.3 Generation of cDNA

The creation of expression constructs, labelled RNA probes and expression analysis via quantitative PCR (qPCR) requires reverse transcription of RNA into cDNA. For all applications, except qPCR, the RNA was transcribed with Invitrogen's Superscript II reverse transcriptase. For quantitative expression analysis with qPCR, the cDNA was produced with the TaqMan Reverse Transcription Reagents (Applied Biosystems) using random hexamers.

3.1.4 Linear mRNA amplification

Very low amounts of RNA from dissected AERs (3.4.2) needed to be amplified prior to analysis with qPCR (3.1.5.6). For this purpose, double-stranded cDNA was produced with Superscript Double-Stranded cDNA Synthesis Kit (Invitrogen) using T7-oligo dT primers according to the protocol of the manufacturer. Following phenol-chloroform purification, RNA was transcribed in large amounts with the MEGAScript Kit (Ambion) and T7 RNA polymerase. The amplified RNA was phenol-chloroform extracted and dissolved in 20 µl nuclease-free water. Since this procedure amplifies polyA-mRNA specifically and hence alters the mRNA/rRNA ratio,

the complete amplified RNA was used as template for a 100 μ l reaction with the TaqMan Reverse Transcription Reagents (Applied Biosystems), which was diluted 1:10 for later qPCRs (4 μ l template / reaction).

3.1.5 Polymerase chain reaction (PCR)

3.1.5.1 Standard PCR protocol

DNA amplification was performed with *Taq*- and *Pfu*-polymerases produced by the institute. A major advantage of the *Taq*-polymerase is its ability to add an adenosine residue to the 3'-end of the amplified DNA double strand. This characteristic enables quick and easy insertion into pTA-GFP vector (Dr. J. Hecht) for later applications. However, this polymerase shows no proof-reading activity. *Pfu*-polymerase with 3'-5' exonuclease activity was employed for applications requiring high fidelity DNA. In cases, where both characteristics were desirable, a mixture of both polymerases (1 part *Pfu* : 10 parts *Taq*) was applied. The reagents were pipetted into a chilled 0.2 ml reaction tube and incubated in a thermocycler with following program:

Phase	Temperature	Time	Cycles
initial denaturation	94°C	3 min	
denaturation	94°C	30 sec	35 cycles
primer annealing	depends on T_m	30 sec	
elongation	72°C / 68°C	<i>Taq</i> / <i>Pfu</i> 1 min per 1000bases	
final elongation	72°C / 68°C	10 min, <i>Taq</i> / <i>Pfu</i>	
end	4°C	∞	

Amount	Reagent
20-100 ng	DNA template
5 μ l	10x reaction buffer (provided by the institute)
1 μ l	dNTPs (1.25 mM, Fermentas)
1 μ l	5'-primer (10 μ M)
1 μ l	3'-primer (10 μ M)
0.5 μ l	DNA polymerase
→ add to 50 μ l with ddH ₂ O	

The PCR products were analyzed on 1% or 3% agarose gels.

3.1.5.2 Amplification of genes for expression constructs

Generally, genes were amplified from appropriate cDNA with a *Pfu/Taq*-polymerase mixture and cloned into pTA-GFP, where their sequence identity and fidelity was determined by Sanger-sequencing. The primers for amplification contained suitable restriction sites for subcloning into the target vector, in addition to gene-specific sequences.

3.1.5.3 PCR-based site-directed mutagenesis

In order to rebuild the precise human mutations in Ror2, PCR-based site-directed mutagenesis was employed. The primers were designed to carry the desired mutation, which leads to the introduction of the mutation in the first PCR-cycle. Furthermore, the primers are located adjacent to each other in an inverted manner, so that the complete construct (pTA-GFP + Ror2) is amplified (Figure 14).

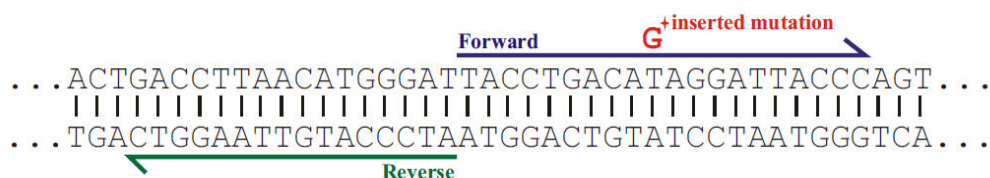


Figure 14: Primer design for site-directed mutagenesis

The PCR reaction was set up with *Phu*-polymerase as described in the standard protocol and executed using following program optimized for long PCR products.

Phase	Temperature	Time	Cycles
initial denaturation	94°C	2 min	
denaturation	94°C	30 sec	18 cycles
primer annealing	depends on T_m	30 sec	
elongation	68°C	17 min	
final elongation	68°C	15 min	
end	4°C	∞	

Following the PCR reaction, the template DNA was digested with 10u *DpnI* (Fermentas) for 2 hours at 37°C. The remaining PCR product was gel-purified, phosphorylated with T4 polynucleotide kinase (T4 PNK, Fermentas) and ligated with the T4 DNA ligase (Fermentas), according to the protocols of the manufacturer. Subsequently, the ligation product was transformed into *E. coli* and colonies were screened for successful mutagenesis.

3.1.5.4 Amplification of probe-sequences

The probes were mainly designed to reside at the 3' end of the candidate gene. In order to secure the specificity of the probe, the target area was analyzed for its uniqueness. The probe sequence was amplified by PCR on mouse cDNA and cloned into pTA-GFP. The orientation and identity of the sequences were determined by colony PCR and Sanger-sequencing.

3.1.5.5 Colony PCR

Colony PCR can serve as fast and easy method to identify with appropriate primers successful sequence insertion and its orientation in the vector. Instead of DNA, bacterial colonies are used directly as PCR template. The colonies were picked with sterile pipette tips, streaked out on replica-plates and dipped into a standard PCR reaction mix.

3.1.5.6 Quantitative real-time PCR (qPCR)

The expression level of specific genes can be quantified with quantitative real-time PCR – in this case employing SYBR green, which binds specifically double-stranded DNA. During the PCR reaction, the rise in fluorescence due to the increase of PCR product is measured in real-time. Suitable primers were designed with VectorNTI and the target sequence included exon/intron boundaries whenever possible, to exclude signal variation due to genomic DNA contamination. The reaction was carried out in 384 well plates in a volume of 12 µl containing 4ng cDNA, 4.5 pmol of forward and reverse primer and 50% 2x SYBR Green PCR Master Mix (Applied Biosystems). The standard curve was produced with 1:2 dilutions, starting with 6 ng cDNA decreasing down to 0.375 ng cDNA. If not denoted otherwise, relative quanti-

fication was achieved by calibrating the individual cDNAs to the levels of the housekeeping gene GAPDH. The data analysis was performed with the software SDS 2.1 (Applied Biosystems).

3.1.5.7 Genotyping of mice

For genotyping, the genomic DNA was extracted from amnions or tail-cuts. The following PCR-programs were applied to genotype the mouse-strains used in this study.

DAC:

Amount	Reagent
20-50 ng	DNA
5 μ l	10x buffer
0.8 μ l	dNTPs (1.25 mM)
1 μ l	5'-primer (8 μ M)
1 μ l	3'-primer (8 μ M)
0.5 μ l	<i>Taq</i> polymerase
→ add to 50 μ l with ddH ₂ O	

Temp.	Time	Cycles
94°C	5 min	
94°C	30 sec	30 cycles
56°C	45 sec	
72°C	45 sec	
94°C	30 sec	8 cycles
53°C	45 sec	
72°C	45 sec	
72°C	10 min	
4°C	∞	

Primer: D19Mit10-F, D19Mit10-R

Product size: wt =152 bp; mutant = 130 bp

Conductin-LacZ:

Amount	Reagent
20-50 ng	DNA
2.5 μ l	10x buffer
1 μ l	dNTPs (1.25 mM)
1 μ l	each primer (10 μ M)
1.5 μ l	DMSO
0.5 μ l	<i>Taq</i> polymerase
→ add to 25 μ l with ddH ₂ O	

Temp.	Time	Cycles
94°C	2 min	
94°C	6 sec	35 cycles
56°C	15 sec	
72°C	90 sec	
72°C	10 min	
4°C	∞	

Primer: AS, NLS, Cklon4

Product size: wt =500 bp; mutant = 400 bp

3.1.5.8 Microsatellite-PCR

Microsatellite markers were selected spacing the initial ~25Mb interval at distances of 1.5 – 2Mb. For this, the MGI database was searched for markers with variable simple sequence length polymorphisms (SSLP), which were subsequently validated for their informational capacity to distinguish between C57Bl/6 and DAC genomic DNA. The analysis of SSLPs is achieved with capillary electrophoresis sequencing (3.1.6.2). In order to reduce costs, the published protocol of Markus Schülke [104] was followed, which utilizes an FAM-labelled M13-adaptor primer.

Amount	Reagent	Temp.	Time	Cycles
20-50 ng	DNA	94°C	5 min	
5 µl	10x buffer	94°C	30 sec	30 cycles
0.8 µl	dNTPs (1.25 mM)	56°C	45 sec	
1 µl	5'-primerM13 (2 µM)	72°C	45 sec	
1 µl	3'-primer (8 µM)	94°C	30 sec	8 cycles
1 µl	FAM-M13 (8 µM)	53°C	45 sec	
0.5 µl	<i>Taq</i> polymerase	72°C	45 sec	
→ add to 50 µl with ddH ₂ O		72°C	10 min	
		4°C	∞	

3.1.5.9 PCR for SNP-sequencing

Known microsatellite markers are limited in their mapping resolution. Hence, densely available single nucleotide polymorphisms (SNPs) were used for fine mapping (~100kb resolution) of the *mdac*-region. These were selected from the SNP-database of the Jackson Laboratory. For later multiplex single base extension sequencing (3.1.6.3), the template PCR product was generated as described in the standard PCR protocol.

3.1.6 DNA sequencing

Sequencing was conducted by Mohsen Karbasiyan (Institute for Medical Genetics, Charité) on a ABI 3700 capillary sequencer (Applied Biosystems).

3.1.6.1 Sanger sequencing

The sequencing-PCR was set up using BigDye v3.1 (Applied Biosystems), according to the specifications of the manufacturer. The reaction was cleaned by ethanol precipitation before it was transferred to the Charité for capillary electrophoresis.

3.1.6.2 SSLP detection by glass capillary electrophoreses

For the detection of simple sequence lengths polymorphisms (SSLP) of microsatellites, 0.5 µl crude PCR-product (3.1.5.8) and 0.5 µl GeneScan™ 500 ROX™ Size Standard were added to 9 µl Hi-Di™ formamide prior to sequencing. Data analysis was performed with the ABI PRISM® GeneMapper™ Software (all Applied Biosystems).

3.1.6.3 SNP sequencing by multiplex single-base extension

In order to save cost, the ABI PRISM SNaPshot Multiplex Kit (Applied Biosystems) was used to detect 4 different single nucleotide polymorphisms (SNPs) in a single reaction. Accordingly, the primers were designed to be either 27 bp or 35 bp in length and care was taken, that the predicted polymorphisms were mutually exclusive, if detected with primers of the same length in a single reaction. The reaction itself was prepared according to the protocol of the manufacturer, including pooling and *ExoI*/SAP-purification of the PCR-products (3.1.5.9), and SAP-purification of the single-base extension products. Prior to sequencing, 2 µl reaction product and 0.5 µl GeneScan™ 120 LIZ™ Size Standard were added to 7.5 µl Hi-Di™ formamide. Data analysis was performed with the ABI PRISM® GeneMapper™ Software (all Applied Biosystems).

3.2 Cell culture

HEK293T and COS-1 cells were generally cultivated in DMEM (high glucose, Gibco) supplemented with 10% heat-inactivated FCS (Biochrome), 2% L-glutamine, 1% penicillin/streptavidin (both Gibco), which was always warmed up to 37°C before use. The cells were kept in an humidified incubator at 37°C and 5% CO₂ and medium was changed every 2 or 3 days.

3.2.1 Thawing of cells

The cells were thawed quickly in a 37°C water bath and immediately transferred into a Falcon tube containing 10 ml standard medium. After the suspension was centrifuged at 800 rpm for 5 min, the cells were resuspended in 10 ml fresh medium and plated into a cell culture flask. The following day, the medium was changed to remove last traces of DMSO.

3.2.2 Splitting of cells

In case the cultured cells reached 80-90% confluency, the cells were split into a new culture flask. For this purpose, HEK293 cells were gently tapped off the bottom of the flask, singularized by pipetting and resuspended 1:10 in fresh medium in a new flask. Since COS-1 cells are more adherent, they were washed with PBS and trypsinised with 0.25% trypsin (Gibco) for at 37°C until they detached from the flask. Immediately after, the cells were taken up in medium, centrifuged, and resuspended 1:10 in fresh medium.

3.2.3 Cryopreservation of cells

Approximately 10⁷ cells were resuspended in 1 ml freezing-medium and transferred into a cryo-vial. These were immediately placed into a cooled (4°C) isopropanol-freezing container, which ensures freezing of the cells at a constant rate of ~1°C/min. The container was placed at -80°C over night and the cryo-vials were transferred to liquid N₂ storage the next day.

3.2.4 Cell number determination

In case a defined cell number was required for an experiment, cells were counted in a Neubauer-chamber and plated out accordingly.

3.2.5 Cell transfection

In order to generate transient or stable cell lines, the cells were transfected with expression constructs using ExGen500 or Superfect (both Fermentas) according to the protocol of the manufacturer.

3.2.6 Generation of stable cell lines

Transient transfection of cells has the major disadvantage, that cells may take up to several hundred plasmids at once, leading to dramatically high expression of the introduced protein and, hence, to artefacts due to the disruption of normal protein production, quality control and transport. In addition, the expression is extremely variable from cell to cell, which leaves analysis of protein localisation free to the interpretation of the experimenter and quantitative biochemical approaches are prone to be not reproducible.

In order to generate stable and inducible cell lines, Invitrogen's Flp-In T-REx system was chosen. Here, the insertion into a single, pre-engineered FRT site in the genome of the HEK293 Flp-In T-REx cell line ensures single-copy expression at near to physiological level. The cell line was cultured with hygromycin B and zeocin according to the specifications of the manufacturer, until they were transfected with the gene of interest in the pcDNA5/FRT/TO vector and pOG44, the construct carrying the FLP-recombinase gene. Both constructs were co-transfected in a ratio of 8:1, respectively, and the cells were selected for genomic integration with 10 µg/ml blasticidin. As soon as all cells of the untransfected negative control were dead, the selection process was finished and the colonies of the newly generated cell line were pooled and propagated.

The integrated gene is under the control of CMV/TetO₂ promoter, which is silenced by the products of the tetracycline repressor gene *TetR*. Upon the addition of tetracycline, the repressor is removed from the promoter and transcription takes place.

Hence, 24h prior to any experiments with inducible cell lines, the cells were treated with 1 µg/ml tetracycline.

3.2.7 Immunocytochemistry (ICC)

Analyses of cellular distribution of protein was carried out by immunocytochemistry, where the protein of interest is labelled by primary antibody (2.10) and detected with a fluorophore-coupled secondary antibody. For this purpose, cells were cultivated on round cover-slips in 12 well-plates. After washing with PBS, the cells were fixed with ice-cold methanol for 8 min at -20°C. Subsequently, cells were washed again 3x with PBS and blocked with 10% FCS in PBST for at least 1 h at RT. 50 µl diluted primary antibody was dropped on parafilm in a humidified dark chamber and the cover-slips with adherent cells were carefully placed upon it for overnight incubation at 4°C. The following day, the cells were washed 3x in PBS and incubated with secondary antibody and DAPI (1:5000) for 1 h at RT in the dark. After 3 further washes, the cover-slips were mounted with Fluoromount G (SouthernBiotech) on a glass slide.

PBST: PBS, 0,02% Tween20

3.2.8 Cell-surface protein biotinylation

This method enables the precise calculation of the relative amount of Ror2 at the plasma membrane in relation to intracellularly retained Ror2.

HEK293 FlpIn T-REx cell lines were cultivated in 6-well plates, washed with PBS and treated with 1 mg/ml EZ-Link Sulfo-NHS-LC-Biotin Reagent (Pierce) for 30 min at 4°C. Excess reagent was neutralized with 100 mM glycine/PBS prior to lysis in 200 µl lysis buffer. 20 µl of cell lysate was retained as Ror2 expression control, whereas 140 µl were subjected to 50 µl immobilized streptavidin (Pierce) for 1h. After incubation, 40 µl supernatant was reserved for the determination of intracellular Ror2, and the streptavidin beads were boiled in SDS sample buffer (3.3.2.2). The complete fraction containing biotinylated protein, the supernatant and the untreated lysate were loaded on an acryamide gel and subjected to SDS-PAGE and Western blotting (3.3).

In order to calculate the relative fraction of ROR2 at the plasma-membrane, the ratios of biotinylated ROR2 and the corresponding intracellular fraction were determined and the resulting values were normalised to the ROR2 wt ratio. For statistical analysis the individual experiments were averaged and the standard error was calculated from the individual standard deviations according to [106] and statistical significance was calculated by using a Student's t test. As control, the relative amount of membrane-localized pan-cadherin was determined.

Lysis buffer: 50 mM HEPES pH 7.4, 50 mM NaCl, 10 mM EDTA, 10% glycerine, 1% Triton-100, inhibitors: 5 μ M phenylmethanesulfonyl fluoride, 5 μ M sodium fluoride, 5 μ M activated sodium orthovanadate, 1 μ g/ml Aprotinin, 10 μ M Pepstatin, 10 μ M Leupeptin (all Sigma-Aldrich)

3.3 Biochemical methods

3.3.1 Determination of protein concentration

The determination of protein concentration was carried out using the BCA Protein Assay Reagent Kit (Pierce) according to the manufacturer. The extinction at 562 nm was determined with a titre-plate reader and unknown protein concentration was calculated by comparison to a BSA standard curve.

3.3.2 SDS-PAGE

3.3.2.1 Preparation of polyacrylamide gels

Depending on the expected protein sizes, gels with appropriate percentages of acrylamide were prepared according to Sambrook, et al., 1989 [105], using the Mini Protean II System (Biorad).

3.3.2.2 Preparation of samples

The protein samples were usually derived from cell-culture cells and lysed as described in 3.2.8. Prior to electrophoresis, loading-buffer was added to the samples, which were subsequently boiled for 10 min. Additionally a pre-stained protein ladder (Fermentas) was loaded to the gel, in order to determine the molecular weight of detected proteins.

4x loading-buffer: 2ml 1M Tris, 4ml glycerine, 2ml 20% (w/v) SDS, 400 μ l 1% bromophenol blue, 600ml ddH₂O, 1ml 40x reducing agent (i.e. β -mercaptoethanol); pH 7.5

3.3.2.3 Electrophoresis

The gels were run with 80V, until the bromophenol blue reached the lower edge of the glass slides. For better separation of large proteins, the running time was elongated.

5x running-buffer: 25mM Tris, 250mM glycine, 0.1% (w/v) SDS

3.3.3 Western Blot (WB)

3.3.3.1 Protein transfer

According to the size of the gel, a suitable piece of nitrocellulose membrane was activated in methanol and equilibrated in transfer-buffer. The proteins were transferred to this membrane using the semi-dry blotting chamber (BioRad), considering the direction of transfer for the assembly of the gel-membrane sandwich. The blotting procedure was taking place at 20 V for 45 min.

1x transfer-buffer: 25mM Tris, 192mM glycine, 20% MeOH

3.3.3.2 Protein detection

After blotting, the membrane was blocked in 5% milk in PBST for at least one hour, followed by overnight-incubation with primary antibody (2.10) in blocking solution at 4°C. The next day, the membrane was washed 3x in PBST for 5 min and incubated with a suitable HRP-coupled secondary antibody for 1 h at RT. Finally, the membrane was washed and protein was visualised with enhanced chemoluminescence (ECL) solution (Rotilumin, Carl Roth). The signals were detected by the LAS-4000 Imaging System (Fuji) and quantified with the AIDA Image Analyzer (Raytest).

PBST: PBS, 0,02% Tween20

3.4 Animal sample preparation

3.4.1 Embryo dissection

Gestating mice were sacrificed at stage E10.5 and the uteri were removed. Embryos were dissected and precisely staged by counting their somites. Then, either whole embryos or their dissected torsi were placed in 4% PFA/PBS for overnight fixation at 4°C. If necessary, the embryonic amnions were collected and processed for genotyping.

3.4.2 AER dissection

The embryos were initially dissected as described in 3.4.1. After counting their somites, their torsi were dissected and the heart was removed, to ensure flat positioning on agar plates. The torsi were transferred into tubes containing 50 µl 1% BSA/PBS supplemented with 1 U/ µl RNase inhibitor (Applied Biosystems) and stored on ice. For AER dissection, the embryos were placed on a 2% agar plate and quickly washed twice with RNAlater. This step stiffens and loosens the epidermal layer due to dehydration and removes disengaged cells, that may contaminate the AER. Then, the AER was carefully removed with a sharpened tungsten needle, where great care was taken not to contaminate the specimen with additional epidermis or underlying mesenchyme. The dissected AER was then sucked into a glass capillary and transferred to a “low-binding” tube containing 10 µl RNAlater. Finally, 500µl peqGold TriFast (peqLab) was added for later RNA extraction (3.1.2) and the samples were stored at -20°C.

RNAlater: 6.1M ammonium sulphate, 10mM EDTA, 25mM sodium citrate;
pH 5.3 with sulphuric acid

3.4.3 Skeletal preparations

Animals were skinned, disembowelled and placed overnight in 100% EtOH. It was stained with alcian blue for two days, washed in 50% EtOH for one day and finally stained with alizarin red. Alcian blue dyes polysaccharides in cartilage blue, while alizarin red causes a red colour to mineralized extracellular matrix (i.e. bone). Dis-

pensable tissue was digested off with 1% KOH and the skeletal preparations were transferred to 80% glycerine.

Alcian blue: 500 mg alcian blue, 800 ml 100% EtOH, 200 ml glacial acetic acid

Alizarin red: 50 mg alizarin red in 1 l 1% KOH

3.5 Histology

3.5.1 Paraffin embedding and sectioning

Fixed embryos or torsi (3.4.1) were washed twice in PBS, before dehydrating in 50% and 70% EtOH for at least 30 min each. Further dehydrating steps and paraffin impregnation took place with the use of an automated device, programmed as follows:

3 h 90% EtOH, 3 h 95% EtOH, 2 h 100%EtOH, 2 h 100%EtOH, 2 h 100%EtOH, 15 min UltraClear (UC), 15 min UC, 30 min UC, 3 h UC/paraffin, 3 h paraffin.

The paraffin-impregnated tissues were embedded in paraffin in the desired orientation and sectioned with a paraffin-microtome (Mikrom). Usually, the tissues were processed into 6 μm thick sections and dried overnight at 37°C.

3.5.2 Immunohistochemistry (IHC)

Immunohistochemistry serves for the antibody-detection of specific proteins in tissues. For this work, all immunohistological analyses were conducted with 6 μm paraffin sections and fluorophore-coupled secondary antibodies. The tissue sections were deparaffinised and rehydrated with following protocol:

45 min UC, 2 min 100% EtOH, 2 min UC, 2 min 100% EtOH, 2 min 90% EtOH, 2 min 70% EtOH, 3x 5 min ddH₂O.

Following rehydration, the sections were boiled in citrate buffer (DAKO) for 10 min for antigen retrieval and allowed to cool to RT. Subsequently, sections were washed 3x with PBS and blocked with 10% FCS in PBST for at least 1 h at RT. Diluted primary antibody was dropped on the sections for overnight incubation at 4°C in a humidified dark chamber. The following day, sections were washed 3x in PBS and incubated with secondary antibody and DAPI (1:5000) for 1 h at RT in the dark. After 3 further washes with PBS, the sections were mounted with Fluoromount G.

PBST: PBS, 0,02% TritonX

3.5.3 RNA *In situ* hybridisation (ISH)

In situ hybridization (ISH) is a type of hybridization that uses a labelled complementary RNA strand to localise a specific RNA sequence in a portion or section of tissue or in the entire tissue (whole mount ISH). Hence, this method facilitates the analysis of expression pattern, and to some degree, expression level of the gene of interest in development.

3.5.3.1 Generation of DIG-labelled probes

Probe sequences with a length of around 500bp were present in pTA-GFP vector (3.1.5.4), which contains either a T7 or Sp6 recognition sequence at each side of insertion. Depending on probe orientation in the vector, either Sp6- or T7-RNA polymerases were used for the *in vitro* transcription of digoxigenin-labelled complementary probes, which was conducted with DIG RNA Labelling Kit (Roche) according to the manufacturer's protocol. After the reaction was stopped, the RNA was cleaned with a LiCl-precipitation and resuspended in 100 μ l RNase-free water. The success of the reaction was tested with an agarose gel and the probes were stored at -80°C until further use.

3.5.3.2 *In situ* hybridisation on sections

Paraffin-sections were deparaffinised, rehydrated and fixed using following protocol:

2x 15 min UC, 2x 10 min 100% EtOH, 5 min 65% EtOH/PBS, 5 min 50% EtOH/PBS, 5 min 25% EtOH/PBS, 2x 5 min PBS, 10 min 4% PFA/PBS, 3x 5 min PBST

After the sections were digested for 3 min with proteinase K (1.5 μ g/ml, Roche), they were re-fixed for 5 min in 4% PFA/PBS, washed 3x in PBST and acetylated. For this step, fresh acetylation-solution was prepared and the slides were incubated for 10 min under constant movement. The sections were washed again 3x in PBST and blocked with hybridisation-buffer for at least 4 h at 65°C in humid chamber, which was provided with 5x SSC / 50% formamide. The probe was diluted in hybridisation-buffer to a final concentration of approximately 0.25 μ g/ μ l and denatured

for 5 min at 85°C prior to hybridisation. The hybridisation was performed at 65°C overnight in the humidified chamber. The next day, excess probe was removed with subsequent washes with 5x SSC, 1x SSC / 50% formamide and an RNase A treatment step. For this purpose the slides were at first washed 1x in RNase washing-buffer and subsequently treated with 10 µg/ml RNase A at 30°C for 30 min. After a final wash in RNase washing-buffer, the slides were washed 1x 20 min in 2x SSC at 65°C and 2x 20 min in 0.2x SSC at 65°C. In order to prepare the sections for antibody incubation, the slides were washed twice in MABT and were blocked in 20% HISS/MABT for at least 2 h in a humidified chamber. During the blocking step, alkaline phosphatase-coupled anti-DIG-AP antibody (1:2500, Roche) was pre-incubated in 5% HISS/MABT at 4°C and the sections were treated with this dilution overnight at 4°C. For antibody detection, the slides were washed at first 3x in MABT, 1x in ALP-buffer and finally the enzymatic reaction was started using NBT/BCIP (Roche). As soon as a clear signal was visible, the slides were washed 3x in ALP-buffer and fixed in 4% PFA/PBS for 30 min. After two final washes in ddH₂O, the slides were mounted with HydroMatrix (Hydro-Tech-Lab) and evaluated.

Acetylation-solution: 0.1M TEA, 500µl acetic anhydride, 200ml ddH₂O

ALP-buffer: 100mM NaCl, 100mM Tris pH9.5, 50mM MgCl₂, 0.1% Tween20

Hybridisation-buffer: 10mM Tris pH7.5, 600mM NaCl, 1mM EDTA, 0.25% SDS, 10% dextrane sulfate, 1x Denhardt's, 200µg/ml yeast t-RNA, 50% formamide

MABT: 100mM maleic acid, 150mM NaCl, 0.1% Tween20; pH 7.5 with NaOH

PBST: PBS, 0.1% Tween20

RNase wash-buffer: 400mM NaCl, 10mM Tris pH7.5, 5mM EDTA

3.5.3.3 Whole mount *in situ* hybridisation

Fixed embryos (3.4.1) were washed twice in PBST, before dehydrating in 50% and 100% MetOH for at least 15 min each. For the hybridisation the embryos were rehydrated in a decreasing MetOH series, washed twice in PBST and bleached in 6% hydrogen peroxide in PBST for 1h at 4°C. The, the embryos were treated for 3 min with proteinase K (10 µg/ml, Roche). After thorough washing with PBST, PBST/glycine (2mg/ml) and RIPA-buffer, the embryos were fixed in 4% PFA / 0.2% glutaraldehyde and washed again with PBST, PBST / hybridisation-buffer (1:1) and

hybridisation-buffer. Pre-hybridisation took place at 65°C for at least 2h. The probe was diluted in hybridisation-buffer to a final concentration of approximately 0.25 µg/µl, denatured for 5 min at 85°C prior to hybridisation and added to the embryos for overnight incubation at 65°C. The next day, the embryos were washed and prepared for antibody incubation according to following protocol:

2x 30 min hybridisation buffer at 65°C, 5 min 1:1 hybridisation/RNase wash-buffer at RT, 2x 30 min 100 µg/ml RNase A treatment at 37°C, 5 min 1:1 RNase wash-buffer / SSC/FA/T at RT, 10x SSC/FA/T at 65°C (total ~4h), 10 min 1:1 SSC/FA/T / MABT at RT, 2x 10 min MABT at RT.

The embryos were blocked in 10% BBR (Boehringer's Blocking Reagent, Roche) in MABT for 1 h, while the alkaline phosphatase-coupled anti-DIG antibody was pre-absorbed 1:5000 in blocking solution. Subsequently, the embryos were incubated with the antibody dilution at 4°C overnight. Unbound antibody was removed with washes in 500 mg/l tetramisole in PBST for at least 6 h. For antibody detection, embryos were washed 2x 20 min in ALP-buffer and were placed in BM Purple AP Substrate (Roche), until a clear signal could be observed. Finally, the embryos were stored at 4°C in 4% PFA, 0.2% glutaraldehyde, 5 mM EDTA in PBS to preserve the signal.

ALP-buffer: 100mM NaCl, 100mM Tris pH9.5, 50mM MgCl₂, 0.1% Tween20, 500 mg/l tetramisole

Hybridisation-buffer: 5x SSC pH4.5, 50µg/ml heparin, 0.1% Tween20, 50% formamide

RIPA: 0.05% SDS, 1% NP40, 5g/l deoxcholate, 150mM NaCl, 50mM Tris pH8, 1mM EDTA

SSC/FA/T: 2x SSC, 50% formamide, 0.1% Tween20

MABT, RNase wash buffer and PBST were prepared as described in 3.5.3.2.

3.6 Bioinformatics and data processing

All *Mus musculus* nucleotide sequence positions denoted in this thesis are according to the Build 37 assembly by NCBI and the Mouse Genome Sequencing Consortium.

3.6.1 SNP data and haplotype analysis

SNP data of 12 mouse strains was retrieved as Excel file from the dense data set (Perlegen2) of the Mouse Phenome Database (MPD). SNPs were excluded if they contained no information for the C57Bl/6 reference strain or less than 75% allele

information for all strains, which resulted in 6541 valuable SNPs within chr13: 60.854.563-63.834.775. In order to obtain a colour-coded graph of biallelic SNP distribution pattern as depicted in Figure 25B, the conditional formatting function of Excel was employed: C57Bl/6 was set as reference and identical alleles were coloured in red, whereas the corresponding variant allele was coloured in blue. Positions without allele information remained white.

Haplotype analysis was conducted with Haploview 4.1 (Broad Institute) with default settings. For a better display of strain distribution patterns (SDP, Figure 25C), the resulting haplotype blocks were manually colour coded within the Excel SNP data. Colour-coded SNP and SDP distribution data were transferred in 100 kb intervals to the vector-based graphics editor CorelDRAW (Corel) and scaled accordingly.

3.6.2 3D-reconstruction of embryonic limbs

For 3D-reconstructions of phospho-histone 3 (pH3) and cleaved-caspase 3 (CC3) signals in the AERs of embryonic limbs, fluorescent microscopic images of 50 consecutive sections per limb were processed as follows: In order to display pH3 and CC3 signals exclusively in the AER, the signals were enhanced in this structure using an imaging processing program (Photoshop, Adobe). The same sections were used to create the transparent surface of the limb and AER by manually outlining the limb and AER shape on each section. Both datasets were used for 3D-rendering with Amira (Visage Imaging GmbH) and merged.

4 Results

4.1 Molecular analysis of ROR2 mutations leading to dominant BDB1, recessive RRS and intermediary phenotypes

4.1.1 A novel recessive mutation in *ROR2* exhibiting features of RRS and severe brachydactyly

Mutations in *ROR2* either cause the dominantly inherited brachydactyly type B1 (BDB1) or recessive Robinow syndrome (RRS). The distinct patterns of inheritance argue for a simple gain versus loss of function model, in which BDB1 causing mutations may still reach the plasma membrane to interfere with normal signalling, whereas RRS mutated protein loses its function completely. The first indication for a more complex model provided a patient homozygous for the p.R441fsX15 [18] mutation. Although the parents showed BDB1 with missing distal phalanges, this individual had almost complete absence of phalanges and nails in hands and feet. In addition, the patient displayed some but not all hallmarks of RRS and hence an intermediate phenotype between BDB and RRS.

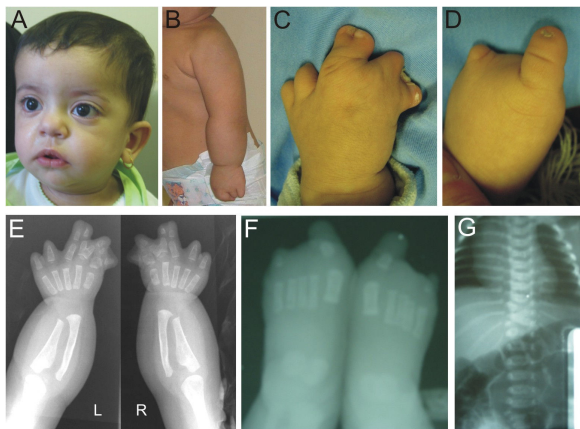


Figure 15: Clinical phenotype associated with the mutation c.1324C>T/p.R441X. Note mild facial dysmorphism with hypertelorism (A), mesomelic limb shortening (B), and severe malformations of hands (C) and feet (D). (E) X-rays of arms (L-left and R-right) showing short and abnormally shaped radii and ulnae and complex, symmetric brachy/syn/polydactyly in the hands. (F) X-ray picture of feet showing aplasia of phalanges of toes 2-4. (G) X-ray of spine displaying multiple vertebral malformations.

Anna Rajab and her colleagues discovered a novel patient displaying severe recessive brachydactyly in conjunction with acromesomelic shortening of the limbs, mild facial dysmorphism and malformed vertebrae (Figure 15) in the Sultanate of Oman. Subsequent mutation analysis carried out at the Institute for Medical Genetics, Charité, revealed a homozygous mutation leading to a premature stop (p.R441X), hence at the very same position as in the case p.R441fsX15 [18]. However, here, the

heterozygous parents are phenotypically normal. This discovery strengthened the idea of a model, in which overlapping phenotypes between the distinct BDB1 and RRS malformations are possible.

4.1.2 Exact copies of human ROR2 were generated for molecular analysis

Major importance for this work has the finding, that a mutation either truncating the protein by a frame shift or a nonsense at the same position result in different phenotypical outcomes. Therefore, expression constructs that do not exactly copy human mutations are inappropriate for mutational analysis. Human full-length ROR2 cDNA was generated and the exact copies of known human mutations were introduced via site-directed mutagenesis. The selection of mutations was based on the intention to investigate the occurrence of intermediate phenotypes that questions the classical gain of function (GOF) / loss of function (LOF) hypothesis. Furthermore, the clinical variability of BDB1 mutations leading to truncation of ROR2 proximal and distal of the tyrosine kinase domain was to be examined in this study.

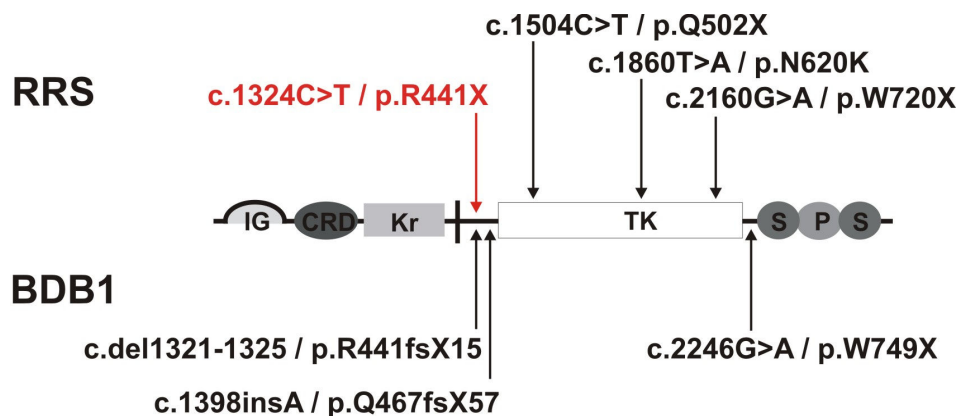


Figure 16: Graphical illustration of mutations causing Robinow syndrome (RRS, top) and brachydactyly type B1 (BDB1, bottom) used in this study.

The novel mutation **c.1324C>T / p.R441X** is depicted in red. IG: immunoglobulin-like domain, CDR: cysteine-rich domain, Kr: kringle domain, Tk: tyrosine kinase domain, S: serine-rich domain, P: proline-rich domain.

In previous work, Chen et al. [26] have shown that protein carrying missense mutations in the extracellular domains are retained in the endoplasmic reticulum (ER). In

addition, they assessed the location of the intracellular missense mutation p.N620K [16], which was used as “positive control” in this study. As further RRS mutations, the protein truncations p.Q502X [16] and p.W720X [15] were chosen for analysis. On the BDB1 side, the distal p.W749X [17] and the proximal p.Q467fsX57 [18] mutations were used in experiments together with p.R441fsX15 [18] and p.R441X, the mutations leading to an intermediary phenotype in the homozygous state. Figure 16 summarises all generated mutations and shows their location in the ROR2 protein.

4.1.3 Cellular distribution of wt ROR2 and the BDB1 and RRS mutations

Protein distribution was first analysed in transiently transfected Cos-1 cells by immunocytochemical detection of ROR2 with a specific antibody raised against its N-terminal domain and by co-staining for endogenous BAP31, a marker for the endoplasmic reticulum (Figure 17). As expected for a cell surface receptor, wild-type ROR2 was predominantly localised at the plasma membrane, which is also the case for the distal BDB1 mutation p.W749X.

The RRS mutation p.N620K shows strong retention in the ER as described by Chen et al. [26]. The same effect can be seen with the previously not investigated intracel-

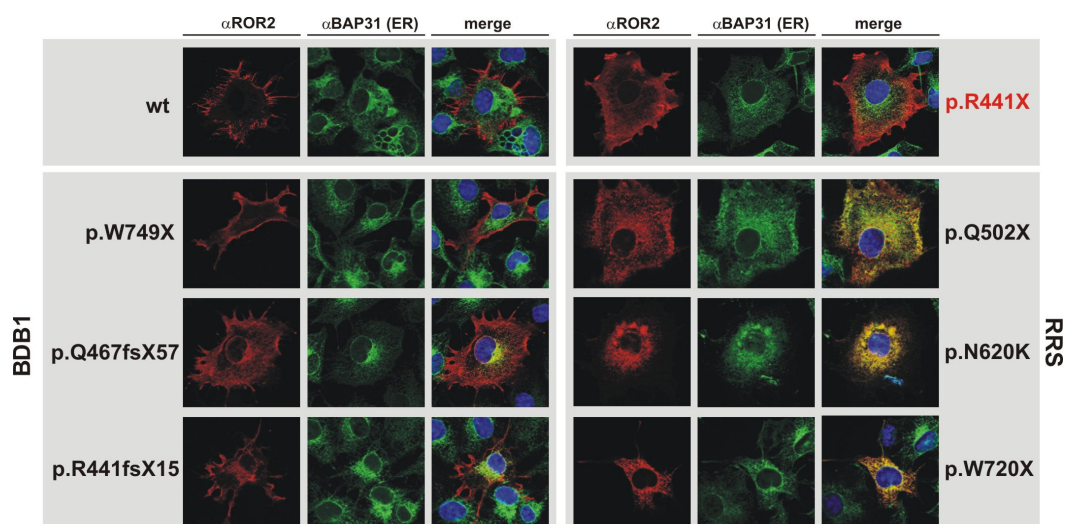


Figure 17: Immunocytochemistry for ROR2 (red) and the endoplasmic reticulum (ER) marker BAP31 (green).

Wild-type (wt) and BDB1 isoforms show cell surface labelling, whereas RRS forms only show overlap with the ER marker BAP31.

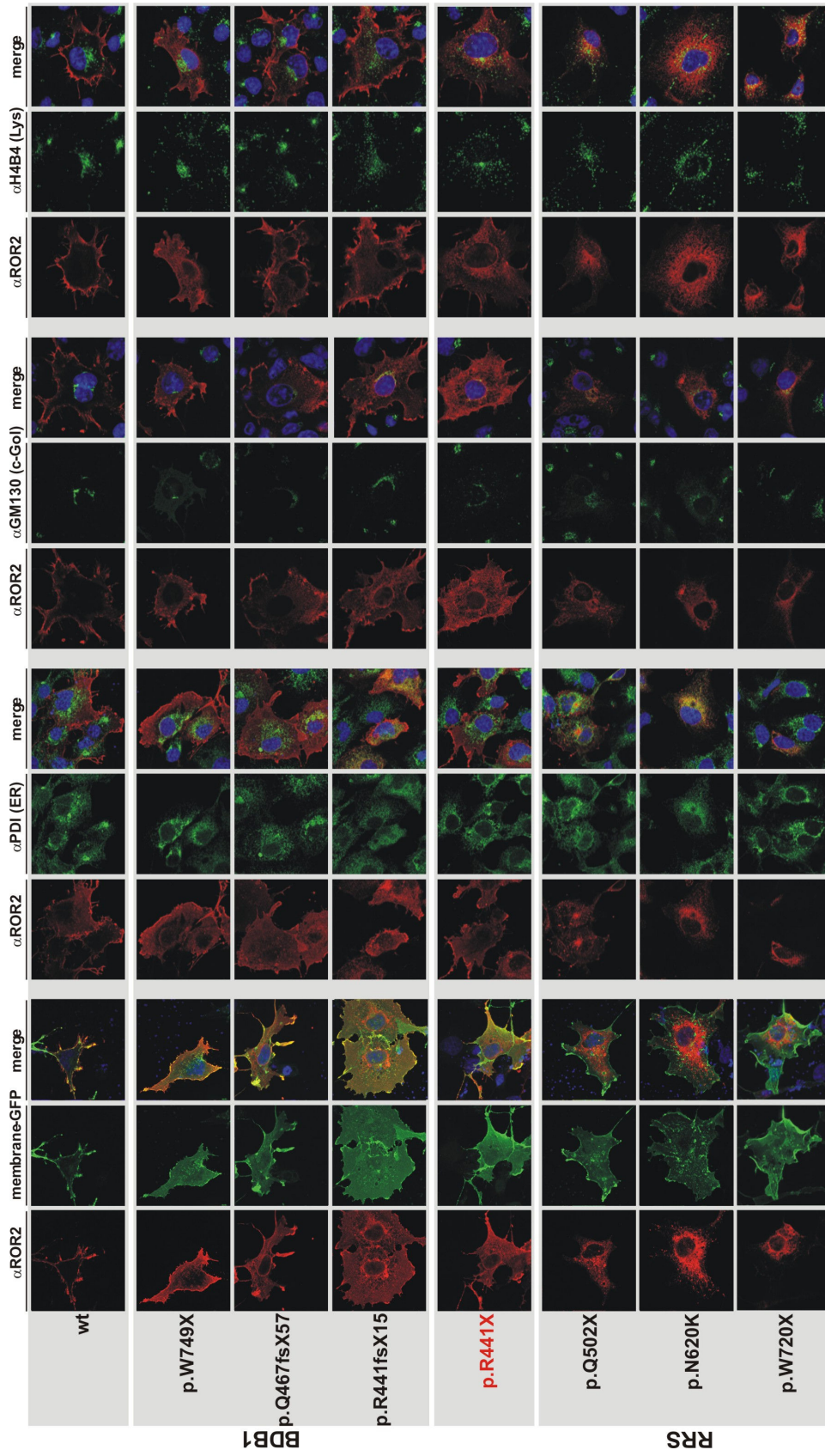


Figure 18: Co-localisation of wt and mutant ROR2 constructs in transiently transfected Cos-1 cells. Co-transfection with membrane-targeted GAP43-GFP shows cell surface localisation for wt, BDB1 and p.R441X mutant, but not for RRS mutants. PDI, GM130 and H4B4 were used as markers for the endoplasmic reticulum (ER), the cis-Golgi (c-Gol) and for lysosomes (Lys), respectively.

ular truncations causing RRS (p.Q502X and p.W720X), which are clearly retained intracellular and co-localise with BAP31. The N-terminal truncations resulting in the less severe form of dominant BDB1 (p.Q467fsX57, p.R441fsX15) also showed clear ER retention. However, a substantial fraction of the protein escapes and is able to reach the plasma membrane. Interestingly, the novel mutation p.R441X causing only recessive BDB shows a protein localisation comparable to the N-terminal BDB1 mutants.

For further verification, co-localization of the ROR2 protein with additional markers in transiently transfected Cos-1 cells was analysed (Figure 18). Membrane labelling with GFP fused to the plasma membrane protein Gap43 (Gap43-GFP) demonstrated surface localization of wt ROR2, the BDB1 constructs and also the p.R441X mutant, but not for the RRS mutants. Co-staining with endogenous PDI as an alternative ER marker corroborated the intracellular retention of the RRS variants. In addition, partial overlap between the cis-Golgi marker GM130 and the RRS mutants, the p.R441X mutant and also the BDB1 mutant p.R441fsX15 is observed. Finally, it was analysed if the mutant ROR2 protein located to the lysosomal compartment by co-staining for endogenous H4B4 and no significant overlap was identified.

4.1.4 Relative quantification of ROR2 protein at the plasma membrane

Analysis of protein distribution by immunocytochemistry alone is not capable to explain the differences in clinical phenotypes and inheritance of the dominant, proximal BDB1 mutations and the recessive p.R441X mutant. Hence, as a first step, the relative amount of ROR2 protein at the plasma membrane needed to be precisely quantified.

Transient transfection owns major disadvantages including dramatically high expression of introduced protein and extremely variable transfection efficiencies from cell to cell. Additionally, localisation of ROR2 mutants depend on protein quality control and transport, that are prone to be impaired due to the massive protein load. The precise quantification of the minute localisation changes between the novel and proximal BDB1 mutants require constant gene expression at near to physiological level. Stable and inducible HEK293 FlpIn T-Rex cell lines were therefore generated. Using this system, cells with a single genomic transgene integration were obtained,

that overexpress ROR2 wt and mutant protein approximately 10-fold on average (data not shown).

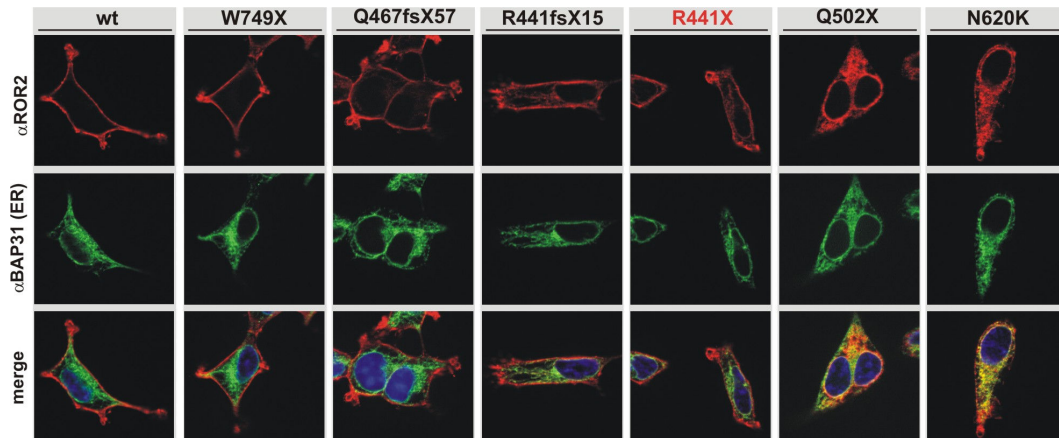


Figure 19: Immunocytochemical staining of ROR2 and endogenous BAP31 in stable HEK293 FlpIn T-Rex cells.

Immunocytochemistry for ROR2 and the ER marker BAP31 in these cells showed a protein distribution similar to that observed in Cos-1 cells (Figure 19). However, variabilities in gene expression levels and protein localisation, as well as overexpression-artefacts frequently observed in transiently transfected Cos-1 cells (data not shown), were cleared in HEK293 FlpIn T-Rex cell lines.

A surface protein biotinylation assay was used to investigate the fraction of membrane-localized ROR2 versus intracellular ROR2 (Figure 20). The amount of membrane-localized relative to intracellular ROR2 was determined for each construct by western blot analysis in six independent experiments and wt ROR2 was set as 1. As shown in Figure 20B, a gradual decrease of membrane localisation was observed, when comparing the different mutants. The BDB1 mutant p.W749X was similar to the wt, but the N-terminal BDB1 mutants p.Q467fsX57 and p.R441fsX15 showed a significantly higher retention than wt or the p.W749X mutant. The RRS mutants p.Q502X and p.N620K were almost completely retained intracellularly. Surprisingly, the p.R441X mutant was comparable to the N-terminal BDB1 mutations.

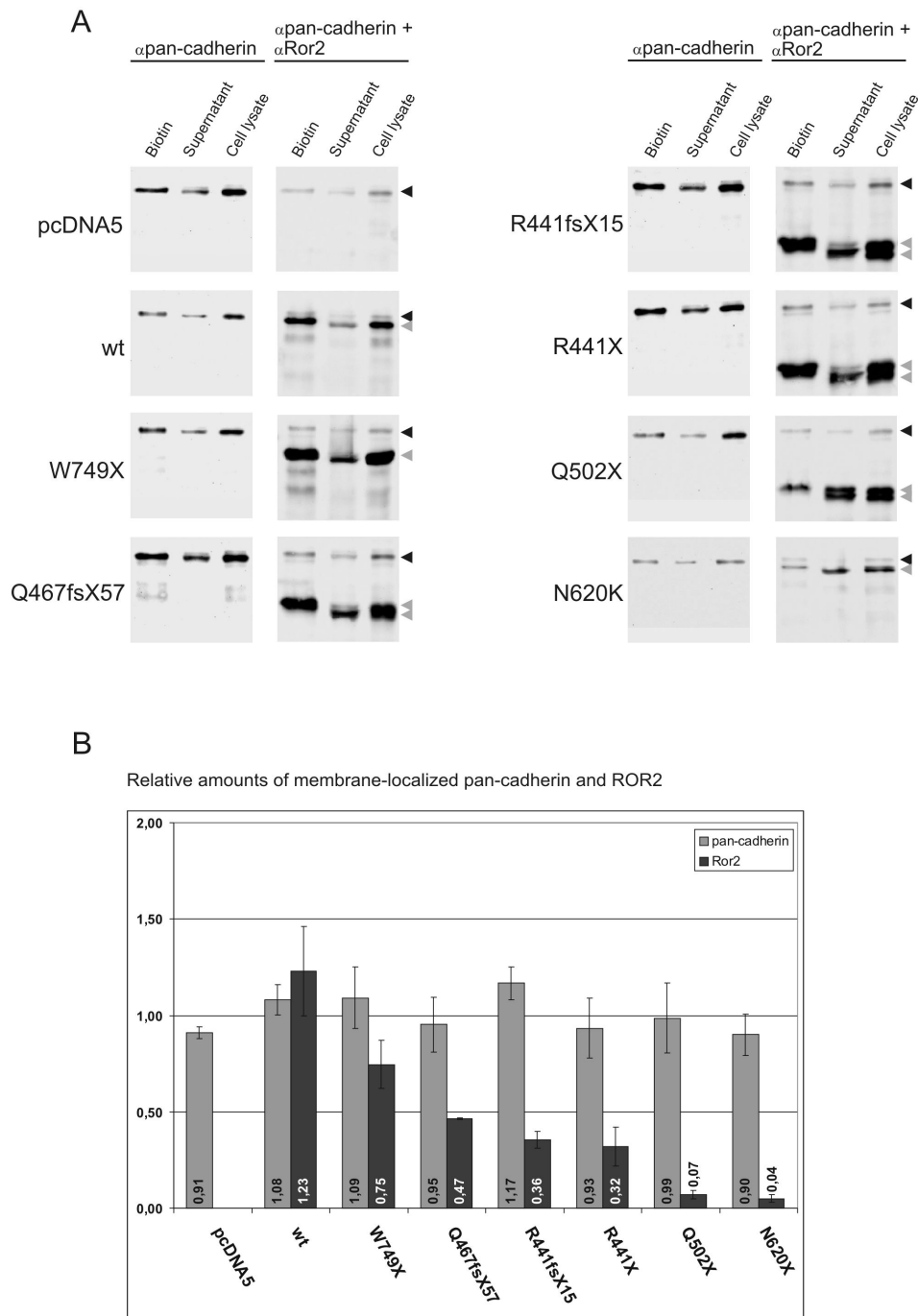


Figure 20: Relative surface localisation of ROR2 and endogenous pan-cadherin as control in stable HEK293 FlpIn T-Rex cell lines determined by surface biotinylation assay.

(A) Western blot analysis shows representative data. Blots have been first probed for endogenous pan-cadherin (left panel) and subsequently were re-probed for ROR2 (right panel; black arrowheads: pan-cadherin, grey arrowheads: ROR2). Note that surface-localized pan-cadherin and ROR2 have a higher molecular weight than the intracellular fraction due to glycosylation and / or biotinylation. (B) Quantification of relative surface localisation of pan-cadherin and ROR2.

These results confirm the observations made by immunocytochemistry. The novel mutant shows no significant changes in protein localisation compared to the N-terminal BDB1 mutants (Figure 21B). To exclude global changes in protein trafficking, the relative distribution of an unrelated protein, pan-cadherin was examined, which was present at equal levels on the surface of all cell lines analysed (Figure 20).

4.1.5 Additional quantification of protein levels reveal a gradient model for BDB1 versus RRS

The fact that the novel mutation showed no significant difference compared to the N-terminal BDB1 mutants came to quite a surprise. However, the biotinylation assay only determines the fraction of ROR2 at the plasma membrane relative to intracellularly retained ROR2. Changes in protein levels, i.e. effects due to altered degradation and /or translation efficiencies, are not examined with this method. ROR2 wild-type and mutant protein have to pass protein quality control in the ER, may be trafficked to the plasma membrane, and are eventually internalised and degraded. Hence, alterations in any of the degradation processes may have an effect on the absolute amount of ROR2 protein at the plasma membrane independent of the relative protein distribution.

In order to obtain an estimate for the degradation and /or translation efficiencies of the different ROR2 mutants, ROR2 protein levels were determined in respect to the corresponding mRNA. The material for mRNA and protein quantification was harvested at the same day and were both normalised to actin expression. The amount of protein was then normalised to the respective mRNA in three independent experiments and wt was set as 1. The BDB1 mutations p.W749X and p.Q467fsX57 showed a weak increase in total ROR2 protein content while the BDB1 construct p.R441fsX15 showed no difference to the wt (Figure 21A). In contrast, the p.R441X mutant was significantly less abundant than the wt and the BDB1 mutations. The RRS mutations p.Q502X and p.N620K were reduced even to a higher extent. These results show that BDB1 mutants generally exhibit a higher protein level than RRS mutants, as well as the novel mutant p.R441X.

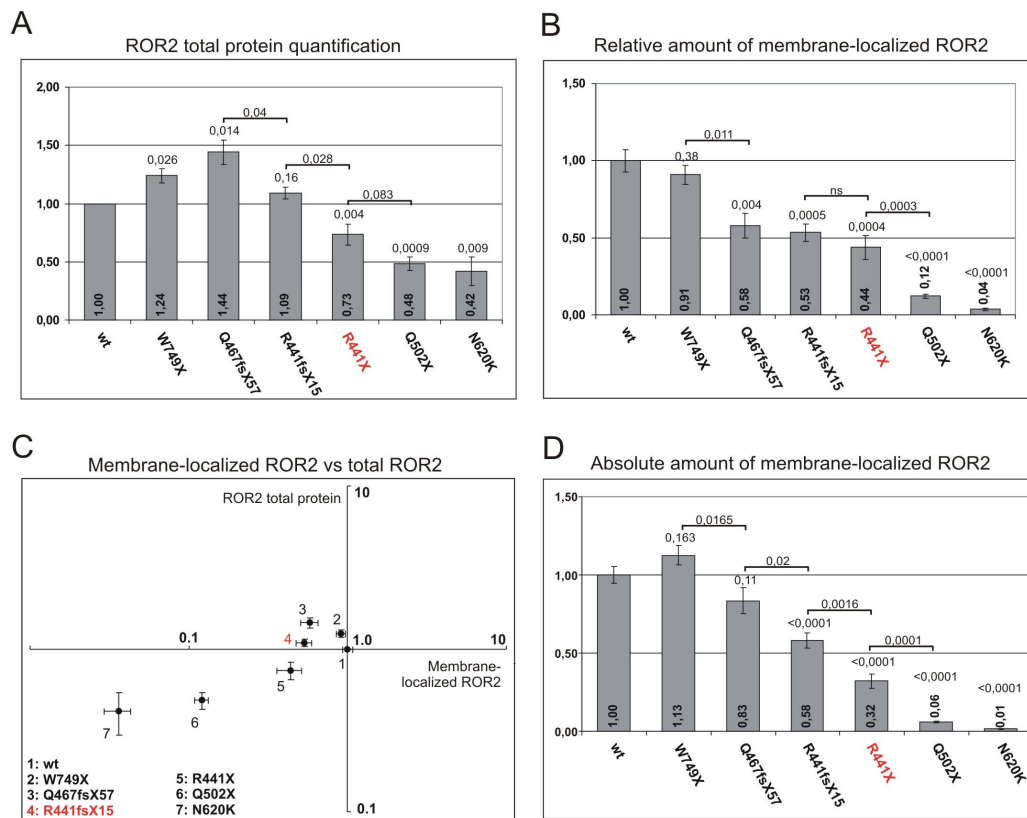


Figure 21: Absolute quantification of membrane-localized ROR2 in HEK293 FlpIn T-Rex cells. (A) Quantification of protein expression of different ROR2 constructs. Protein measurement was normalized to mRNA expression for each construct and to β -actin as loading control. (B) Relative amount of membrane localized ROR2 determined by surface biotinylation assay as shown in Figure 20. (C) Scatter blot depiction of membrane localized ROR2 (relative values) versus total protein amount on a double logarithmic scale. Note intermediate position of R441X mutant. (D) Absolute amount of membrane localized ROR2 determined by multiplication of total ROR2 protein levels with factor for membrane fraction obtained by surface biotinylation assay. Error bars represent standard errors, p-values depicted above columns representing t-test versus wild type, p-values depicted above brackets represent paired t-test between two particular constructs.

This indicated that the ROR2 protein levels play a significant role in addition to the relative protein localisation. To better discriminate the BDB1 from the RRS mutations, the relative membrane localisation of ROR2 versus the total protein amount were plotted on a double logarithmic scale (Figure 21C). Using this form of presentation, BDB1 mutations cluster in the left upper quadrant whereas the RRS mutations localize to the left lower quadrant. The R441X mutation appears in an intermediate position.

Furthermore, the knowledge about protein levels in the cells facilitates the determination of the absolute amount of membrane-bound ROR2 for each construct/cell line. Values for total ROR2 protein quantification were used as a factor and multiplied with the surface biotinylation values obtained from the same experiment (Figure 21D). This calculation demonstrates a continuous gradual decrease in surface ROR2 protein along the allelic series tested in this study. The mutations exhibiting intermediate phenotypes in homozygous human patients are placed at intermediate positions between the other BDB1 and RRS mutations. Concordant with the higher total ROR2 protein amount observed for the frame shift mutation R441fsX15, this mutation also shows a statistically significant higher total surface ROR2 amount than the nonsense mutation R441X.

4.1.6 An allelic series of Ror2 mutations in the mouse confirms BDB1 versus RRS phenotype gradient

The Ror2^{-/-} mouse [9] exhibits complete loss of Ror2 function and shows numerous features of Robinow syndrome including craniofacial and vertebral malformations, heart defect and severe mesomelic limb shortening [31]. Recently, a novel mouse mutant for Ror2 that carries the exact copy of a human BDB1 mutation (Ror2^{W749X}) was generated. This mouse mutant exhibits recessive brachydactyly with complete lack of the middle phalanges (p2). In the homozygous state, this mouse also shows features of RRS, albeit to a weaker degree than the Ror2^{-/-} mouse [32]. These mouse mutants were used to challenge the gradient model in vivo.

The mesomelic limb shortening and p2 shortening were used as readout for RRS and BDB1 features, respectively (Figure 22). The radius of newborn Ror2^{W749X/W749X} mice showed moderate shortening compared to their wild type littermates, whereas Ror2^{-/-} mice showed a severe reduction in size (Figure 22A). Consistent with the biochemical data presented above, mice carrying one truncating and one functional null allele (Ror2^{W749X/-}), thus possessing a reduced amount of membrane-bound truncated Ror2, displayed an intermediate phenotype. The Ror2^{W749X/W749X} mouse showed the most severe brachydactyly phenotype exhibiting an aplasia of p2, while Ror2^{-/-} mice had only a minor hypoplasia of p2 (Figure 22B). Altogether, Ror2^{W749X/-}

mice had a more severe phenotype than $Ror2^{-/-}$ mice demonstrating a gain of function of the remaining W749X allele on a null background.

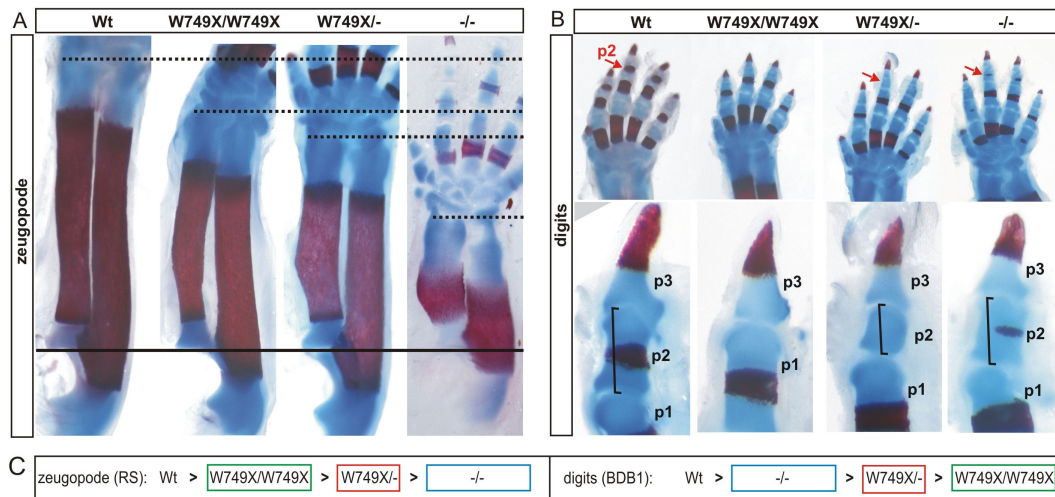


Figure 22: Allelic series of $Ror2$ mutations in the mouse.

(A) $Ror2^{-/-}$ was used as model for RRS; $Ror2^{W749X/W749X}$ was used as model for BDB1. (A) Mesomelic limb shortening (here: radius) was used as readout for Robinow-syndrome-like features. (B) Shortening of the middle phalanx (p2) was used as BDB1 readout. Note that the W749X/W749X mutant exhibits mild RRS features that can be increased by replacing one allele with a functional null. Vice versa the $Ror2$ -null mouse shows only mild hypoplasia of p2 while the W749X/W749X mutant exhibits complete loss of p2. The W749X/- mutant displays an intermediate phenotype. (C) Reciprocal development of phenotypic severity in the allelic series. RS phenotype increases towards the -/- (blue box), BDB1 phenotype towards the W749X/W749X (green box) genotype. Compound heterozygous embryos (red box) display an intermediate phenotype in both cases.

The allelic series presented here supports the *in vitro* findings demonstrating that the W749X mutant functions as a gain of function allele and as such induces a brachydactyly phenotype in a dose dependent manner. The mesomelic shortening, in contrast, is caused by a loss of $Ror2$ function. Figure 22C illustrates the observed reciprocal gradient, in which the RRS phenotype increases towards the $Ror2^{-/-}$ mutant and the BDB1 phenotype increases towards the $Ror2^{W749X/W749X}$ mutant.

4.2 Mapping the modifier of dactylaplasia (*mdac*)

Phenotypic variability in genetic disorders may not only be due to the type of mutation as exemplified in the Ror2 project. In most cases, the genetic background also has a modulating effect on the phenotypic outcome. A very dramatic example for this finding is the dactylaplasia mutation (*dac*) in the mouse, which occurred twice spontaneously in the Jackson Laboratory (Bar Harbour, Maine). Initial experiments to determine the mode of inheritance have shown, that the phenotype of these animals is completely lost when crossed out to specific mouse strains (Table 7). Results of C. K. Chai [93] suggest a two locus model, in which a dominant modifier in the genetic background in some of the tested mouse strains suppresses the development of dactylaplasia.

Previous to this work, *Mdac* was roughly mapped to a ~27 Mb interval on chromosome 13 [94] between the microsatellite markers D13Mit10 (49.82 Mb) and D13Mit99 (76.94 Mb). This area comprises approximately 200 known protein coding genes and needs to be reduced to identify the modifier of dactylaplasia.

Table 7: List of mouse strains with known allele of *mdac* [93].

Dac mice were crossed to different mouse strains. If the F₁ generation displayed no phenotype, the dominant allele *Mdac* is present in the tested strains. Accordingly, the recessive *mdac* allele is present in case the F₁ generation showed the phenotype.

Mouse strain	<i>Mdac</i> (no phenotype in F ₁)	<i>mdac</i> (phenotype in F ₁)
C57Bl6/J	+	-
AKR/J	+	-
C3H/J	+	-
CBA/J	+	-
DBA/2J	+	-
SWR/J	+	-
129/J	-	+
BALB/cByJ	-	+
NZB/BinJ	-	+
LG/J	-	+
SM/J	-	+
MRL/MpJ	-	+

4.2.1 Genetic mapping reduces the *Mdac* interval to ~ 3 Mb

4.2.1.1 Hybrid F₁ backcross

Homozygous or heterozygous *dac* mice were crossed out to C57Bl6/J to generate a hybrid F₁ generation. The resulting mice are heterozygous or wild-type for the *dac* mutation and always heterozygous for the modifier of dactylaplasia (*Mdac/mdac*). Hence, they do not display the phenotype. These animals were genotyped for the presence of the *dac* allele and backcrossed to *dac/dac* or *dac/+* ; *mdac/mdac* mice.

Due to an insufficient amount of homozygous *dac* animals to start with, not all animals in the F₁ generation are true hybrids, i.e. do not carry the *dac* allele (+/+). If these animals were crossed to *dac/+* ; *mdac/mdac* mice, only 50% of the F₂ generation carried the *dac* allele. As a consequence, it could not be determined if the lack of phenotype is due to the presence of the dominant *Mdac* allele or the mere absence of *dac*. Therefore, only dactylaplastic F₂ mice were analysed for recombination in the *Mdac* region on chromosome 13.

Table 8 summarises the results obtained from the hybrid backcross. In total 2006 F₂ animals were generated, of which 849 were analysed.

Table 8: Summary of F₁ hybrid backcross

F ₁ hybrid	backcrossed with	total animals	phenotype	no phenotype	expected ratio	observed ratio
+/+ or <i>dac/+</i> ; <i>Mdac/mdac</i>	<i>dac/dac</i> ; <i>mdac/mdac</i>	1115	538	577	0.5	0.49
<i>dac/+</i> ; <i>Mdac/mdac</i>	<i>dac/+</i> ; <i>mdac/mdac</i>	558	209	349	0.375	0.375
+/+; <i>Mdac/mdac</i>	<i>dac/+</i> ; <i>mdac/mdac</i>	333	102	231	0.25	0.31
Totals		2006	849	1157	0.42	0.42

4.2.1.2 Microsatellite and SNP mapping

Genomic DNA of the 849 dactylaplastic animals was examined for recombination in the *Mdac* interval. 16 highly polymorphic microsatellite markers were tested for their capacity to distinguish between DAC and C57Bl/6 genomic information. D13Mit248, D13Mit54 and D13Mit283 showed no polymorphism between these two strains, however, the remaining thirteen markers were polymorphic and their differential lengths are summarised in Figure 23. Twenty six of 849 offspring exhibited recombination events that were informative for further mapping between D13Mit10 and D13Mit99. Among these, eight independent recombination events placed *Mdac* within a 5-Mb interval between D13Mit186 and D13Mit310 (Figure 23) and the recombination breakpoints were further characterised by SNP mapping.

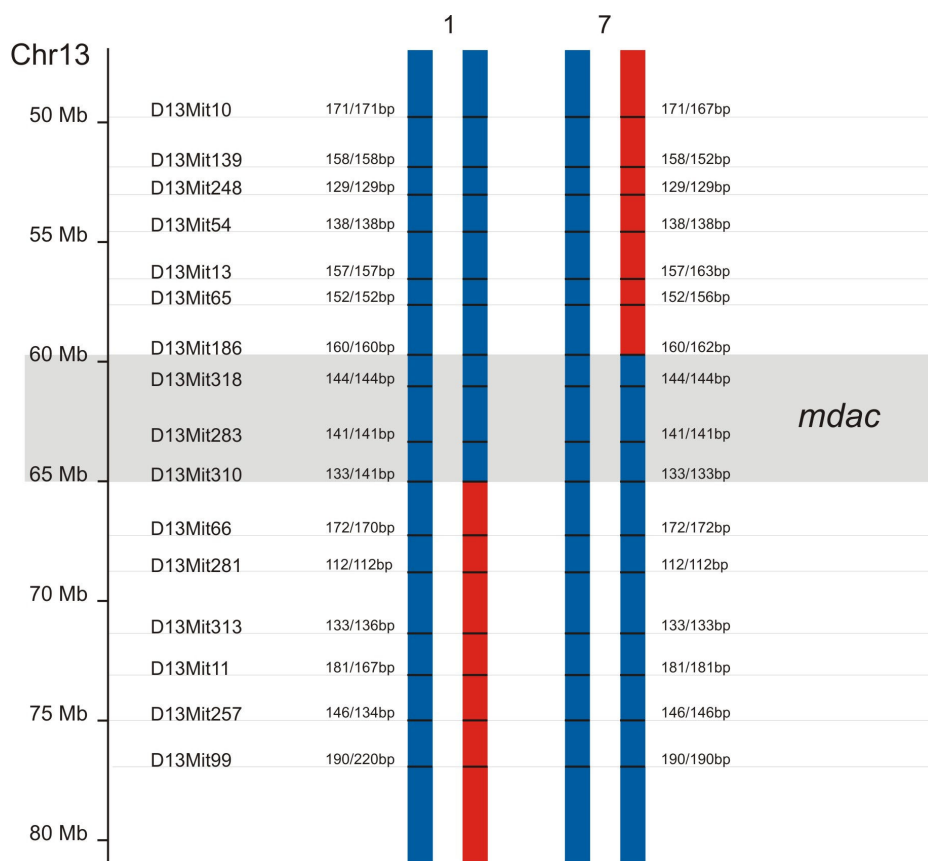


Figure 23: Microsatellite mapping reduces *mdac* interval to ~ 5 Mb.

One animal has a recombination breakpoint at D13Mit310 (65.1 Mb) and 7 animals show recombination at D13Mit186 (59.8 Mb). Observed sequence length polymorphisms of microsatellites are depicted (DAC/C57Bl/6). Genomic origin of DAC and C57Bl/6 mice is illustrated in blue and red, respectively. The inferred *mdac* region is shaded in grey.

The innermost proximal recombination breakpoint resides between rs29636656 and rs13481840, the distal between rs29584348 and rs3726453 (Figure 24). Hence, the *mdac* interval is defined to the region between 60.854 Mb and 63.835 Mb on chromosome 13.

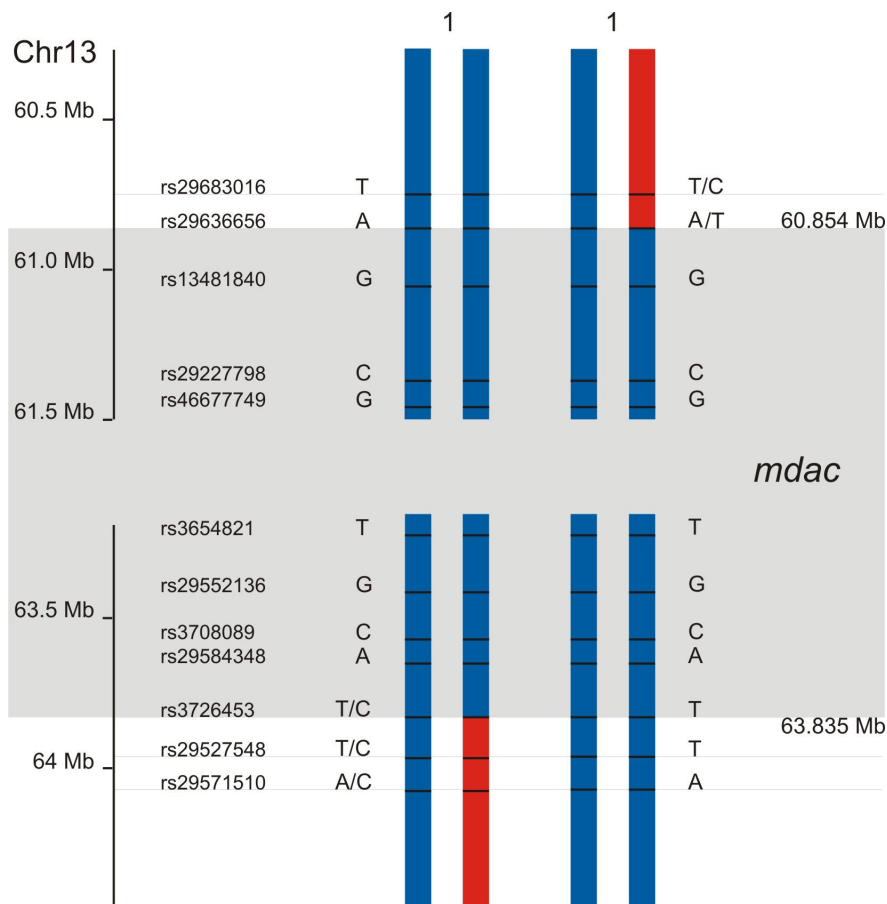


Figure 24: SNP mapping limits *mdac* interval to ~ 3 Mb.

Two independent recombination events occurred at rs29636656 and rs3726453. Observed single nucleotide polymorphisms are depicted (DAC/C57Bl/6). Genomic origin of DAC and C57Bl/6 mice is illustrated in blue and red, respectively. The inferred *mdac* region is shaded in grey.

Among many predicted genes, pseudogenes, miRNA and other non-coding RNAs, this genomic region contains 24 validated protein-coding genes. Yet none of the genes renders an obvious candidate to modify the dactylaplasia phenotype and, under this perspective, the informational content of the 3-Mb interval is still relatively large. Further genetic mapping is hampered by the low probability of recombination

events in the small genomic region. However, recent advances may overcome this bottleneck. High density SNP coverage of 16 inbred mouse strains [107] allows investigation of accumulated recombinations and, hence, facilitates mapping *in silico*.

4.2.2 Analysis of haplotype structures refines the potential *mdac* region

The European "fancy" mouse, the genetic ancestor of widely-used classical inbred mouse strains, is derived from European wild mice *Mus musculus domesticus* and East Asian "fancy" mice, a product of interbreeding the Asian subspecies *M. m. musculus*, *M. m. castaneus* and *M. m. molossinus* to generate varieties of mice with different coat colours and behavioural characteristics as pets [107, 108]. At the beginning of the 20th century, William Castle and few other colleagues started to study inheritance in European "fancy" mice in a number of mouse colonies. Inbreeding and exchange of mice in the small research community lead to the generation of classical inbred strains [109], which are highly interrelated and own dramatically reduced genetic variability compared to wild mice [110, 111], since they derived from a limited number of founder animals.

These special characteristics of classical strains enable *in silico* mapping of genetic traits by analysing haplotype structures in several strains [112, 113]. Genetic variation within species is not randomly distributed, but is shared in discrete haplotype blocks, which arise from meiotic crossovers between parental chromosomes. Over many generations, genomic segments representing ancestral genotypes are shuffled around in the genomes of an inbred population, resulting in a mosaic block-wise pattern of variability [110]. Due to the reduced genetic variability and common ancestry of classical inbred strains, patterns of allelic similarities and differences (strain distribution patterns or SDPs) can be discerned for every variable locus [112]. This makes it possible to map specific traits (i.e. *mdac*) by correlating genotype and phenotype strain distribution patterns, because a common trait is rather caused by an ancient polymorphism than independently acquired mutations in different strains.

Until recently, the reliable determination of haplotype structure was hampered by the lack of dense SNP data for a large number of strains. The situation changed when Frazer et al. [107] published SNP data for 16 classical and wild-derived mouse strains in 2007. In total, 8.27 mio SNPs were discovered using oligonucleotide ar-

rays covering 58% of the C57Bl/6 reference genome, which were made publically available in the Mouse Phenome Database (MPD, Jackson Laboratory). Of the 16 mouse strains analysed, four are known to carry the dominant modifier of dactylaplasia *Mdac* (C57BL/6J, AKR/J, C3H/HeJ, DBA/2J), whereas three strains are permissive for the phenotype (129S1/SvImJ, BALB/cByJ, NZW/LacJ) and hence contain the recessive allele *mdac*. Additionally, DAC mice were crossed to NOD/ShiLtJ mice available at the institute, which confirmed them to carry the *mdac* allele.

SNP data for the eight classical and four wild derived strains were downloaded from MPD and filtered to contain > 75% typed strains per SNP. In total, 6541 SNPs qualified between 60.854 Mb and 63.835 Mb, which corresponds to a median SNP density of approx. 2.2 SNP per kilobase. A more detailed overview on the SNP coverage in the *mdac* interval is shown in Figure 25A. The biallelic nature of murine SNPs allows a two-colour coded depiction of a reference genotype (C57BL/6J, red) and the corresponding alternative allele (blue, Figure 25B). This form of visualisation reveals distinct patterns of genetic variability often shared between members of different strains, which resemble the ancient phenotypes inherited in block-wise structure. Boundaries of haplotype blocks were calculated using HaploView and strain distribution patterns (SDPs) of common and divergent ancestry were generated for each strain (Figure 25C). In concordance with the assumption that the modifier of dactylaplasia is an ancient polymorphism, the candidate region can be defined as area, in which no haplotype is shared between *Mdac* and *mdac* strains.

Two genomic intervals that agree with the prerequisites to harbour *mdac* could be determined. The first comprises ~18 kb between 60.854 Mb - 60.873 Mb at the proximal end of the region defined by SNP mapping. The second area is incomparably larger, consisting of an 1.5 Mb interval between 61.554 Mb - 63.062 Mb.

An additional level of information regarding genetic variability in this genomic region can be acquired by the pair wise comparison of strains with respect to their SNP density. For this approach, SNPs that are polymorphic to the C57Bl/6 genotype were counted and averaged over a 40 kb interval for each strain. The resulting graph is depicted in Figure 26, which essentially shows two areas in which all *mdac* strains

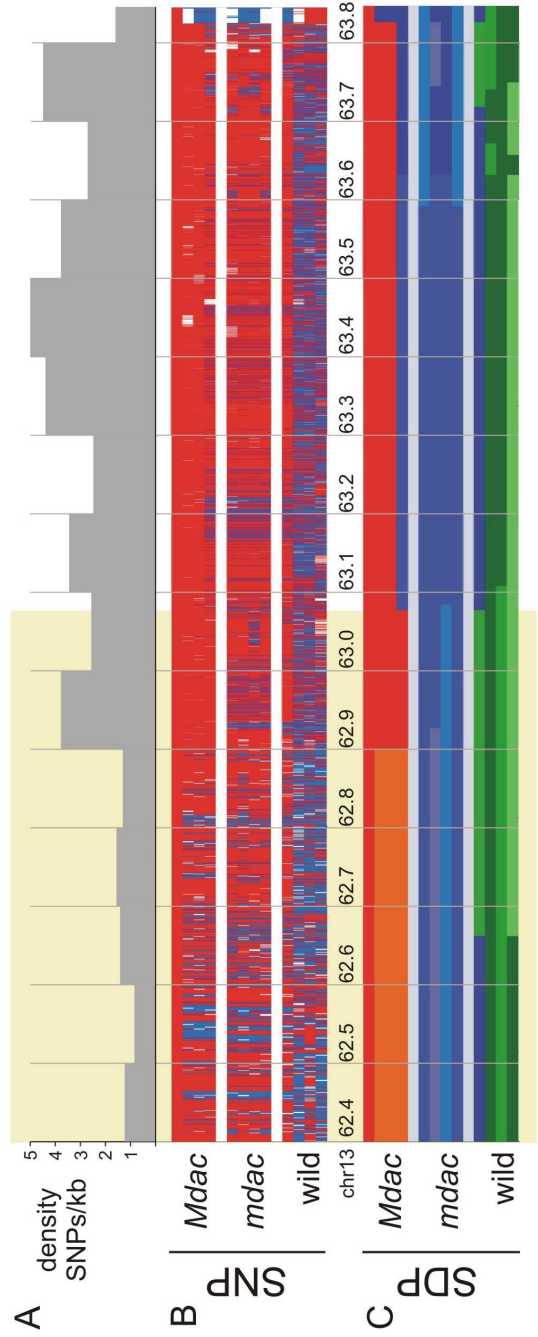
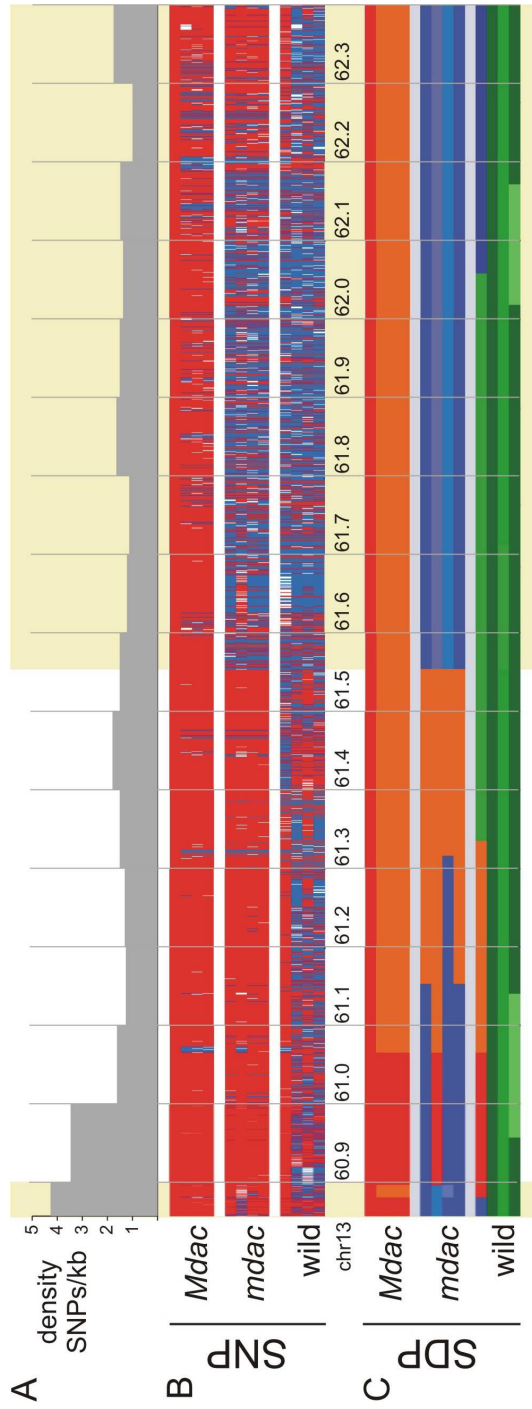


Figure 25: Single nucleotide polymorphisms (SNPs) and strain distribution patterns (SDPs) in the *mdac* interval.

(A) SNP density of the dataset in the *mdac* region. The number of SNPs per kb was determined and averaged over 100-kb intervals. (B) SNP data for mice carrying the dominant allele *Mdac* (C57BL/6J, AKR/J, C3H/HeJ, DBA/2J), the recessive allele *mdac* (129S1/SvImJ, BALB/cByJ, NOD/ShiLtJ, NZW/LacJ) and wild-derived strains (WSB/EiJ, MOLF/EiJ, PWD/PhJ, CAST/EiJ). Allele1 is depicted in red, whereas the corresponding allele 2 is shown in blue. White: not typed. The genotype of C57BL/6J is set as reference. (C) Corresponding strain distribution patterns (SDPs) of mice carrying *Mdac* or *mdac*, and wild-derived strains. Haplotypes predominant in mice carrying *Mdac* are depicted in red/orange, predominant *mdac* haplotypes are shown in blue shades, and haplotypes unique to wild-derived mice are depicted in green shades. Only 2 to 5 different haplotypes are present in the 8 classical inbred strains. Areas that agree with the prerequisites to harbour *mdac* are underlain in bright yellow.

are highly polymorphic (~60 SNPs / 40 kb) to C57Bl/6 and other *Mdac* strains: 61.54 - 62.10 Mb and 62.90 - 63.02 Mb.

It had been suggested, that areas of high sequence divergence and hence SNP density is due to different subspecies origins [110], although intra-subspecies variation due to ancient recombinations within the wild *M. m. domesticus* may also be the cause [114]. In either case, the highly polymorphic nature of the mentioned areas increase the likelihood, that an ancient polymorphism influencing the dactylasplasia phenotype resides within them.

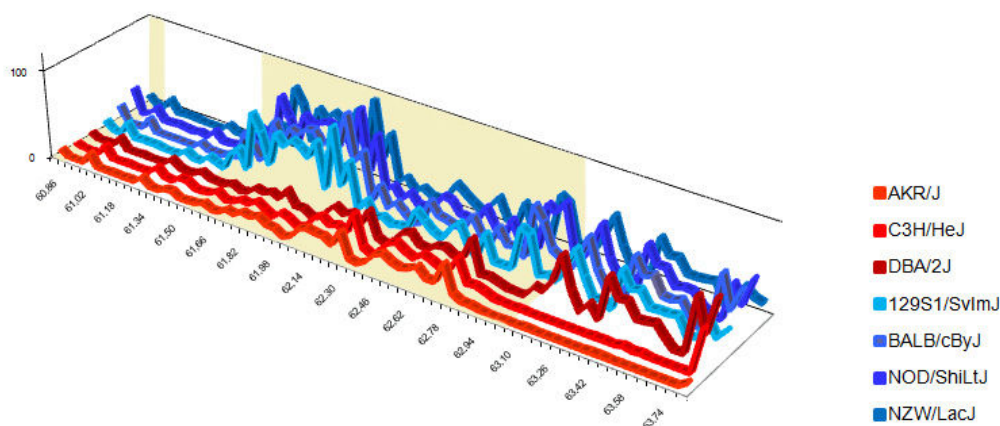


Figure 26: SNP density of strains in respect to C57Bl/6.

For each analysed mouse strain, SNPs that are polymorphic to the C57Bl/6 genotype were counted and averaged over a 40 kb interval. Mouse strains carrying *Mdac* are depicted in red/orange, mice carrying the *mdac* allele are shown in blue shades. Areas that agree with the prerequisites to harbour *mdac* are underlain in bright yellow.

4.2.3 Genomic features of the *Mdac* region

Kano et al. [97] showed in 2007, that the activation of the MusD element causing dactylaplasia leads to the formation of the phenotype. This activation depends on the presence of *mdac*, whereas the presence of *Mdac* inhibits MusD activity via DNA methylation of its 5'-LTR. Hence, the function of *mdac* / *Mdac* may relate to this specific methylation rather than modulating signalling processes leading to the degradation of the AER, the cause of dactylaplasia.

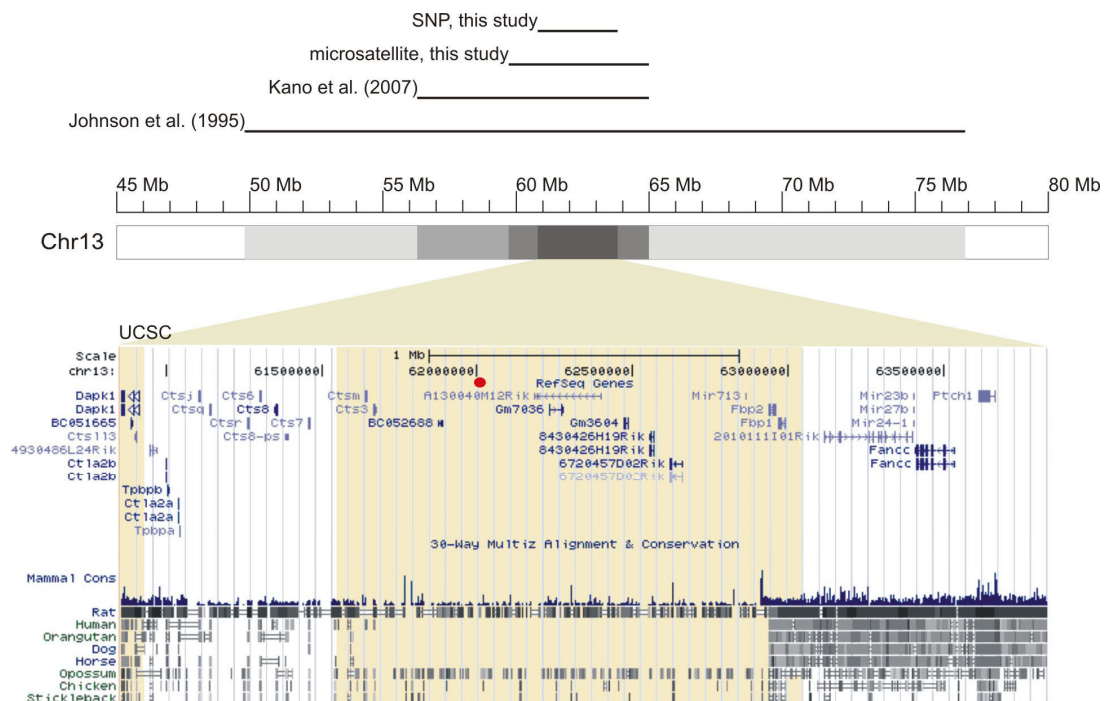


Figure 27: Overview of the *Mdac* interval.

Mapping results of this and two other studies are summarised. A UCSC genome browser screen shot depicts the genomic details (RefSeq genes, species conservation) of the *Mdac* region as defined by genetic SNP mapping (Chr13: 60.854 - 63.835 Mb). Areas that agree with the prerequisites to harbour *Mdac* according to haplotype mapping are underlain in bright yellow. The position of the potentially active MusD element is marked by a red dot.

As mentioned above, none of the annotated features in the initial 3 Mb *Mdac* interval renders a good candidate to modify the phenotype of dactylaplasia. However the amount of genomic features could be significantly reduced by *in silico* mapping (Figure 27, Table 9). The remaining 10 protein coding genes defined by haplotype

mapping include 5 genes outside of the polymorphic region: 4 zinc finger (Gm7036, Gm3604, 8430426H19Rik, 6720457D02Rik) and one hypothetical krab-box protein (BC053725) for which no further data is available. Furthermore, the region contains two placenta-specific cysteine-type peptidases (GNF Expression Atlas 2) and two fructose-bisphosphatases expressed in liver, kidney and testis, but not during development (GNF Expression Atlas 2, whole mount in situ hybridisation; data not shown). The most interesting protein coding gene is the death associated protein kinase 1 (Dapk1), which has been shown to have promoting and attenuating effects on apoptosis [115-117]. However, Dapk1 is predominantly expressed in the developing notochord and brain at stage E10.5 and no signal was observed in the apical ectodermal ridge or the limb in general (whole mount in situ hybridisation; data not shown).

Table 9: Summary of genomic features.

The number of genomic features could be significantly reduced by haplotype (SDP) mapping. Within this region, a subset with increased probability could be defined due to the highly polymorphic nature of haplotypes at this position.

Feature	Genetic map (3 Mb)	Haplotype map (1.5 Mb)	Highly polymorphic (0.8 Mb)
Protein coding	29	10	5
Non-coding gene	1	1	1
miRNA	4	1	0
Pseudogene	2	1	1
Ensembl predicted	17	14	6

The lack of a clear candidate requires a more detailed search to detect interesting features in the *mdac* interval. In 2004, a study identified a potentially active MusD element within the highly polymorphic region of the *mdac* interval (Chr13: 62.052.281 - 62.059.772) [118], which owns 96% sequence homology with both dactylaplasia-causing MusD insertions, respectively [98]. Genomic DNA of mouse strains with known *mdac* / *Mdac* phenotype were tested for the presence of this particular MusD element. Interestingly, *Mdac* perfectly segregates with the existence of

the MusD element, whereas the element is always absent in the *mdac* strains tested (Figure 28). This result was expected for strains with dense SNP data available, since it resembles the haplotype distribution pattern at this locus. However, the segregation in strains with unknown haplotype structure but known *Mdac* or *mdac* genotype (i.e. CBA/J, LG/J, SM/J, SWR/J) suggests, that *mdac* may be positioned at this locus.

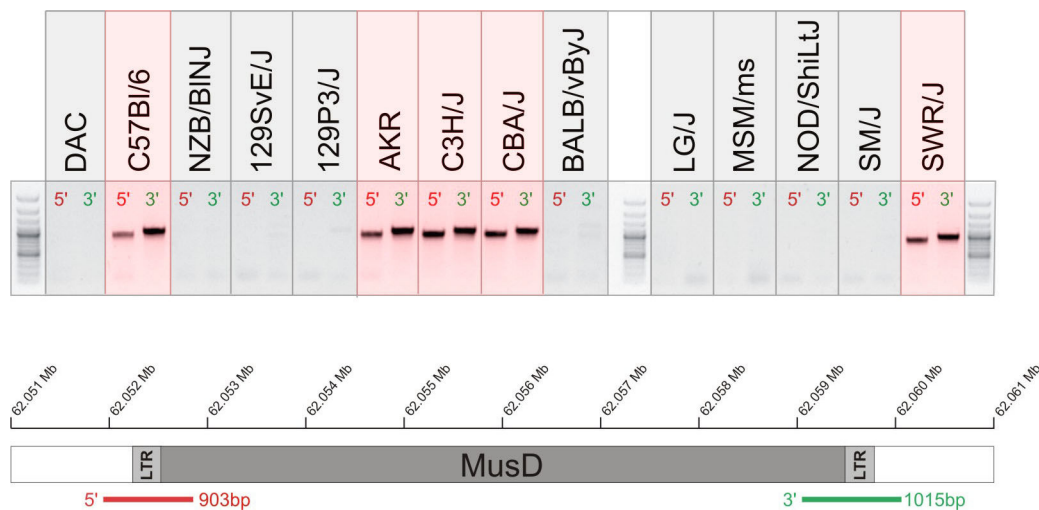


Figure 28: A MusD element segregates with *mdac* /*Mdac*.

Primers specific for the 5' and 3' ends of the MusD element on Chr13 were used to detect its presence in the genetic background of several mouse strains with known *mdac* (shaded in gray) /*Mdac* (shaded in red) phenotype. *Mdac* perfectly segregates with the presence of the MusD element, whereas the MusD element is absent in the *mdac* strains tested.

Several short RNA-mediated defence mechanisms against retrotransposable elements have been described, which involve DNA methylation of the respective transposons (5.2.3). Hence the possibility exists, that the specific MusD element on chromosome 13 may act as an RNA template, which eventually silences the MusD element leading to dactylaplasia.

4.3 Characterisation of mutational consequences leading to ectrodactyly in the dactylaplasia mouse

Due to the similarity in phenotype and location of the mutation, the dactylaplasia mouse has been suggested as model for the human split hand and foot malformation

3 (SHFM3). Although these mice have been available for more than two decades, the molecular mechanisms leading to ectrodactyly have not been elucidated to date. Several studies on gene expression in *Dac* limbs could not identify a misregulated pathway and contradicting results on the mechanism of AER degradation have been published [96, 100]. Further detailed analyses of these mice are necessary to identify a common misregulation in dactylaplasia and SHFM3.

4.3.1 The defect in AER maintenance is caused by increased apoptosis

Previously, two different mechanisms of AER degradation have been proposed leading to the observed ectrodactyly in dactylaplasia mice. Seto et al. [100] suggested that increased apoptosis leads to the loss of AER, whereas Crackower [96] and colleagues identified a lack of proliferation to be the cause. Since neither set of data is particularly convincing and the onset of the phenotype was never precisely determined, cell death and proliferation were examined in wild-type and *Dac* mutant limbs via immunohistochemistry (IHC) with α Cleaved-caspase 3 and α Phosphohistone 3 antibodies, respectively. All embryos were precisely staged by counting somite numbers to ensure comparability of the results.

First, apoptosis and proliferation were analysed in whole AERs. The number of cleaved-caspase 3 positive cells and the number of proliferating cells were determined in at least 50 sections per limb. Three-dimensional reconstructions of 34 somite stage limb sections reveal excessive cell death throughout the entire AER of *Dac* mutant limbs, where only limited apoptosis is observed in the wild-type controls (Figure 29). Interestingly, proliferation even increased in *Dac* mutant AERs, which stands in sharp contrast to the results obtained by Crackower et al. [96].

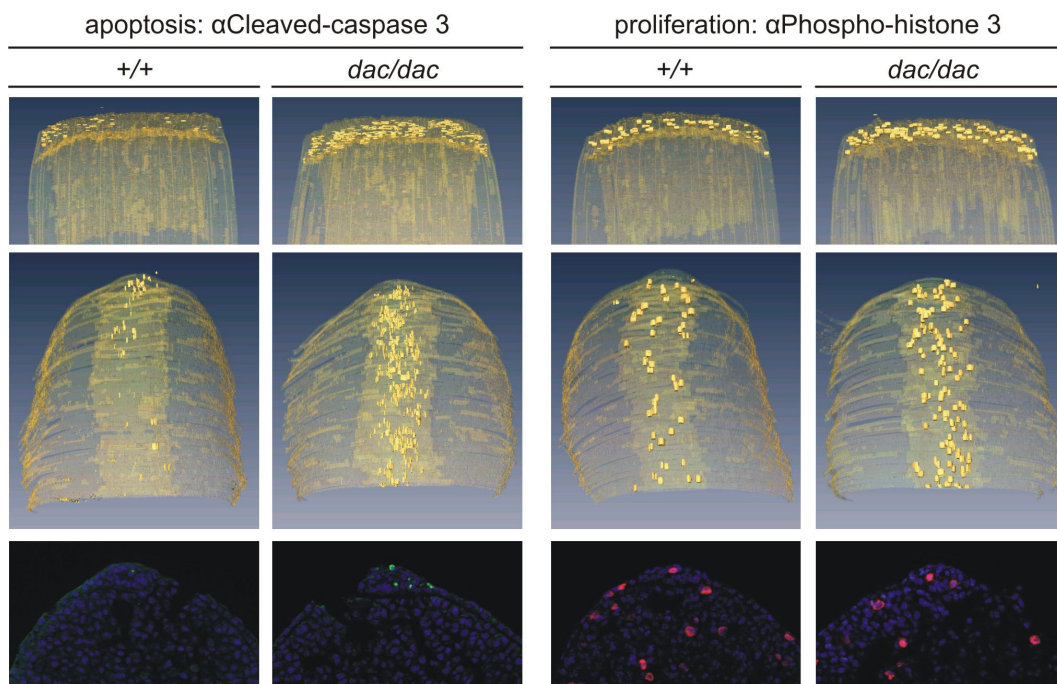


Figure 29: Apoptosis and proliferation are increased in *dac/dac* mutants at the 34S stage. Three-dimensional reconstruction of longitudinal IHC-sections of wild-type and mutant limbs treated with α Cleaved-caspase 3 (apoptosis) and α Phospho-histone 3 (proliferation). The outlines of limbs and AERs are depicted transparently. Top panel: side-view of the AER. Middle panel: top-view of the AER. Bottom panel: representative sections used for reconstructions: cleaved-caspase 3 (green), phospho-histone 3 (red), DAPI (blue).

In order to determine the onset of increased apoptosis and to follow changes in proliferation, sections of wild-type and mutant limbs from 11 different somite stages were prepared. Statistical analysis revealed an abnormal increase of apoptosis starting at stage 32S / 33S in mutant AERs. From stage 36S onwards, excessive cell death occurs, which is approximately 30-40 fold increased compared to wild-type (Figure 30A). The increase in proliferation, however, appears to be only a transient phenomenon. Between stages 32S and 36S an approximately 2 fold increase in proliferative cells is observed, which is subsequently reduced to wild-type levels at later stages (Figure 30B).

In conclusion, these results confirm the observations made by Seto and colleagues [100], who proposed aberrant cell death in the AER to be the cause for its degradation.

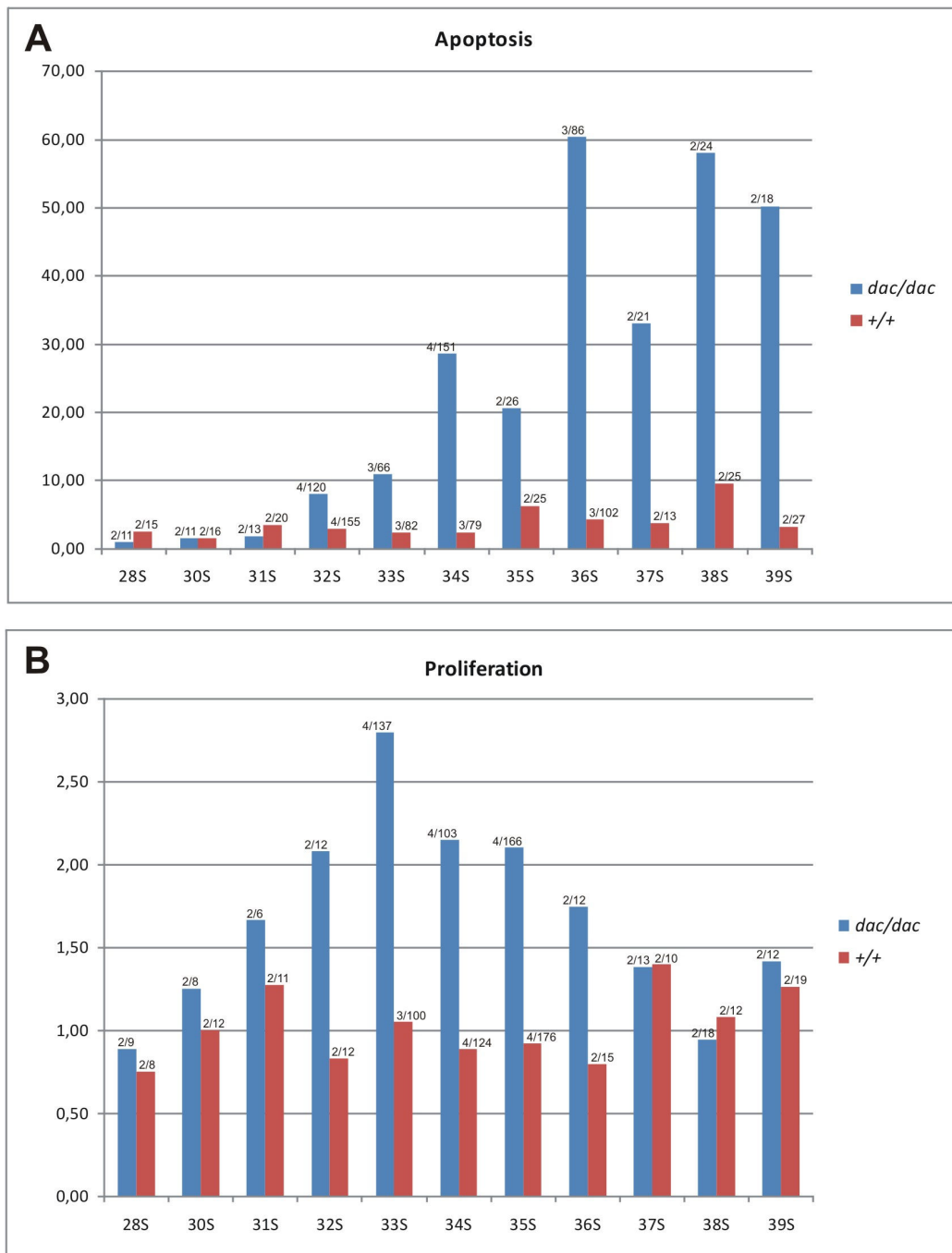


Figure 30: Quantitative analysis of apoptosis and proliferation between stages E9.75 and E10.75. (A) Fold-changes of apoptosis signal (α Cleaved-caspase 3) compared to wild-type at the 30 somite stage (30S, E10.0). In *lac/dac* AERs (blue) apoptosis increases significantly from stage 32S/33S onward, whereas the level remains constant in *+/+* AERs. Number of limbs / number of sections analysed are indicated above bars. (B) Fold-changes of AER-proliferative cells (α Phospho-histone 3) normalised to wild-type at the 30 somite stage (30S, E10.0). A transient increase in proliferation can be observed *lac/dac* AERs between somite stages 32S and 36S. Number of limbs / number of sections analysed are indicated above bars.

4.3.2 Expression analysis indicates deregulation of canonical Wnt-signalling in the mutant AER

Although Dactylaplasia mice have been suggested a model for human SHFM3, expression analyses for common candidate genes involved in AER maintenance and function except for *Fgf8* have not been published to date. Figure 31 displays *in situ* hybridisations of selected genes within or nearby the human duplicated region as well as further candidates important for AER maintenance. The down-regulation of *Fgf8* [95, 96] and up-regulation of MusD transcripts [97] in *Dac* mutant limbs could be reproduced with this method. *Fbxw4*, the gene disrupted by the human duplication and the murine *Dac*^{2J} insertion, shows ubiquitous low-level mRNA expression. However, no differences between *Dac*^{1J} mutant limbs and wild-type control could be observed. Similar results were obtained with *in situ* hybridisations of *Poll* and *Btrc*, the genes always duplicated in human SHFM3. Gene expression studies on lymphoblastoid cell lines of SHFM3 patients by qPCR suggested transcriptional upregulation of *SUFU* [58] in affected individuals.

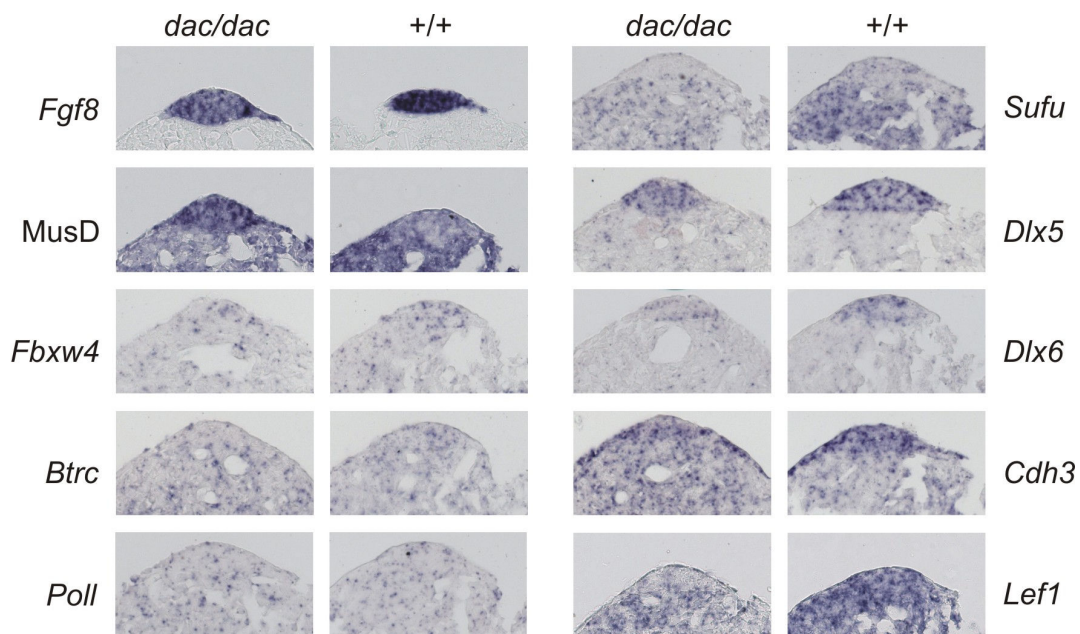


Figure 31: *In situ* hybridisation on longitudinal sections of wild-type and mutant limbs at stage 33S.

However, expression analysis by the means of *in situ* hybridisation on *Dac* mutant limbs does not show significant changes in *Sufu* expression, but it rather appears to be downregulated. *TP63* and its downstream targets, *DLX5/6* and *CDH3*, have been shown to be central factors in the pathogenesis of SHFM3 and related disorders in human and mice [85-92]. Expression analysis of *Dlx5/6* and *Cdh3* on RNA level and p63 on protein level (Figure 32B), however, revealed no changes in expression intensity.

A different picture evolves when examining components of the Wnt / β -catenin pathway. Disruption of this pathway was shown to impair AER maintenance due to an increase of apoptosis [84] as observed in dactylaplasia mice. *Lef1* is a downstream mediator of Wnt / β -catenin signalling [reviewed in 119] and transcriptionally upregulated by activated β -catenin [120, 121]. *In situ* hybridisation of this gene

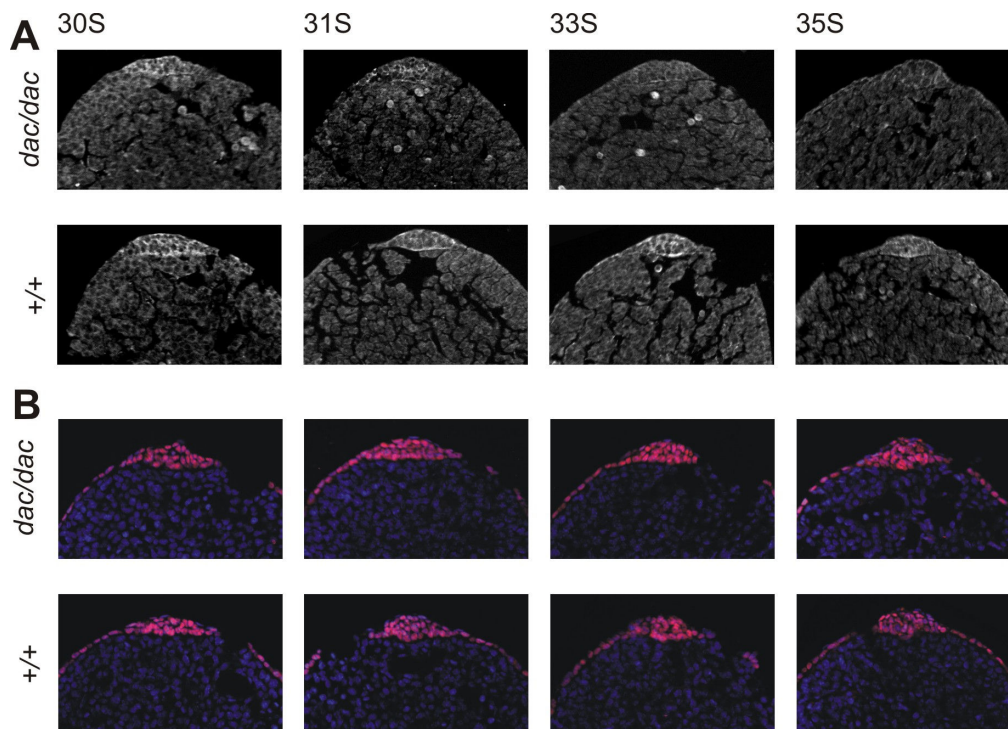


Figure 32: Immunohistochemistry of activated β -catenin and p63 on longitudinal sections of wild-type and mutant limbs.

(A) Activated β -catenin signal in wild-type and mutant limbs. The AER signal in *dac/dac* limbs is strongly decreased at stages 33S and 35S. (B) p63 signal in wild-type and mutant limbs. No difference in signal intensity between wild-type and mutants can be observed.

shows downregulation in *Dac* mutant limbs, which seems to be exceptionally strong in the AER. In concordance with these results, the level of activated β -catenin appears to be significantly reduced in the AER in *dac/dac* animals from stage 33S onwards (Figure 32A). Taken together, the results indicate that downregulation of canonical Wnt-signalling is the crucial factor in the pathogenesis of ectrodactyly in the dactylaplasia mouse.

However, the results generated by *in situ* hybridisation and immunohistochemistry are by no means quantitative and can only serve as strong indication. Furthermore, the causative misregulation leading to dactylaplasia and SHFM3 could not be identified. In order to overcome these flaws, AERs from mutant and wild-type animals were collected at stages 29S/30S and 33S/34S and their RNA was isolated to perform RNAseq. Unfortunately, new generation sequencing of these probes could not be conducted to date due technical problems.

5 Discussion

5.1 *ROR2* - the common genetic cause for two developmental disorders

There are numerous examples for mutations in a single gene causing different congenital disorders. In some cases, phenotypic outcomes depend on the functional domain of the protein at which the mutation occurs. Good examples for this phenomenon are mutations in p63, that can lead to seven syndromic and non-syndromic developmental disorders [reviewed in 85]. Mutations clustering at the C-terminal domains of the protein commonly lead to AEC syndrome (ankyloblepharon, ectodermal defects, cleft lip/palate; OMIM 106260), whereas mutations causing EEC syndrome (ectrodactyly, ectodermal dysplasia, cleft lip/palate; OMIM 129900) are mainly clustered in the N-terminal DNA-binding domain.

Alternatively, mutations in a gene may lead to its loss-of-function (LOF) or to gain-of-function (GOF) effects and hence to differential disorders commonly inherited in a recessive or dominant fashion, respectively. Mutations in *ROR2* are prominent examples for this mechanism, where LOF mutations lead to recessive Robinow syndrome (RRS) and GOF cause dominantly inherited brachydactyly type B1 (BDB1) [reviewed in 22].

5.1.1 Patients exhibiting intermediary phenotypes challenge the classical gain-of-function and loss-of function hypotheses

RRS and BDB1 are clinically distinct and clearly separable congenital malformations. However, a patient homozygous for the dominant BDB1 mutation p.R441fsX15 has been previously described exhibiting a severe form of brachydactyly in conjunction with RRS features. While the parents showed BDB1 with missing distal phalanges, this individual had almost complete absence of phalanges and nails in the hands and feet [18]. In addition he had mesomelic limb shortening and multiple vertebral malformations but no facial dysmorphism, thus displaying some but not all of the hallmarks of Robinow syndrome.

The novel nonsense mutation described in this thesis (p.R441X) terminates the *ROR2* polypeptide chain at the same position, but without adding additional amino acids. In contrast to the p.R441fsX15 mutation, both parents had normal hands and

feet. In concurrence with the recessive inheritance the patient showed features of Robinow syndrome including mild facial dysmorphism, vertebral malformations and mesomelic limb shortening. In addition a brachydactyly phenotype was seen that is somewhat similar to the p.R441fsX15 mutation in the feet (absence of toes 2 to 5), but the hands show a more complex picture with polydactyly, syndactyly and distal hypoplasia. Thus, the frame shift mutation causes a dominant BDB1 phenotype in which the homozygous state results in severe limb reduction defects and Robinow-like features, whereas the nonsense mutation is recessive, also with Robinow-like features and a limb phenotype that is intermediate between BDB1 and homozygosity for the BDB1 frame shift mutation.

These observations of intermediary phenotypes challenge the classical gain-of-function versus loss-of-function hypothesis for *ROR2* mutations. Especially the existence of a recessive mutation leading to a brachydactyly phenotype demonstrates the need for a more sophisticated model that accounts for these observations.

5.1.2 Trafficking defects of intracellular ROR2 mutants causes RRS

In BDB1 and RRS the position of the mutation is of importance, based on the finding that only truncating mutations immediately N-terminal or C-terminal of the tyrosine kinase domain lead to BDB1, whereas the RRS associated mutations are scattered throughout the molecule. In addition, the type of mutation appears to play a role, since all N-terminal BDB1 mutations reported so far are frame shift mutations. This is particularly accentuated by lack of dominant BDB1 in heterozygous carriers of the p.R441X mutation, whereas a frame shift at the very same position (p.R441fsX15) leads to dominant BDB1. In contrast, nonsense and frame shift mutations have been reported to be associated with the C-terminal BDB1 mutations. The situation is further complicated by the finding that nonsense mutations that are located within the tyrosine kinase domain, only 35 amino acids apart from the N-terminal and 29 amino acids apart from the C-terminal BDB1 mutations, result in RRS.

The explanation for the observed discrepancy in phenotypes may be altered cellular response to the mutated proteins. Receptors like ROR2 are generally processed through the endoplasmic reticulum (ER), folded and thereafter transported to the

Golgi apparatus where post-translational modification takes place. Finally, an elaborate trafficking system transports the receptor to the cell membrane. Mutated and misfolded protein is frequently recognised in the ER and subsequently retained and subjected to protein degradation. In general, mutations occurring in highly conserved parts of proteins and /or within complexly folded domains are more prone to misfolding (and thus degradation) than mutations found in regions displaying a looped structure. This may contribute to the low protein abundance and also minimal membrane trafficking observed for the intracellular RRS mutations p.Q502X and p.N620K.

Intriguingly, a FLAG-tagged version of the p.N620K mutant was recently employed by the lab of Roel Nusse to assess the role of the kinase activity of ROR2 in WNT5A signalling [122]. The asparagine residue at amino acid 620 is predicted to bind a magnesium ion within the catalytic cleft of tyrosine kinases with homology to ROR2 [123, 124], where its mutation may lead to impaired kinase activity. Functional analysis of the p.N620K-FLAG mutant revealed no changes in WNT5A signalling in contrast to wild-type ROR2, which the authors claimed to be due to the lack of kinase activity. However, the detailed analysis of the cellular distribution of p.N620K presented here indicates that the mutant protein is not able to reach the plasma membrane in sufficient amounts to influence cellular signalling. Although a FLAG-tag may alter the cellular response to overexpressed protein, it is highly unlikely to increase protein stability and membrane localisation in this context (see below). Hence, it is critical to thoroughly assess the subcellular localisation of mutant protein prior to biochemical analyses.

Nonsense-mediated mRNA decay (NMD) is widely accepted as a mechanism by which the cell inhibits the production of truncated proteins [125]. Van Bokhoven and colleagues [15] reported lower amplification efficiency of mRNA from the W720X allele suggesting that NMD is implicated in the pathogenesis of the RRS loss of function phenotype. Contrasting this, Ben-Shachar et al [126] recently demonstrated NMD for the extracellular truncating mutations, but specifically not the p.W720X mutation, again leaving the question open how this mutation causes RRS. The massive ER localisation with lacking membrane localization demonstrated argues that protein retention and degradation plays the major role in this mutant, drastically re-

ducing the amount of ROR2 protein. In the system employed in this thesis effects exerted by NMD are unlikely, since full-length cDNA was used for expression and protein amounts measured by Western blot were normalised to mRNA levels quantified by real-time PCR. Generally, the constructs were variably expressed but this did not correlate with the type of mutation, and can thus be attributed to intrinsic differences between the different cell lines.

5.1.3 A gradient of Ror2 protein stability and membrane localisation confers BDB1 or RRS phenotypes

The major difference between the p.R441X mutation and the mutations associated with full RRS appears to be their intracellular distribution. While all classical RRS mutants are almost completely retained in the ER, a significant fraction of the R441X protein is able to reach the cell membrane. Again, this is likely to be caused by less protein misfolding due to the mutation being located in a loop region vs. in a conserved domain. This may lead to an escape from intracellular recognition machinery and from protein retention and degradation. The p.R441X mutant has a similar intracellular distribution but a significantly lower total protein level than the p.R441fsX15 mutant. Thus, protein stability appears to be a major difference between those mutants ultimately leading to lesser membrane-associated R441X protein. How the 15 amino acid peptide resulting from the p.R441fsX15 mutation affect protein stability remains to be determined.

These results highlight that small alteration of the polypeptide chains of protein constructs may result in striking changes in protein stability and intracellular distribution. As a consequence, protein tags might influence protein stability and/or trafficking and ultimately distort quantification measurements and other procedures. Indeed, C-terminally FLAG-tagged ROR2-constructs showed an overall higher amount of intracellular retention than the untagged constructs (not shown). Similar observations demonstrating an influence of tags on protein distribution or stability have been reported before [127-129]. To further stabilise the experimental situation the Flp-in system was used, which allows single-copy integration and thus a moderate level of expression. In addition, cell lines were generated from transfected Cos-1 cells and also used for surface biotinylation. Although these assays showed the same

general tendency as the experiments performed in HEK293 FlpIn T-Rex cells, the results were more variable and difficult to interpret indicating that single- or low-copy expression systems are preferable. This has to be taken into account when designing studies analysing the consequence of human mutations on protein stability and/or trafficking. Thus, for proper analysis untagged constructs exactly copying human mutations that are expressed at low levels in a controlled system should be used.

The fact that FLAG-tagged ROR2 constructs in cell culture showed a higher degree of intracellular retention also offers a possible explanation for the recessive nature of the BDB1 phenotype observed in the *Ror2*^{W749X} mouse [32], which carries a FLAG-tag fused to the truncated *Ror2*. It is possible that the total truncated *Ror2* protein amount reaching the cell membrane is too low to cause a dominant phenotype but is high enough to cause a BDB1-like phenotype in the homozygous situation, thus reflecting the situation observed in the patient harbouring the p.R441X mutation.

The quantitative analysis of mutant ROR2 protein localised at the plasma membrane also provide a possible explanation for the different degrees of severity observed in BDB1 patients [18]. In general, mutations N-terminal of the tyrosine kinase domain cause a less severe phenotype than those located C-terminally. The results show that protein levels are comparable between BDB1 mutants, but the N-terminal mutations show a higher degree of intracellular retention than the C-terminal p.W749X mutation thus resulting in a higher degree of LOF (and hence less GOF protein at the membrane) and, consequently, a milder BDB1 phenotype.

In summary the study provides a quantitative biochemical explanation for the variable severity seen in BDB1 and for the appearance of overlapping features of BDB1 and RRS in single patients (Figure 33). In dominant BDB1 the appearance of RRS-like features is precluded by the presence of one wt allele. Truncating alleles found in both conditions appear to have dual functions: mutant proteins exhibit a partial loss of function due to intracellular retention and decreased protein stability, but can also act via a gain of function whenever they are able to reach the cell membrane. The results argue for a model in which the phenotypic outcome of the ROR2 mutations is determined by two threshold levels: the degree of degradation/retention determines the RRS phenotype, whereas the amount of truncated protein that reaches

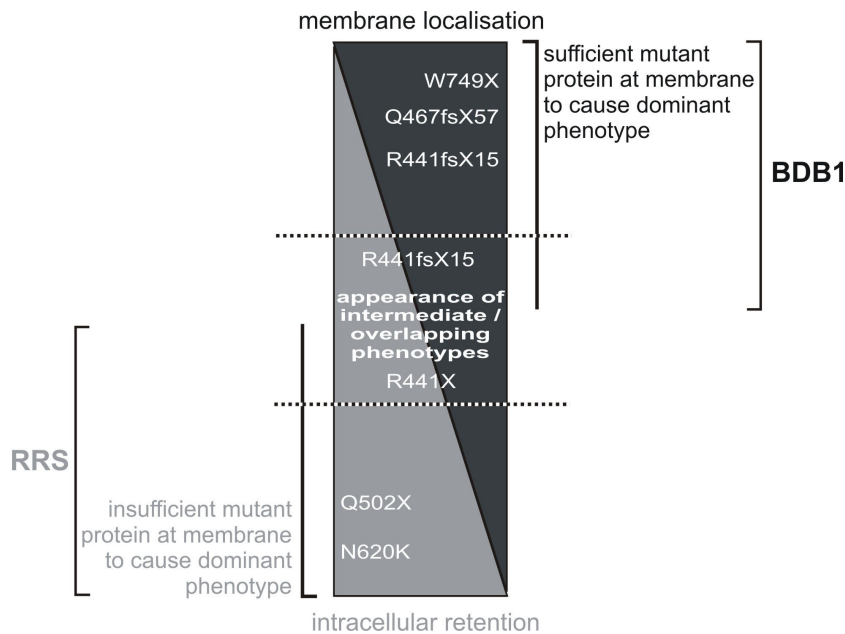


Figure 33: Schematic of the consequences of ROR2 intracellular distribution.

the cell membrane determines the severity of the BDB1 phenotype. A mixture of both effects can result in a balance of gain- and loss of function and, consequently, overlapping phenotypes.

5.1.4 Possible pathogenetic mechanisms leading to BDB1 and RRS

One interesting feature of truncated ROR2 proteins is that they seem to be able to fulfill a residual “normal” function, as both homozygous patients carrying the p.R441fsX15 and p.R441X mutations show some but not all features of RRS. In concordance the *Ror2*^{W749X/W749X} mouse mutant shows a less severe RRS-like phenotype than the *Ror2*^{-/-} mutant. This could be attributed to functions of ROR2 that are independent of the presence of the intracellular proline/serine/threonine-rich domain as it was demonstrated in *C. elegans* [130, 131]. A possible function of a membrane-tethered variant of ROR2 lacking the intracellular domains may be to serve as a co-receptor as it has been suggested for Wnt signalling in different contexts [132].

Interestingly, missense mutations in *WNT5A* were recently identified in patients with dominant Robinow syndrome (DRS), which potentially lead to a partial inactivation of the protein [21]. The strong phenotypic similarity of RRS and DRS indicate that a

common pathway of WNT5A and ROR2 is involved in the pathogenesis of Robinow syndrome. ROR2 has been shown to mediate WNT5A signals in planar cell polarity, convergent extension movements and cell migration [4, 8, 132-135]. Defects in this pathway may explain the various outgrowth defects observed in Robinow syndrome, which is exemplified in mammalian palate development. Here, Wnt5a mediates directed cell migration via Ror2 and the abolishment of this pathway in *Wnt5a*^{-/-} and *Ror2*^{-/-} mice results in cleft palates [7]. Also other phenotypes of *Wnt5a*^{-/-} and *Ror2*^{-/-} mice are highly similar: both display dwarfism, facial abnormalities, short limbs and respiratory dysfunction, however, these effects are generally milder in *Ror2*^{-/-} mice [reviewed in 136]. Interestingly, the severity of these phenotypes increases in *Ror1/Ror2* double knockout mice, indicating that *Ror1* and *Ror2* are partially redundant.

In contrast to *Ror2* or *Ror1/Ror2* double knockout mice, *Wnt5a*^{-/-} mice lack proximal and medial phalanges [137], indicating an additional function of this protein in these structures. Interestingly, recent research shows the upregulation of canonical Wnt-signalling and a subsequent decrease of Bmp-signalling in the phalanx forming region (PFR) to be responsible for the BDB phenotype in *Ror2*^{W749X/W749X} mice [138]. The PFR is a cell population with active Bmp-signalling just distal of the growing condensation, which determines digit elongation and phalange numbers by driving commitment of distal mesenchymal cells into cartilage condensation. *Ror2*^{W749X/W749X} mice display ectopic canonical Wnt-signalling in the PFR, which has been shown to act antagonistic to Bmp-signalling in the distal mesenchyme and cartilage condensations [139, 140]. Hence, excess canonical Wnt-signalling in this structure may inhibit PFR function and eventually cause the brachydactyly phenotype.

Wnt5a is known to be able to repress canonical Wnt-signalling either via Frizzled-receptors in a calcium dependent manner [141] or by interaction with Ror2 [5, 142], upon which it binds phosphorylated Dishevelled via its C-terminal proline/serine/threonine-rich domain thereby triggering inhibition of canonical Wnt-signalling [143]. A potential mechanism for the gain of function effect seen with truncated ROR2 in BDB1 patients may be envisaged as follows: truncated ROR2 binds to WNT5a, but is unable to repress canonical Wnt-signalling due to the lack of its C-terminal domain. Simultaneously, ROR2 withdraws WNT5A available for al-

ternative WNT5A/Ca²⁺ signalling, which may sufficiently rescue the lack of ROR2 in RRS patients or *Ror2*^{-/-} mice. Hence, it may be conceivable that the truncated ROR2 protein may act as a scavenger for WNT5A in BDB1 patients and *Ror2*^{W749X/W749X} mice.

5.2 The modifier of dactylaplasia - a second locus defines a disease phenotype

Phenotypic variability frequently observed in Mendelian disorders can be caused by alternative alleles as exemplified by the ROR2 project. However, environmental factors and modulating genetic background contribute significantly to penetrance, pleiotropy and severity of simple monogenetic traits. In humans, the environmental and genetic influences are difficult to dissect and only few modifier genes have been identified [reviewed in 144, 145]. The use of inbred laboratory mouse strains alleviates these difficulties due to the defined genetic background and constant environment they inhabit. A mutational phenotype often varies depending on the mouse strain the mutation is introduced to [146] and numerous modifiers could be mapped to specific chromosomal intervals. However, only few modulating genes have been identified so far and even fewer functional relationships to disease-causing alleles have been elucidated. Further research in this area will provide insight into developmental pathways and physiological processes regulating disease phenotype. In addition, insights may be gained into mechanisms by which organisms modulate biological processes to accommodate the adverse effects of genetic mutations. This knowledge will help genetic counsellors to predict the phenotypic outcome of specific mutations and may even drive advances in therapeutic strategies against late onset genetic diseases.

The modifier of dactylaplasia is a striking example for the modulating effect of genetic background. The presence of the dominant allele of *Mdac* completely suppresses the phenotype of dactylaplasia [93]. Therefore, the phenotype is clearly dependent on a single second locus, which renders a simple model to identify and characterise the modulating effect of the modifier locus. However, despite this genetic simplicity, its potential relevance to the reduced penetrance seen in human SHFM3, and the prolonged availability of these mice, the identity of *Mdac* has not been elucidated to date.

5.2.1 The molecular effect exerted by *Mdac* provides cues for candidate search

The initial 27 Mb interval harbouring *Mdac* contained several promising candidates which could potentially mediate the suppressive effect of *Mdac*. *Msx2*, for instance, is strongly expressed in the AER [147] and appears to be regulated by *Dlx5* [148, 149], a gene associated with ectrodactyly phenotype. Interestingly, *Ror2* is also found within this genomic region. Several cases of recessive Robinow syndrome in conjunction with ectrodactyly had been reported [23] and *Ror2* protein is expressed in the AER [personal communication]. These two exemplary candidates were thought to possibly act in a common molecular pathway responsible for the development of ectrodactyly and thereby altering the phenotypic outcome.

Most modifier genes identified so far can be placed in such a common regulatory pathway, albeit the mode of interaction can be quite different: a differentially expressed modifier may directly regulate the expression of the mutant protein [150, 151], could encode for functional redundancy in the same [152] or a parallel pathway [153], or may directly regulate the activity of the mutant protein [154]. In contrast, the modifying effect exerted by *Mdac* seems to be independent of the pathophysiological pathway. During the course of this thesis, Kano and colleagues have shown, that the MusD elements integrated in dactylaplasia mice are differentially methylated depending on which allele of *Mdac* is present [97]. Upon the presence of the dominant allele of *Mdac*, the excessive DNA methylation at the 5' LTR of the MusD element inhibits its activity as demonstrated by the lack of ectopic MusD transcripts in the AER [97, Figure 31]. It is conceivable, that the activity of the endogenous retrovirus may be a prerequisite to mediate the mutagenic effect leading to dactylaplasia.

The importance of the epigenetic state of mutagenous retroviral elements on phenotype expression has been studied on several alleles associated with insertions of the closely related intracisternal A particle (IAP) retrotransposon. For instance, several different IAPs drive ectopic *Agouty* expression (A^{hvy} , A^{iapy} , A^{vy}) resulting in highly variable phenotypes which largely correlate with LTR-methylation [155-158]. An IAP insertion in intron 6 of the *Axin* gene ($Axin^{Fu}$) causes truncated mRNA fused to IAP sequence [159] and the expression of aberrant transcripts and the corresponding

phenotype is again dependent on the methylational state of the transposon. The molecular cause for the observed differential methylation has not been elucidated, but it has been shown to be either maternally or paternally inherited in the aforementioned cases. This stands in strong contrast to the Mendelian inheritance of *Mdac*, which appears to regulate the methylational state of in a deterministic manner: the 5'LTR of the *Dac*-MusD transposon is either completely methylated (*Mdac*) or demethylated (*mdac*) and the phenotype of homozygous *dac/dac* animals is not variable. All animals with the permissive *mdac* allele show monodactyly, whereas all animals with the non-permissive *Mdac* allele are phenotypically normal.

In mammals, the mechanisms of transposon methylation are only starting to be deciphered [reviewed in 160]. DNA methylation of endogenous retroviruses is a major line of defence against these parasitic sequences and is targeted to transposons via RNA-dependent mechanisms. Transposons are particularly active in germ cells and preimplantation embryos. Correspondingly, a novel class of small RNAs, the PIWI-interacting RNA (piRNA), was recently discovered to target repetitive elements specifically in the germ-cell lines of drosophila, mice and several other model organisms [161, 162]. In preimplantation embryos and ES cells evidence is accumulating that repetitive elements are silenced via endogenous siRNAs [163-165] and both classes of small RNAs will be discussed later in detail.

The involvement of *Mdac* in differential methylation of the mutagenous MusD element leading to dactylaplasia generates new challenges for its identification. Many aspects of host defence mechanisms against retrotransposons are currently unclear. However, the unexpected effects of *Mdac* outside a pathophysiological pathway changes the prerequisites of the candidate search and may help to elucidate the identity of *Mdac*.

5.2.2 Minimising the genomic interval of *Mdac* is a step towards elucidating its identity

Classical genetic mapping has reduced the relevant genomic area to approximately 3 Mb containing 29 protein coding genes and numerous annotated features. None of these features renders a clear candidate for modulating AER physiology or DNA methylation of MusD. Due to the lack of knowledge of what could target MusD to

differential methylation, it is crucial to reduce the genetic information to a minimum to make further search feasible. To achieve this, the use of classical genetic mapping is very labour intensive and prone to produce no further results. The genetic interval comprises 0.02 cM according to the MGI genetic map and recombination events in this region are predicted to occur once in 5000 meioses.

In silico mapping uses the unique genealogy of inbred mouse strains which results in discrete haplotype structures due to ancient recombination events. This accumulation of recombination helps to dissect this low-recombination genomic interval into regions of common and divergent genetic ancestry and therefore facilitates fine mapping of *Mdac*. The occurrence of both dominant and recessive alleles of *Mdac* in several mouse strains strongly argues *Mdac* to be an ancient polymorphism in the genetic background of inbred mouse strains rather than an independent novel mutation. Hence it is most likely to find *Mdac* in a genomic interval, which shows distinct ancestry between mouse strains carrying the dominant and the recessive *mdac* allele.

Genome-wide association studies (GWAS) using SNP data and haplotype structures of inbred mouse strains successfully identified quantitative trait loci (QTL) and susceptibility genes for many genetic traits [representative references: 166, 167]. However, a recent paper suggests that GWA studies in mouse inbred strains can suffer a high rate of false-positive results and should be used in conjunction with classical linkage mapping in genetic crosses [168]. In the case of *Mdac*, the haplotype structures were used for fine mapping in a small defined genomic interval. Interestingly, the 3 Mb interval defined by classical linkage mapping includes the only loci owning the prerequisites to harbour *Mdac* within the originally defined 27 Mb interval according to rough analyses using the SNP comparison display (MPD, Jackson laboratory, data not shown). Although this is not a proof of principle, it strongly argues that *Mdac* truly is an ancient polymorphism and that haplotype analysis is applicable for fine mapping in this case.

In silico mapping has reduced the genomic area harbouring *Mdac* to approximately 1.5 Mb. Accordingly, the amount of annotated features are also significantly reduced. To date, it is common notion that small RNA pathways impose specificity to target DNA to methylation [reviewed in 169] and it is intriguing that a potentially

active MusD element is found within the highly polymorphic region of the 1.5 Mb interval. Approximately, 100 copies of MusD elements can be found in the C57Bl/6J reference genome, of which only 3 elements, including the MusD element in the *Mdac* interval, are transposition competent [118]. The presence of this particular MusD element perfectly segregates with the suppression of the dactylaplasia phenotype not only in the mouse strains used for *in silico* mapping, but also in all other strains tested. This segregation does not necessarily implicate that the MusD element is the modifier of dactylaplasia, since other features in the vicinity may segregate similarly due to the block-like structure of inheritance in classic inbred mouse strains. However, it confirms the prerequisites and a potential role for this particular MusD element in silencing the mutagenous MusD element otherwise leading to dactylaplasia is discussed below.

5.2.3 The modifier of dactylaplasia: another MusD element?

Transposon activity can be highly detrimental to their hosts, leading to germ cell mutations [reviewed in 170] and may cause cancerous transformations in the soma [171]. The integration within or nearby a gene can disrupt its coding sequence or perturb its expression pattern [158, 172] and examples in which new transposon insertions compromise genome integrity have been reported [171]. Due to these potentially harmful effects of new transposition events, several lines of defence against active retrotransposons have been evolved in eukaryotes which include the post-transcriptional targeting of their replication cycle [reviewed in 173]. Importantly, most transposable elements are additionally silenced by heterochromatin formation involving DNA methylation and histone modifications [160]. This raises the fundamental question of how an organism can distinguish between protein coding genes and repetitive sequences targeted for selective silencing. Recent work points to several small RNA-mediated mechanisms, whose sequence specificity helps to explain the observed silencing.

Retrotransposons are particularly active in germ cells and preimplantation embryos, which is likely due to the fact that the regulatory sequences of transposons are adapted to expression in these particular stages which allow transmission across generations [174]. Furthermore, host cells undergo two rounds of DNA demethyla-

tion during gametogenesis and after fertilisation [175]. Hence, defence mechanisms targeting transposons must be particularly active at these stages to ensure *de novo* methylation of these elements. Interestingly, the methylation level of IAP elements decreases only to 62% after fertilisation, staying considerably higher than the genome average [176]. This similarity to imprinted genes may explain the parental epigenetic inheritance seen for *Axin^{Fu}* and *Agouty* alleles. In the case of dactylaplasia, however, no parental epigenetic effect is notable, which indicates that the mutagenous MusD element is demethylated either during gametogenesis or after fertilisation. A tissue specific demethylation can be excluded since it seems to be an ubiquitous effect [97] and the ectopic expression of MusD in the AER is most likely driven by transcription factors specific for this tissue. Therefore, the *Mdac*-dependent differential methylation of the MusD element leading to the dactylaplasia phenotype is likely taking place in the germ cell or the preimplantation embryo.

Two major defence mechanisms have been recently described, which target repetitive sequences to *de novo* methylation during these stages. One is a specialised small RNA pathway in germ cells [177]. The 24-30 nucleotide long Piwi-interacting RNAs (piRNA) are mainly directed against transposon sequences and are generated and amplified via the so-called "ping-pong" model (Figure 34).

Importantly, murine generation of piRNAs seems to depend on the presence of actively transcribed transposons as input for the ping-pong cycle. In the model proposed by Aravin et al. [178], primary piRNAs derived from transposon transcripts associate with homologous proteins of the Piwi-family (Mili, Miwi2) and are used to screen antisense transcripts likely derived from so-called "piRNA clusters". Partially complementary, secondary piRNAs are subsequently generated which in turn target transposon mRNA transcripts and initiate DNA methylation of corresponding transposons by an yet unknown mechanism. In correspondence with this model, transcripts of the potentially active MusD element in the *Mdac* region may serve as template to prime the piRNA pathway to eventually silence the mutagenous MusD element. This pathway is thought to be germ cell specific, but recent work has suggested an additional role in preimplantation development [179]. In addition to the presence of maternally and/or paternally inherited piRNAs and maternally inherited

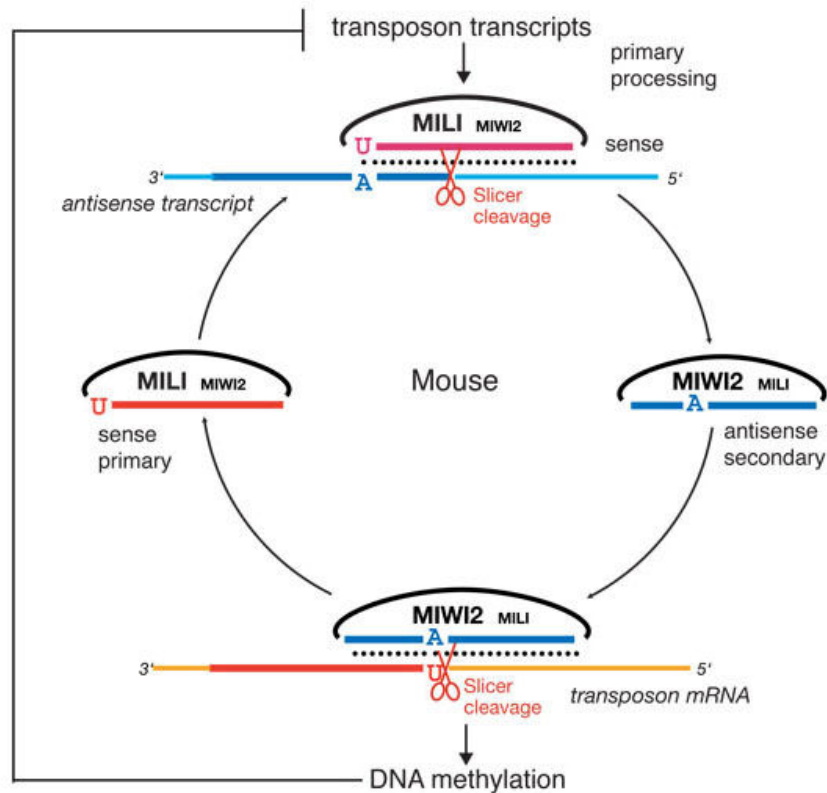


Figure 34: Ping-Pong amplification of piRNA in the mouse. Description see text. Adapted from [178].

associated proteins (Mili, Miwi2), some piRNAs are transiently upregulated in the zygote and transient *Mili* expression could be detected at the 8-cell stage.

In addition to the piRNA pathway, endogenous siRNAs seem to play an equally important role in silencing transposons. This is exemplified by the failures of gametogenesis in mice carrying loss of function of either the *Piwi*-family genes [180-182] or *Dicer* [183, 184], a gene associated with siRNA/miRNA production. The generation of naturally occurring double stranded RNAs necessary for siRNA production is not well understood. However, it has been hypothesised that bidirectional transcription in *cis* via an external or cryptic antisense promoter within the transposon may lead to dsRNA. Furthermore, the generation of dsRNA in *trans* may be possible, in which transcripts from active transposons hybridise to antisense transposon fragments transcribed from piRNA clusters [185, 186]. siRNAs derived from trans-

posons are abundantly present in germ cell and preimplantation embryos [179, 185-187] and are thought to silence the corresponding elements on the DNA level via the RNA-induced silencing complex (RITS) [reviewed in 169]. Similarly to the situation described above, the potentially active MusD element in the *Mdac* region may trigger the production of siRNAs to silence the mutagenous MusD element in *trans*.

Despite this potential relevance of an active MusD element in the *Mdac* region, several questions remain unanswered. Kano and colleagues [97] have suggested specific methylation of the mutagenous MusD element, since DNA methylation on a single control MusD element is not influenced by the presence of the *Mdac* allele. The involvement of *Mdac* in a general, small-RNA mediated defence mechanism, however, would suggest global changes in the methylation status of MusD elements. Several possible scenarios could explain this flaw. The control element may escape demethylation during preimplantation development similar to the majority (62%) of IAP elements [176], leaving global changes to the methylation status of the previously demethylated elements undetected. In addition, retrotransposons in the genomic background have frequently acquired numerous mutations. Due to the sequence specificity of piRNAs or siRNAs, small RNAs derived from the MusD element in the *Mdac* region may only be able to affect a subset of closely related MusD elements, which may not include the control element. Alternatively, a yet unidentified mechanism may exist, which is able to target single specific transposable elements to DNA methylation and may or may not be dependent on an active MusD copy in the *Mdac* region. Lastly, *Mdac* may impose heterochromatin formation at the *Dac* locus independent of the mutagenous MusD insertion, in which the *mdac*-dependent MusD activity is a unspecific byproduct.

Interestingly, the obviously active mutagenous MusD element is not able to silence itself. One would expect that this MusD is actively transcribed during gametogenesis and preimplantation development, hence supplying the small RNA defence systems with perfect input sequence. Possibly, a position effect at the integration site may inhibit the expression at these developmental stages. It cannot be excluded, however, that the differential methylation of the mutagenous MusD element may be completely independent on the activity of any other MusD element.

Despite the questions remaining, the MusD element within the *Mdac* region may well be the modifying feature. It is intriguing, that one of only three active MusD elements within the C57Bl/6J genome resides in the *Mdac* genomic interval. Small RNA defence mechanisms depend on transcribed transposon sequence and are the only means known to date, by which a host cell can specifically target transposon sequences to DNA methylation and histone modifications.

Several experiments could elucidate the potential relevance of the MusD element in the *Mdac* interval. First, dynamics of the methylation status of the mutagenous MusD element should be determined in germ cells and preimplantation embryos. Cultured ES-cells of *Dac*-mutant mice could be transfected with the potential modifying MusD element, in order to test its capability to inflict *de novo* methylation upon the mutagenous MusD element. Finally, *mdac/mdac* mice transgenic for the MusD element within the *Mdac* region should be generated and tested for their potential to suppress the dactylaplasia phenotype.

Independent on the identity of the modifier of dactylaplasia, its characterisation will most likely shed light on fundamental cellular processes. The influence of a single genomic locus on the epigenetic state of another is highly intriguing and future research should be conducted to elucidate the mechanisms behind this modifying effect on a genetic disease.

5.3 From phenotype to genotype of Dactylaplasia mice

In comparison to the modifier of dactylaplasia, the molecular causes leading to the phenotype of dactylaplasia mice had received higher attention so far. The potential relevance to a human congenital disorder, split hand and foot malformation 3 (SHFM3), has led to an increased interest in the molecular mechanisms causing the disease. However, research conducted prior to this thesis had failed to identify a mis-regulated pathway leading to AER degradation and contradictive results concerning apoptosis in this process had been published. In the following sections, advances made in this topic are being discussed. In addition, the central question on which gene / genes are deregulated to cause the common disease phenotype in mice and humans will be examined.

5.3.1 Many roads to destruction: deregulation of Wnt-signalling may eventually lead to Dactylaplasia

Defects in the function or maintenance of the apical ectodermal ridge (AER) are common themes in the pathogenesis of ectrodactylies, which accentuates its role as main signalling centre during limb development. The AER owns a highly dynamic and transient morphology [reviewed in 64], that is most likely adopted to focalise a higher number of cells at the distal tip of the limb to produce a sufficient amount of growth factors necessary for signalling [67]. In this structure, the number of cells needs to be tightly regulated. The concomitant presence of cell proliferation and apoptosis may account for this need. In Dactylaplasia mice, this regulation is obviously severely disturbed. The excess amount of apoptosis observed in mutant AERs leads to a severe reduction growth factor-producing cells and eventually to the complete regression of the median portion of the AER. Moreover, the knowledge that increased cell death rather than a lack of proliferation is the underlying cause may help to identify the deregulated signalling pathway involved in this process.

Interestingly, pathologic regression of the AER has been described to occur via two distinct mechanisms. Several mouse mutants solely display increased apoptosis similar to *dac/dac* mice, whereas others show alterations in AER morphology which first appears flattened and eventually regresses. An example for the latter is the AER-specific knock-out of *Fgfr2*, which results in the loss of distal skeletal elements [188]. A similar flattening and regression of the median AER has been observed in *Dlx5/Dlx6* double-mutant mice [88, 91] and in *p63^{EEC}* mutant mice [88], which results in a phenocopy of human SHFM. Intriguingly, AER flattening is a normal physiological event at the end of the lifespan of the AER at stage E13.0 [189], that seems to be under control of BMP-signalling [83]. P63, in turn, appears to be a ectoderm-specific direct target of BMP-signalling at least in the zebrafish [190]. Hence the possibility exists, that the p63-Dlx5/6 pathway protects the AER from adverse effects of BMP-signalling, preventing premature regression of the AER via a negative feedback loop.

In contrast, dactylaplasia mutant mice do not display a flattened AER morphology prior to degradation. At stage E11.0, only few AER cells are remaining, which still have an elevated appearance. Hence, it seems that the *Dac* mutation exerts an effect

independent of the p63-Dlx5/6 pathway, which eventually leads to the same phenotypic outcome. Interestingly, the increased apoptosis in *Dac*-mutant mice is highly reminiscent to mice with disrupted canonical Wnt-signalling in the AER. If β -catenin is conditionally ablated in the AER using the *Msx2Cre* transgene, the AER is degraded due to increased apoptosis in this tissue [84]. Degradation initiates at stage E9.75 in the median portion of the AER and spreads to the anterior and posterior margins, until the AER completely vanishes at stage E10.75. This pattern may indicate, that the central part of the AER is especially sensitive to disruptions in canonical Wnt-signalling. Later onset and incomplete degradation in *Dac* mutant mice may explain the phenotypic differences observed: the forelimbs of β -catenin^{n/c}; *Msx2Cre* mutants are truncated at the end of the humerus. The apparent downregulation of *Lef1* and the reduced levels of activated β -catenin in *Dac* mutant AERs point to a disruption of Wnt-signalling in this tissue, which may also explain the decreased amount of *Fgf8* transcripts in the mutant AER. It had been shown that canonical Wnt-signalling in the limb ectoderm is necessary and sufficient to drive *Fgf8* expression during AER induction [84, 191-194]. Accordingly, during AER maintenance, *Fgf8* expression is abolished in β -catenin^{n/c}; *Msx2Cre* mutants prior to degradation [84].

It has been frequently hypothesised that a downregulation of *Fgf8* expression is causative for the Dactylaplasia phenotype. This gene lies in close proximity to the genomic interval duplicated in human SHFM3 and downstream of the MusD insertions leading to Dactylaplasia. However, Fgf-signalling is apparently not necessary for AER maintenance. The conditional ablation of *Fgf8* and *Fgf4* results in a morphological normal AER [75]. In addition, *Fgf8/Msx2Cre* mutant mice display a relatively mild phenotype, only lacking the second digit [72]. It is therefore unlikely, that a downregulation of *Fgf8* alone is sufficient to cause the Dactylaplasia phenotype.

5.3.2 Dactylaplasia and human SHFM3 - a common genetic misregulation?

Dactylaplasia mice have commonly been acknowledged to be a model for human SHFM3 due to highly similar phenotypes and the position of *Dac* mutations in the syntenic region of the duplications in SHFM3. However, it is difficult to envisage

how a transposon insertion and a duplication may have similar effects. The molecular consequences of both types of mutations are variable and often complex. This is further complicated by the fact that transposon insertions leading to Dactylaplasia are the only reported *de novo* mutagenous MusD insertions to date [170], and hence no experience on the mutational mechanisms of this type of retrotransposon exists. It is therefore not surprising, that little is known about the molecular causes leading to dactylaplasia and SHFM3 to date.

Apart from *Fgf8*, the F-box protein *Fbxw4* has been frequently suggested as candidate gene for dactylaplasia. The distal breakpoints of the human duplication always reside within this gene, resulting in a disrupted extra copy. In mice, the *Dac*^{2J} insertion causes an abnormally large *Fbxw4*-transcript [95], which most likely contains MusD sequence. This effect has been frequently described for IAP element insertions within introns [reviewed in 170]. The *Dac*^{1J} insertion, however, did not result in abnormal *Fbxw4* transcription with respect to size or abundance in several adult tissues [95]. Upstream insertions of IAP elements in antisense direction have been reported to constitute the 5'end of adjacent transcripts [157, 170] or to reduce transcript levels, which is most likely due to a separation of the promoter from upstream *cis*-regulatory elements [195]. Such effects might well be tissue-specific, leaving a possible mutagenic effect of *Dac*^{1J} on *Fbxw4* transcripts undetected.

As already mentioned, *Fbxw4* is a member of the F-box gene family, which encodes subunits of ubiquitin ligases that present specific protein targets to ubiquitin-conjugating enzymes to ensure their proteolytic destruction [196 and references therein]. It consists of a N-terminal F-box domain, which mediates protein binding to the ubiquitin ligase, and a C-terminal WD40 repeat that is necessary for interaction with specific protein targets. A truncation in this WD40 repeat has been suggested to explain the dominant negative nature of the *Dac*^{2J} mutation [95], resulting in a protein with intact F-box but which cannot bind its target. Similarly, *Dac*^{1J} may cause defects at the N-terminus of *Fbxw4*, disrupting the F-box and, hence, resulting in a protein that may still be able to bind to its target, but fails to integrate in the ubiquitin ligase complex.

Specific targets of *Fbxw4* are currently unknown. However, a second F-box protein is located within the duplicated region in SHFM3, for which several targets have

been elucidated. *Btrc*, or otherwise known as *Fbxw1* or β -TrCP, has been shown to participate in the regulation of several signal transduction pathways, transcriptional regulation and cell cycle control [197-201]. Most interestingly, specific isoforms of *Btrc* are involved in the degradation of β -catenin [202, 203]. *Btrc* isoforms are differentially expressed in several tissues and ectopic expression or overexpression of β -catenin-specific splice variants in the AER could explain the reduction of canonical Wnt-signalling in *Dac*-mutant AERs. Such a deregulation *Btrc* may be caused by a dosage effect due to the duplication or the separation of this gene from tissue- and/or isoform-specific enhancer/repressor elements.

Unfortunately, both *Fbxw4* and *Btrc* are expressed at low levels in the AER, rendering analyses of potentially tissue-specific transcript-alterations very difficult. In addition, potential long-range regulatory effects of the *MusD* insertion or human duplication may exist. A microduplication at the long-range *Shh* enhancer (ZRS), for instance, is associated with the human triphalangeal thumb and polysyndactyly syndrome [204]. This enhancer is an extreme example of long-range transcriptional regulation as it is positioned approximately 1 Mb upstream of *Shh* coding sequence [205]. However, even transcriptional regulation in *trans* between non-homologous chromosomes in mammals has been reported [206].

This multitude of possible genetic consequences due to mutations in *Dactylaplasia* and *SHFM3* requires a global approach to elucidate the underlying mechanism. The use of next generation sequencing to determine the transcriptome of wild-type and mutant AERs will provide insight to the misregulation caused by these mutations. Precise staging of the phenotype onset and subsequent collection of appropriate probes may help to identify the initial misregulation as well as the pathways involved in the disruption of the AER. As soon as these data are available, follow-up experiments can be planned to eventually prove consequences of the *Dactylaplasia* mutation. Revealing the AER transcriptome may, furthermore, trigger future research of this developmental structure, which owns high relevance in limb regenerative processes. Hence, these data are much anticipated, but technical problems impeded processing and no inappropriate risk wants to be taken with these precious samples.

6 Summary

6.1 Summary in English

Phenotypic variability in Mendelian disorders is caused by the influence of environmental factors, diverse genetic background or differences in the underlying mutation. In most cases, these influences are complex and difficult to dissect, leaving the molecular causes for variation often obscure. This work should help to explain the phenotypic variability observed in two monogenic disorders involving skeletal abnormalities. First, the question on how mutations in a single gene, *ROR2*, can give rise to two distinct developmental disorders with variable severity is examined on a molecular level. Secondly, the effect of genetic background on phenotypic outcome is analysed in the case of the dactylaplasia mouse.

Dependent on their position and nature, mutations in *ROR2* may either lead to the dominantly inherited brachydactyly type B1 (BDB1) or the recessive Robinow syndrome (RRS), each characterised by distinct phenotypic features. A homozygous patient carrying a novel nonsense mutation in *ROR2* (c.1324C>T; p.R441X) reported here, however, exhibits features of RRS in conjunction with severe recessive brachydactyly. Membrane protein fraction quantification of this mutation together with wild-type, BDB1 and RRS mutant protein revealed a gradient of distribution and stability correlating with the clinical phenotypes: RRS mutant protein was retained intracellularly, whereas BDB1 mutant protein localised at the plasma membrane in varying amounts, correlating with the severity of the BDB1. The novel mutation showed an intermediate behaviour. In heterozygous carriers of the p.R441X mutation the amount of mutant protein at the plasma membrane is insufficient to cause dominant BDB1, however, it leads to severe recessive brachydactyly in conjunction with RRS features in the homozygous state. This gradual model was confirmed by crossing mouse models for RRS and BDB1, yielding double heterozygous animals that exhibited an intermediate phenotype.

In the case of *dactylaplasia* (*dac*) mice, the model for human split hand and foot malformation 3 (SHFM3), the phenotype is determined by a second locus present in the genetic background of inbred laboratory mouse strains. The so-called *modifier of*

dactylaplasia (*Mdac*) completely suppresses the ectrodactyly phenotype of *dac*, if its dominant allele is present. In order to determine the identity of *Mdac*, the interval known to harbour this genetic feature was reduced to approximately 3 Mb by classical genetic linkage analysis and further narrowed to ~1.5 Mb by *in silico* mapping. No protein coding gene within this genomic region could be identified as good candidate for *Mdac*.

The phenotype of the dactylaplasia mouse is caused by the insertion of a MusD element, which was shown to be differentially methylated depending on which *Mdac* allele is present. Interestingly, another putatively active MusD element within the *Mdac* interval was exclusively found in mouse strains suppressing the dactylaplasia phenotype, but not in those permissive for the phenotype. Its presence could explain the hypermethylation seen in the MusD element otherwise leading to the phenotype. The possibility exists, that the specific MusD element on chromosome 13 may act as an RNA template, which eventually silences the MusD element leading to dactylaplasia via an RNA-mediated defence mechanism.

To date, the molecular consequences of the mutations leading to dactylaplasia and SHFM3 are unknown. Thorough analyses conducted during this thesis confirmed that increased apoptosis leads to the loss of the median AER and subsequently the ectrodactyly phenotype. This effect is most likely due to a reduction in canonical Wnt-signalling, as indicated by the downregulation of *Lef1* and the reduced amount of activated β -catenin observed in the AER. However, the direct molecular cause for this deregulation could not be identified so far.

In summary, several important steps have been made towards the understanding of phenotypic variability in monogenic disorders caused by *ROR2* and *dactylaplasia* mutations. A gradual model for *ROR2* mutations is proposed, which explains not only the occurrence and clinical variability of two distinct phenotypes, but also the phenomenon of intermediary phenotypes of otherwise clearly separable congenital disorders. Narrowing of the genomic interval harbouring *Mdac* has led to the identification of the first promising candidate, a MusD element, that may modify the phenotype of *dactylaplasia*. In addition, the experiments underway, deciphering the AER transcriptome of wild-type and *Dac*-mutant animals, may eventually shed light on the common misregulation in dactylaplasia and SHFM3.

6.2 Deutsche Zusammenfassung

Phänotypische Variabilität in Mendelschen Erkrankungen wird durch den Einfluss von Umweltfaktoren, genetischem Hintergrund oder Unterschieden in der zugrunde liegenden Mutation verursacht. In den meisten Fällen sind diese Einflüsse sehr komplex und schwierig zu analysieren, so dass die molekulare Ursache der Variabilität häufig ungewiss bleibt. Diese Arbeit soll nun helfen, die phänotypische Variabilität zweier monogenetischer Erkrankungen mit Skelettfehlbildungen zu klären. Zuerst wird die Frage untersucht, wie Mutationen in einem einzigen Gen, *ROR2*, zu zwei unterschiedlichen Entwicklungsstörungen mit variabler Ausprägung führen kann. Danach wird der Einfluss des genetischen Hintergrundes auf den Phänotyp der Daktylaplasie-Maus analysiert.

Abhängig von Position und Art können Mutationen in *ROR2* entweder zu dominant vererbten Brachydaktylie Typ B1 oder rezessiven Robinow Syndrom führen, die normalerweise durch unterschiedliche Ausprägungsmerkmale klar voneinander unterschieden werden können. Allerdings zeigt ein homozygoter Patient mit einer neuen Nonsense-Mutation in *ROR2* (c.1324C>T; p.R441X) einige Merkmale des RRS zusammen mit einer schweren, rezessiven Brachydaktylie. Quantifizierung des Membran-gebundenen Anteils von diesem mutantern Protein zusammen mit Wildtyp, BDB1- und RRS-mutantern *ROR2* ergab einen Gradienten in Verteilung und Stabilität, die mit den klinischen Phänotypen korrelierte: RRS-mutantes Protein wurde intrazellulär zurückgehalten, wohingegen BDB1-mutantes Protein in unterschiedlichen Mengen an der Plasmamembran lokalisiert war, die wiederum mit dem Schweregrad der Brachydaktylie korrelierten. Die neue Mutation zeigte ein intermediäres Verhalten, wobei im heterozygoten Zustand die Menge des mutanten Protein an der Zellmembran nicht ausreicht, um eine dominante BDB1 hervorzurufen. Im homozygoten Zustand führt sie jedoch zu einer schweren Brachydaktylie mit RRS Merkmalen. Dieses graduelle Modell wurde durch Kreuzungen der Mausmodelle für BDB1 und RRS bestätigt, wobei doppelt heterozygote Tiere ebenfalls einen intermediären Phänotyp aufwiesen.

Im Falle der Daktylaplasie-Maus (*Dac*), dem Modell der humanen Spalthand und -Fuß Malformation 3 (SHFM3), wird der Phänotyp durch einen zweiten Locus im

genetischen Hintergrund von Inzuchtmausstämmen determiniert. Der sogenannte "modifier of dactylaplasia" (*Mdac*) unterdrückt den Ektrodakylie-Phänotyp der *Dac*-Mutation vollständig, falls das dominante Allele vorliegt. Um die Identität von *Mdac* zu klären, wurde das genetische Intervall, welches bekannt ist *Mdac* zu enthalten, durch klassische Kopplungsanalyse auf etwa 3 Mb eingeschränkt und zusätzlich durch *in silico*-Kartierung auf ~1.5 Mb reduziert. Allerdings konnte kein Proteinkodierendes Gen als guter *Mdac*-Kandidat identifiziert werden.

Der Phänotyp der Daktylaplasie-Maus wird durch die Insertion eines MusD-Elements hervorgerufen, welches in Abhängigkeit des vorliegenden *Mdac*-Alleles differentiell methyliert wird. Interessanterweise liegt ein weiteres, möglicherweise aktives MusD-Element innerhalb des *Mdac*-Intervalls ausschließlich bei *Dac*-supprimierenden Mausstämmen vor. Dessen Anwesenheit könnte die Hypermethylierung des MusD-Elements erklären, welches andernfalls für die Ausprägung des Phänotyps verantwortlich ist. Es besteht die Möglichkeit, dass dieses spezifische MusD-Element auf Chromosom 13 als RNA-Vorlage dient, welche das Daktylaplasie-auslösende MusD-Element über einen RNA-vermittelten Abwehrmechanismus inhibiert.

Bis heute sind die molekularen Mechanismen der Mutationen, die Daktylaplasie und SHFM3 verursachen, ungeklärt. Die sorgfältigen Analysen in dieser Arbeit bestätigen die Annahme, dass vermehrte Apoptose zu dem Verlust der mittleren AER und somit zu dem Ektrodakylie-Phänotyp führt. Dieses wird vermutlich durch eine Reduzierung des kanonischen Wnt-Signalwegs verursacht, welche durch die verringerten Mengen von *Lef1*-Transkripten und β -Catenin Proteins angedeutet wird. Allerdings konnte die direkte molekulare Ursache für diese Misregulation bislang nicht geklärt werden.

Zusammengefasst wurden mehrere wichtige Schritte getan, die zum Verstehen der phänotypischen Variabilität in den durch *ROR2* und *Dac*-Mutationen verursachten Erkrankungen beitragen. Ein graduelles Modell für *ROR2*-Mutationen wurde aufgestellt, welches nicht nur das Vorkommen und die phänotypische Variabilität der zwei unterschiedlichen Erkrankungen beschreibt, sondern auch das Phänomen der intermediären Phänotypen erklären kann. Die genetische Eingrenzung des *Mdac*-Intervalls führte zu der Bestimmung des ersten vielversprechenden Kandidaten: ein

MusD-Element, welches möglicherweise den Daktylplasie-Phänotyp modifizieren kann. Zusätzlich sind Experimente im Gange, die das AER-Transkriptom von Wildtyp- und mutanten Tieren entschlüsseln werden und somit hoffentlich die kausale Misregulation in Daktylplasie und SHFM3 offen legen werden.

7 Literature

1. Connor, J.M., Ferguson-Smith, M. A., *Essential Medical Genetics*. 1987, Oxford: Blackwell Scientific Publications.
2. Robinson, D.R., Y.M. Wu, and S.F. Lin, *The protein tyrosine kinase family of the human genome*. *Oncogene*, 2000. **19**(49): p. 5548-57.
3. Masiakowski, P. and R.D. Carroll, *A novel family of cell surface receptors with tyrosine kinase-like domain*. *J Biol Chem*, 1992. **267**(36): p. 26181-90.
4. Oishi, I., et al., *The receptor tyrosine kinase Ror2 is involved in non-canonical Wnt5a/JNK signalling pathway*. *Genes Cells*, 2003. **8**(7): p. 645-54.
5. Mikels, A.J. and R. Nusse, *Purified Wnt5a protein activates or inhibits beta-catenin-TCF signaling depending on receptor context*. *PLoS Biol*, 2006. **4**(4): p. e115.
6. Liu, Y., et al., *Wnt5a induces homodimerization and activation of Ror2 receptor tyrosine kinase*. *J Cell Biochem*, 2008. **105**(2): p. 497-502.
7. He, F., et al., *Wnt5a regulates directional cell migration and cell proliferation via Ror2-mediated noncanonical pathway in mammalian palate development*. *Development*, 2008. **135**(23): p. 3871-9.
8. Schambony, A. and D. Wedlich, *Wnt-5A/Ror2 regulate expression of XPAPC through an alternative noncanonical signaling pathway*. *Dev Cell*, 2007. **12**(5): p. 779-92.
9. Takeuchi, S., et al., *Mouse Ror2 receptor tyrosine kinase is required for the heart development and limb formation*. *Genes Cells*, 2000. **5**(1): p. 71-8.
10. DeChiara, T.M., et al., *Ror2, encoding a receptor-like tyrosine kinase, is required for cartilage and growth plate development*. *Nat Genet*, 2000. **24**(3): p. 271-4.
11. Enomoto, M., et al., *Autonomous regulation of osteosarcoma cell invasiveness by Wnt5a/Ror2 signaling*. *Oncogene*, 2009. **28**(36): p. 3197-208.
12. O'Connell, M.P., et al., *The orphan tyrosine kinase receptor, ROR2, mediates Wnt5A signaling in metastatic melanoma*. *Oncogene*, 2010. **29**(1): p. 34-44.
13. Wright, T.M., et al., *Ror2, a developmentally regulated kinase, promotes tumor growth potential in renal cell carcinoma*. *Oncogene*, 2009. **28**(27): p. 2513-23.
14. Kobayashi, M., et al., *Ror2 expression in squamous cell carcinoma and epithelial dysplasia of the oral cavity*. *Oral Surg Oral Med Oral Pathol Oral Radiol Endod*, 2009. **107**(3): p. 398-406.
15. van Bokhoven, H., et al., *Mutation of the gene encoding the ROR2 tyrosine kinase causes autosomal recessive Robinow syndrome*. *Nat Genet*, 2000. **25**(4): p. 423-6.
16. Afzal, A.R., et al., *Recessive Robinow syndrome, allelic to dominant brachydactyly type B, is caused by mutation of ROR2*. *Nat Genet*, 2000. **25**(4): p. 419-22.
17. Oldridge, M., et al., *Dominant mutations in ROR2, encoding an orphan receptor tyrosine kinase, cause brachydactyly type B*. *Nat Genet*, 2000. **24**(3): p. 275-8.
18. Schwabe, G.C., et al., *Distinct mutations in the receptor tyrosine kinase gene ROR2 cause brachydactyly type B*. *Am J Hum Genet*, 2000. **67**(4): p. 822-31.
19. Bell, J., *On brachydactyly and symphalangism*. In: *The treasury of human inheritance*. Vol. 5. 1951, Cambridge: Cambridge University Press.

20. Mazzeu, J.F., et al., *Clinical characterization of autosomal dominant and recessive variants of Robinow syndrome*. Am J Med Genet A, 2007. **143**(4): p. 320-5.
21. Person, A.D., et al., *WNT5A mutations in patients with autosomal dominant Robinow syndrome*. Dev Dyn, 2010. **239**(1): p. 327-37.
22. Afzal, A.R. and S. Jeffery, *One gene, two phenotypes: ROR2 mutations in autosomal recessive Robinow syndrome and autosomal dominant brachydactyly type B*. Hum Mutat, 2003. **22**(1): p. 1-11.
23. Balci, S., et al., *Robinow syndrome: with special emphasis on dermatoglyphics and hand malformations (split hand)*. Clin Dysmorphol, 1993. **2**(3): p. 199-207.
24. Oldridge, M., et al., *Brachydactyly type B: linkage to chromosome 9q22 and evidence for genetic heterogeneity*. Am J Hum Genet, 1999. **64**(2): p. 578-85.
25. Brunetti-Pierri, N., et al., *Robinow syndrome: phenotypic variability in a family with a novel intragenic ROR2 mutation*. Am J Med Genet A, 2008. **146A**(21): p. 2804-9.
26. Chen, Y., et al., *ER-associated protein degradation is a common mechanism underpinning numerous monogenic diseases including Robinow syndrome*. Hum Mol Genet, 2005. **14**(17): p. 2559-69.
27. Tufan, F., et al., *Clinical and molecular characterization of two adults with autosomal recessive Robinow syndrome*. Am J Med Genet A, 2005. **136**(2): p. 185-9.
28. Ali, B.R., et al., *Novel Robinow syndrome causing mutations in the proximal region of the frizzled-like domain of ROR2 are retained in the endoplasmic reticulum*. Hum Genet, 2007. **122**(3-4): p. 389-95.
29. Bacchelli, C., et al., *ROR2 is mutated in hereditary brachydactyly with nail dysplasia, but not in Sorsby syndrome*. Clin Genet, 2003. **64**(3): p. 263-5.
30. Lv, D., et al., *A novel single-base deletion in ROR2 causes atypical brachydactyly type B1 with cutaneous syndactyly in a large Chinese family*. J Hum Genet, 2009. **54**(7): p. 422-5.
31. Schwabe, G.C., et al., *Ror2 knockout mouse as a model for the developmental pathology of autosomal recessive Robinow syndrome*. Dev Dyn, 2004. **229**(2): p. 400-10.
32. Raz, R., et al., *The mutation ROR2W749X, linked to human BDB, is a recessive mutation in the mouse, causing brachydactyly, mediating patterning of joints and modeling recessive Robinow syndrome*. Development, 2008. **135**(9): p. 1713-23.
33. Niedrist, D., I.W. Lurie, and A. Schinzel, *4q32-q35 and 6q16-q22 are valuable candidate regions for split hand/foot malformation*. Eur J Hum Genet, 2009. **17**(8): p. 1086-91.
34. Duijf, P.H., H. van Bokhoven, and H.G. Brunner, *Pathogenesis of split-hand/split-foot malformation*. Hum Mol Genet, 2003. **12 Spec No 1**: p. R51-60.
35. Gul, D. and C. Oktenli, *Evidence for autosomal recessive inheritance of split hand/split foot malformation: a report of nine cases*. Clin Dysmorphol, 2002. **11**(3): p. 183-6.
36. Ahmad, M., et al., *X-chromosomally inherited split-hand/split-foot anomaly in a Pakistani kindred*. Hum Genet, 1987. **75**(2): p. 169-73.
37. Kano, H., et al., *Genomic rearrangement at 10q24 in non-syndromic split-hand/split-foot malformation*. Hum Genet, 2005. **118**(3-4): p. 477-83.

38. Gurnett, C.A., et al., *Evidence for an additional locus for split hand/foot malformation in chromosome region 8q21.11-q22.3*. Am J Med Genet A, 2006. **140**(16): p. 1744-8.
39. Ugur, S.A. and A. Tolun, *Homozygous WNT10b mutation and complex inheritance in Split-Hand/Foot Malformation*. Hum Mol Genet, 2008. **17**(17): p. 2644-53.
40. Celli, J., et al., *Heterozygous germline mutations in the p53 homolog p63 are the cause of EEC syndrome*. Cell, 1999. **99**(2): p. 143-53.
41. Ianakiev, P., et al., *Split-hand/split-foot malformation is caused by mutations in the p63 gene on 3q27*. Am J Hum Genet, 2000. **67**(1): p. 59-66.
42. van Bokhoven, H., et al., *p63 Gene mutations in eec syndrome, limb-mammary syndrome, and isolated split hand-split foot malformation suggest a genotype-phenotype correlation*. Am J Hum Genet, 2001. **69**(3): p. 481-92.
43. Genuardi, M., et al., *Split hand/split foot anomaly in a family segregating a balanced translocation with breakpoint on 7q22.1*. Am J Med Genet, 1993. **47**(6): p. 823-31.
44. McElveen, C., et al., *Ectrodactyly and proximal/intermediate interstitial deletion 7q*. Am J Med Genet, 1995. **56**(1): p. 1-5.
45. Gurrieri, F., et al., *Exclusion of linkage between autosomal dominant split hand/split foot and markers from chromosome 7q: further evidence for genetic heterogeneity*. Am J Hum Genet, 1994. **55**(4): p. 853-5.
46. Ignatius, J., et al., *Split hand/split foot malformation, deafness, and mental retardation with a complex cytogenetic rearrangement involving 7q21.3*. J Med Genet, 1996. **33**(6): p. 507-10.
47. Fukushima, K., et al., *Deletion mapping of split hand/split foot malformation with hearing impairment: a case report*. Int J Pediatr Otorhinolaryngol, 2003. **67**(10): p. 1127-32.
48. van Silfhout, A.T., et al., *Split hand/foot malformation due to chromosome 7q aberrations(SHFM1): additional support for functional haploinsufficiency as the causative mechanism*. Eur J Hum Genet, 2009. **17**(11): p. 1432-8.
49. Boles, R.G., et al., *Deletion of chromosome 2q24-q31 causes characteristic digital anomalies: case report and review*. Am J Med Genet, 1995. **55**(2): p. 155-60.
50. Bijlsma, E.K., et al., *Increased nuchal translucency and split-hand/foot malformation in a fetus with an interstitial deletion of chromosome 2q that removes the SHFM5 locus*. Prenat Diagn, 2005. **25**(1): p. 39-44.
51. Faiyaz ul Haque, M., et al., *Mapping of the gene for X-chromosomal split-hand/split-foot anomaly to Xq26-q26.1*. Hum Genet, 1993. **91**(1): p. 17-9.
52. Faiyaz-Ul-Haque, M., et al., *Fine mapping of the X-linked split-hand/split-foot malformation (SHFM2) locus to a 5.1-Mb region on Xq26.3 and analysis of candidate genes*. Clin Genet, 2005. **67**(1): p. 93-7.
53. Nunes, M.E., et al., *A second autosomal split hand/split foot locus maps to chromosome 10q24-q25*. Hum Mol Genet, 1995. **4**(11): p. 2165-70.
54. Gurrieri, F., et al., *A split hand-split foot (SHFM3) gene is located at 10q24-->25*. Am J Med Genet, 1996. **62**(4): p. 427-36.
55. Raas-Rothschild, A., et al., *Refined mapping of a gene for split hand-split foot malformation (SHFM3) on chromosome 10q25*. J Med Genet, 1996. **33**(12): p. 996-1001.

56. Ozen, R.S., et al., *Fine mapping of the split-hand/split-foot locus (SHFM3) at 10q24: evidence for anticipation and segregation distortion*. Am J Hum Genet, 1999. **64**(6): p. 1646-54.
57. de Mollerat, X.J., et al., *A genomic rearrangement resulting in a tandem duplication is associated with split hand-split foot malformation 3 (SHFM3) at 10q24*. Hum Mol Genet, 2003. **12**(16): p. 1959-71.
58. Lyle, R., et al., *Split-hand/split-foot malformation 3 (SHFM3) at 10q24, development of rapid diagnostic methods and gene expression from the region*. Am J Med Genet A, 2006. **140**(13): p. 1384-95.
59. Basel, D., et al., *Split hand foot malformation is associated with a reduced level of Dactylin gene expression*. Clin Genet, 2003. **64**(4): p. 350-4.
60. Dimitrov, B.I., et al., *Distal limb deficiencies, micrognathia syndrome (OMIM 246560) and syndromic forms of split hand foot malformation (SHFM) are caused by chromosome 10q genomic rearrangements*. J Med Genet, 2009.
61. Mariani, F.V. and G.R. Martin, *Deciphering skeletal patterning: clues from the limb*. Nature, 2003. **423**(6937): p. 319-25.
62. Logan, M., *Finger or toe: the molecular basis of limb identity*. Development, 2003. **130**(26): p. 6401-10.
63. Duboc, V. and M.P. Logan, *Building limb morphology through integration of signaling modules*. Curr Opin Genet Dev, 2009. **19**(5): p. 497-503.
64. Fernandez-Teran, M. and M.A. Ros, *The Apical Ectodermal Ridge: morphological aspects and signaling pathways*. Int J Dev Biol, 2008. **52**(7): p. 857-71.
65. Guo, Q., C. Loomis, and A.L. Joyner, *Fate map of mouse ventral limb ectoderm and the apical ectodermal ridge*. Dev Biol, 2003. **264**(1): p. 166-78.
66. Fernandez-Teran, M.A., J.R. Hinchliffe, and M.A. Ros, *Birth and death of cells in limb development: a mapping study*. Dev Dyn, 2006. **235**(9): p. 2521-37.
67. Saunders, J.W., Jr., *The proximo-distal sequence of origin of the parts of the chick wing and the role of the ectoderm*. J Exp Zool, 1948. **108**(3): p. 363-403.
68. Summerbell, D., *A quantitative analysis of the effect of excision of the AER from the chick limb-bud*. J Embryol Exp Morphol, 1974. **32**(3): p. 651-60.
69. Rowe, D.A. and J.F. Fallon, *The proximodistal determination of skeletal parts in the developing chick leg*. J Embryol Exp Morphol, 1982. **68**: p. 1-7.
70. Niswander, L., et al., *FGF-4 replaces the apical ectodermal ridge and directs outgrowth and patterning of the limb*. Cell, 1993. **75**(3): p. 579-87.
71. Fallon, J.F., et al., *FGF-2: apical ectodermal ridge growth signal for chick limb development*. Science, 1994. **264**(5155): p. 104-7.
72. Lewandoski, M., X. Sun, and G.R. Martin, *Fgf8 signalling from the AER is essential for normal limb development*. Nat Genet, 2000. **26**(4): p. 460-3.
73. Moon, A.M. and M.R. Capecchi, *Fgf8 is required for outgrowth and patterning of the limbs*. Nat Genet, 2000. **26**(4): p. 455-9.
74. Moon, A.M., A.M. Boulet, and M.R. Capecchi, *Normal limb development in conditional mutants of Fgf4*. Development, 2000. **127**(5): p. 989-96.
75. Sun, X., et al., *Conditional inactivation of Fgf4 reveals complexity of signalling during limb bud development*. Nat Genet, 2000. **25**(1): p. 83-6.

76. Colvin, J.S., et al., *Lung hypoplasia and neonatal death in Fgf9-null mice identify this gene as an essential regulator of lung mesenchyme*. *Development*, 2001. **128**(11): p. 2095-106.
77. Mariani, F.V., C.P. Ahn, and G.R. Martin, *Genetic evidence that FGFs have an instructive role in limb proximal-distal patterning*. *Nature*, 2008. **453**(7193): p. 401-5.
78. Niswander, L., et al., *A positive feedback loop coordinates growth and patterning in the vertebrate limb*. *Nature*, 1994. **371**(6498): p. 609-12.
79. Riddle, R.D., et al., *Sonic hedgehog mediates the polarizing activity of the ZPA*. *Cell*, 1993. **75**(7): p. 1401-16.
80. Zuniga, A., et al., *Signal relay by BMP antagonism controls the SHH/FGF4 feedback loop in vertebrate limb buds*. *Nature*, 1999. **401**(6753): p. 598-602.
81. Khokha, M.K., et al., *Gremlin is the BMP antagonist required for maintenance of Shh and Fgf signals during limb patterning*. *Nat Genet*, 2003. **34**(3): p. 303-7.
82. Zuniga, A., et al., *Mouse limb deformity mutations disrupt a global control region within the large regulatory landscape required for Gremlin expression*. *Genes Dev*, 2004. **18**(13): p. 1553-64.
83. Pizette, S. and L. Niswander, *BMPs negatively regulate structure and function of the limb apical ectodermal ridge*. *Development*, 1999. **126**(5): p. 883-94.
84. Barrow, J.R., et al., *Ectodermal Wnt3/beta-catenin signaling is required for the establishment and maintenance of the apical ectodermal ridge*. *Genes Dev*, 2003. **17**(3): p. 394-409.
85. Rinne, T., H.G. Brunner, and H. van Bokhoven, *p63-associated disorders*. *Cell Cycle*, 2007. **6**(3): p. 262-8.
86. Mills, A.A., et al., *p63 is a p53 homologue required for limb and epidermal morphogenesis*. *Nature*, 1999. **398**(6729): p. 708-13.
87. Yang, A., et al., *p63 is essential for regenerative proliferation in limb, craniofacial and epithelial development*. *Nature*, 1999. **398**(6729): p. 714-8.
88. Lo Iacono, N., et al., *Regulation of Dlx5 and Dlx6 gene expression by p63 is involved in EEC and SHFM congenital limb defects*. *Development*, 2008. **135**(7): p. 1377-88.
89. Shimomura, Y., et al., *P-cadherin is a p63 target gene with a crucial role in the developing human limb bud and hair follicle*. *Development*, 2008. **135**(4): p. 743-53.
90. Robledo, R.F., et al., *The Dlx5 and Dlx6 homeobox genes are essential for craniofacial, axial, and appendicular skeletal development*. *Genes Dev*, 2002. **16**(9): p. 1089-101.
91. Merlo, G.R., et al., *Mouse model of split hand/foot malformation type I*. *Genesis*, 2002. **33**(2): p. 97-101.
92. Kjaer, K.W., et al., *Distinct CDH3 mutations cause ectodermal dysplasia, ectrodactyly, macular dystrophy (EEM syndrome)*. *J Med Genet*, 2005. **42**(4): p. 292-8.
93. Chai, C.K., *Dactylaplasia in mice a two-locus model for development anomalies*. *J Hered*, 1981. **72**(4): p. 234-7.
94. Johnson, K.R., et al., *Mapping the mouse dactylaplasia mutation, Dac, and a gene that controls its expression, mdac*. *Genomics*, 1995. **29**(2): p. 457-64.
95. Sidow, A., et al., *A novel member of the F-box/WD40 gene family, encoding dactylin, is disrupted in the mouse dactylaplasia mutant*. *Nat Genet*, 1999. **23**(1): p. 104-7.

96. Crackower, M.A., J. Motoyama, and L.C. Tsui, *Defect in the maintenance of the apical ectodermal ridge in the Dactylaplasia mouse*. *Dev Biol*, 1998. **201**(1): p. 78-89.
97. Kano, H., H. Kurahashi, and T. Toda, *Genetically regulated epigenetic transcriptional activation of retrotransposon insertion confers mouse dactylaplasia phenotype*. *Proc Natl Acad Sci U S A*, 2007. **104**(48): p. 19034-9.
98. Friedli, M., et al., *Characterization of mouse Dactylaplasia mutations: a model for human ectrodactyly SHFM3*. *Mamm Genome*, 2008. **19**(4): p. 272-8.
99. Keller, S.A., et al., *Kidney and retinal defects (Krd), a transgene-induced mutation with a deletion of mouse chromosome 19 that includes the Pax2 locus*. *Genomics*, 1994. **23**(2): p. 309-20.
100. Seto, M.L., et al., *Pathogenesis of ectrodactyly in the Dactylaplasia mouse: aberrant cell death of the apical ectodermal ridge*. *Teratology*, 1997. **56**(4): p. 262-70.
101. Binato, R., et al., *SMAD 8 binding to mice Msx1 basal promoter is required for transcriptional activation*. *Biochem J*, 2006. **393**(Pt 1): p. 141-50.
102. Lallemand, Y., et al., *Msx genes are important apoptosis effectors downstream of the Shh/Gli3 pathway in the limb*. *Dev Biol*, 2009. **331**(2): p. 189-98.
103. Kim, S.H., et al., *The role of paraxial protocadherin in selective adhesion and cell movements of the mesoderm during Xenopus gastrulation*. *Development*, 1998. **125**(23): p. 4681-90.
104. Schuelke, M., *An economic method for the fluorescent labeling of PCR fragments*. *Nat Biotechnol*, 2000. **18**(2): p. 233-4.
105. Sambrook, J., Fritsch, E. F., Maniatis, T., *Molecular Cloning: A Laboratory Manual*. 2nd ed. 1989, Cold Spring Harbor, NY: Cold Spring Harbor Laboratory Press.
106. Cumming, G., F. Fidler, and D.L. Vaux, *Error bars in experimental biology*. *J Cell Biol*, 2007. **177**(1): p. 7-11.
107. Frazer, K.A., et al., *A sequence-based variation map of 8.27 million SNPs in inbred mouse strains*. *Nature*, 2007. **448**(7157): p. 1050-3.
108. Wade, C.M. and M.J. Daly, *Genetic variation in laboratory mice*. *Nat Genet*, 2005. **37**(11): p. 1175-80.
109. Beck, J.A., et al., *Genealogies of mouse inbred strains*. *Nat Genet*, 2000. **24**(1): p. 23-5.
110. Wade, C.M., et al., *The mosaic structure of variation in the laboratory mouse genome*. *Nature*, 2002. **420**(6915): p. 574-8.
111. Wiltshire, T., et al., *Genome-wide single-nucleotide polymorphism analysis defines haplotype patterns in mouse*. *Proc Natl Acad Sci U S A*, 2003. **100**(6): p. 3380-5.
112. Grupe, A., et al., *In silico mapping of complex disease-related traits in mice*. *Science*, 2001. **292**(5523): p. 1915-8.
113. Pletcher, M.T., et al., *Use of a dense single nucleotide polymorphism map for in silico mapping in the mouse*. *PLoS Biol*, 2004. **2**(12): p. e393.
114. Zhang, J., et al., *A high-resolution multistrain haplotype analysis of laboratory mouse genome reveals three distinctive genetic variation patterns*. *Genome Res*, 2005. **15**(2): p. 241-9.

115. Gozuacik, D., et al., *DAP-kinase is a mediator of endoplasmic reticulum stress-induced caspase activation and autophagic cell death*. Cell Death Differ, 2008. **15**(12): p. 1875-86.
116. Jin, Y. and P.J. Gallagher, *Antisense depletion of death-associated protein kinase promotes apoptosis*. J Biol Chem, 2003. **278**(51): p. 51587-93.
117. Yukawa, K., et al., *Deletion of the kinase domain in death-associated protein kinase attenuates renal tubular cell apoptosis in chronic obstructive uropathy*. Int J Mol Med, 2004. **13**(4): p. 515-20.
118. Ribet, D., M. Dewannieux, and T. Heidmann, *An active murine transposon family pair: retrotransposition of "master" MusD copies and ETn trans-mobilization*. Genome Res, 2004. **14**(11): p. 2261-7.
119. Eastman, Q. and R. Grosschedl, *Regulation of LEF-1/TCF transcription factors by Wnt and other signals*. Curr Opin Cell Biol, 1999. **11**(2): p. 233-40.
120. Driskell, R.R., et al., *Wnt-responsive element controls Lef-1 promoter expression during submucosal gland morphogenesis*. Am J Physiol Lung Cell Mol Physiol, 2004. **287**(4): p. L752-63.
121. Vadlamudi, U., et al., *PITX2, beta-catenin and LEF-1 interact to synergistically regulate the LEF-1 promoter*. J Cell Sci, 2005. **118**(Pt 6): p. 1129-37.
122. Mikels, A., Y. Minami, and R. Nusse, *Ror2 receptor requires tyrosine kinase activity to mediate Wnt5A signaling*. J Biol Chem, 2009. **284**(44): p. 30167-76.
123. Forrester, W.C., *The Ror receptor tyrosine kinase family*. Cell Mol Life Sci, 2002. **59**(1): p. 83-96.
124. Vihinen, M., et al., *Structural basis for chromosome X-linked agammaglobulinemia: a tyrosine kinase disease*. Proc Natl Acad Sci U S A, 1994. **91**(26): p. 12803-7.
125. Neu-Yilik, G. and A.E. Kulozik, *NMD: multitasking between mRNA surveillance and modulation of gene expression*. Adv Genet, 2008. **62**: p. 185-243.
126. Ben-Shachar, S., et al., *Dominant versus recessive traits conveyed by allelic mutations - to what extent is nonsense-mediated decay involved?* Clin Genet, 2009. **75**(4): p. 394-400.
127. Mikalsen, T., M. Johannessen, and U. Moens, *Sequence- and position-dependent tagging protects extracellular-regulated kinase 3 protein from 26S proteasome-mediated degradation*. Int J Biochem Cell Biol, 2005. **37**(12): p. 2513-20.
128. O'Rourke, N.A., T. Meyer, and G. Chandy, *Protein localization studies in the age of 'Omics'*. Curr Opin Chem Biol, 2005. **9**(1): p. 82-7.
129. Ramanathan, M.P., V. Ayyavoo, and D.B. Weiner, *Choice of expression vector alters the localization of a human cellular protein*. DNA Cell Biol, 2001. **20**(2): p. 101-5.
130. Forrester, W.C., et al., *A C. elegans Ror receptor tyrosine kinase regulates cell motility and asymmetric cell division*. Nature, 1999. **400**(6747): p. 881-5.
131. Green, J.L., T. Inoue, and P.W. Sternberg, *The C. elegans ROR receptor tyrosine kinase, CAM-1, non-autonomously inhibits the Wnt pathway*. Development, 2007. **134**(22): p. 4053-62.
132. Yamamoto, S., et al., *Cthrc1 selectively activates the planar cell polarity pathway of Wnt signaling by stabilizing the Wnt-receptor complex*. Dev Cell, 2008. **15**(1): p. 23-36.

133. Nishita, M., et al., *Filopodia formation mediated by receptor tyrosine kinase Ror2 is required for Wnt5a-induced cell migration*. J Cell Biol, 2006. **175**(4): p. 555-62.
134. Yamamoto, H., et al., *Wnt5a modulates glycogen synthase kinase 3 to induce phosphorylation of receptor tyrosine kinase Ror2*. Genes Cells, 2007. **12**(11): p. 1215-23.
135. Nomachi, A., et al., *Receptor tyrosine kinase Ror2 mediates Wnt5a-induced polarized cell migration by activating c-Jun N-terminal kinase via actin-binding protein filamin A*. J Biol Chem, 2008. **283**(41): p. 27973-81.
136. Minami, Y., et al., *Ror-family receptor tyrosine kinases in noncanonical Wnt signaling: Their implications in developmental morphogenesis and human diseases*. Dev Dyn, 2009.
137. Yamaguchi, T.P., et al., *A Wnt5a pathway underlies outgrowth of multiple structures in the vertebrate embryo*. Development, 1999. **126**(6): p. 1211-23.
138. Witte, F., et al., *Control of phalanx-forming region-mediated digit outgrowth by ROR2 and IHH*. Unsubmitted manuscript, 2010.
139. Fischer, L., G. Boland, and R.S. Tuan, *Wnt signaling during BMP-2 stimulation of mesenchymal chondrogenesis*. J Cell Biochem, 2002. **84**(4): p. 816-31.
140. Mukhopadhyay, M., et al., *Dickkopf1 is required for embryonic head induction and limb morphogenesis in the mouse*. Dev Cell, 2001. **1**(3): p. 423-34.
141. Ishitani, T., et al., *The TAK1-NLK mitogen-activated protein kinase cascade functions in the Wnt-5a/Ca(2+) pathway to antagonize Wnt/beta-catenin signaling*. Mol Cell Biol, 2003. **23**(1): p. 131-9.
142. Billiard, J., et al., *The orphan receptor tyrosine kinase Ror2 modulates canonical Wnt signaling in osteoblastic cells*. Mol Endocrinol, 2005. **19**(1): p. 90-101.
143. Witte, F., et al., *Negative regulation of Wnt signaling mediated by CK1-phosphorylated Dishevelled via Ror2*. Faseb J, 2010.
144. Nadeau, J.H., *Modifier genes in mice and humans*. Nat Rev Genet, 2001. **2**(3): p. 165-74.
145. Genin, E., J. Feingold, and F. Clerget-Darpoux, *Identifying modifier genes of monogenic disease: strategies and difficulties*. Hum Genet, 2008. **124**(4): p. 357-68.
146. Doetschman, T., *Influence of genetic background on genetically engineered mouse phenotypes*. Methods Mol Biol, 2009. **530**: p. 423-33.
147. Davidson, D.R., et al., *Position-dependent expression of two related homeobox genes in developing vertebrate limbs*. Nature, 1991. **352**(6334): p. 429-31.
148. Pan, Z.Z., et al., *MSX2 expression in the apical ectoderm ridge is regulated by an MSX2 and Dlx5 binding site*. Biochem Biophys Res Commun, 2002. **290**(3): p. 955-61.
149. Cheng, H.C., C.K. Wang, and W.B. Upholt, *Transcriptional regulation of Msx2 in the AERs of developing limbs is dependent on multiple closely spaced regulatory elements*. Dev Biol, 2004. **270**(2): p. 513-24.
150. Shavit, J.A., et al., *Modifiers of von Willebrand factor identified by natural variation in inbred strains of mice*. Blood, 2009. **114**(26): p. 5368-74.
151. Heaney, J.D., et al., *Deletion of eIF2beta suppresses testicular cancer incidence and causes recessive lethality in agouti-yellow mice*. Hum Mol Genet, 2009. **18**(8): p. 1395-404.

152. Hosking, B., et al., *Sox7 and Sox17 are strain-specific modifiers of the lymphangiogenic defects caused by Sox18 dysfunction in mice*. *Development*, 2009. **136**(14): p. 2385-91.
153. Cukier, H.N., et al., *Genetic modifiers of MeCP2 function in Drosophila*. *PLoS Genet*, 2008. **4**(9): p. e1000179.
154. Kaltenbach, L.S., et al., *Huntingtin interacting proteins are genetic modifiers of neurodegeneration*. *PLoS Genet*, 2007. **3**(5): p. e82.
155. Argeson, A.C., K.K. Nelson, and L.D. Siracusa, *Molecular basis of the pleiotropic phenotype of mice carrying the hypervariable yellow (Ahvy) mutation at the agouti locus*. *Genetics*, 1996. **142**(2): p. 557-67.
156. Michaud, E.J., et al., *Differential expression of a new dominant agouti allele (Aiapy) is correlated with methylation state and is influenced by parental lineage*. *Genes Dev*, 1994. **8**(12): p. 1463-72.
157. Duhl, D.M., et al., *Neomorphic agouti mutations in obese yellow mice*. *Nat Genet*, 1994. **8**(1): p. 59-65.
158. Morgan, H.D., et al., *Epigenetic inheritance at the agouti locus in the mouse*. *Nat Genet*, 1999. **23**(3): p. 314-8.
159. Rakyant, V.K., et al., *Transgenerational inheritance of epigenetic states at the murine Axin(Fu) allele occurs after maternal and paternal transmission*. *Proc Natl Acad Sci U S A*, 2003. **100**(5): p. 2538-43.
160. Maksakova, I.A., D.L. Mager, and D. Reiss, *Keeping active endogenous retroviral-like elements in check: the epigenetic perspective*. *Cell Mol Life Sci*, 2008. **65**(21): p. 3329-47.
161. Aravin, A.A., et al., *Developmentally regulated piRNA clusters implicate MILI in transposon control*. *Science*, 2007. **316**(5825): p. 744-7.
162. Brennecke, J., et al., *Discrete small RNA-generating loci as master regulators of transposon activity in Drosophila*. *Cell*, 2007. **128**(6): p. 1089-103.
163. Svoboda, P., et al., *RNAi and expression of retrotransposons MuERV-L and IAP in preimplantation mouse embryos*. *Dev Biol*, 2004. **269**(1): p. 276-85.
164. Babiarz, J.E., et al., *Mouse ES cells express endogenous shRNAs, siRNAs, and other Microprocessor-independent, Dicer-dependent small RNAs*. *Genes Dev*, 2008. **22**(20): p. 2773-85.
165. Calabrese, J.M., et al., *RNA sequence analysis defines Dicer's role in mouse embryonic stem cells*. *Proc Natl Acad Sci U S A*, 2007. **104**(46): p. 18097-102.
166. Liu, P., et al., *Candidate lung tumor susceptibility genes identified through whole-genome association analyses in inbred mice*. *Nat Genet*, 2006. **38**(8): p. 888-95.
167. Yang, I.V., et al., *Identification of novel genes that mediate innate immunity using inbred mice*. *Genetics*, 2009. **183**(4): p. 1535-44.
168. Manenti, G., et al., *Mouse genome-wide association mapping needs linkage analysis to avoid false-positive Loci*. *PLoS Genet*, 2009. **5**(1): p. e1000331.
169. Verdel, A., et al., *Common themes in siRNA-mediated epigenetic silencing pathways*. *Int J Dev Biol*, 2009. **53**(2-3): p. 245-57.
170. Maksakova, I.A., et al., *Retroviral elements and their hosts: insertional mutagenesis in the mouse germ line*. *PLoS Genet*, 2006. **2**(1): p. e2.

171. Howard, G., et al., *Activation and transposition of endogenous retroviral elements in hypomethylation induced tumors in mice*. *Oncogene*, 2008. **27**(3): p. 404-8.
172. Druker, R., et al., *Complex patterns of transcription at the insertion site of a retrotransposon in the mouse*. *Nucleic Acids Res*, 2004. **32**(19): p. 5800-8.
173. Goff, S.P., *Retrovirus restriction factors*. *Mol Cell*, 2004. **16**(6): p. 849-59.
174. Maksakova, I.A. and D.L. Mager, *Transcriptional regulation of early transposon elements, an active family of mouse long terminal repeat retrotransposons*. *J Virol*, 2005. **79**(22): p. 13865-74.
175. Morgan, H.D., et al., *Epigenetic reprogramming in mammals*. *Hum Mol Genet*, 2005. **14 Spec No 1**: p. R47-58.
176. Lane, N., et al., *Resistance of IAPs to methylation reprogramming may provide a mechanism for epigenetic inheritance in the mouse*. *Genesis*, 2003. **35**(2): p. 88-93.
177. Aravin, A.A., G.J. Hannon, and J. Brennecke, *The Piwi-piRNA pathway provides an adaptive defense in the transposon arms race*. *Science*, 2007. **318**(5851): p. 761-4.
178. Aravin, A.A., et al., *A piRNA pathway primed by individual transposons is linked to de novo DNA methylation in mice*. *Mol Cell*, 2008. **31**(6): p. 785-99.
179. Ohnishi, Y., et al., *Small RNA class transition from siRNA/piRNA to miRNA during pre-implantation mouse development*. *Nucleic Acids Res*, 2010.
180. Deng, W. and H. Lin, *miwi, a murine homolog of piwi, encodes a cytoplasmic protein essential for spermatogenesis*. *Dev Cell*, 2002. **2**(6): p. 819-30.
181. Kuramochi-Miyagawa, S., et al., *Mili, a mammalian member of piwi family gene, is essential for spermatogenesis*. *Development*, 2004. **131**(4): p. 839-49.
182. Carmell, M.A., et al., *MIWI2 is essential for spermatogenesis and repression of transposons in the mouse male germline*. *Dev Cell*, 2007. **12**(4): p. 503-14.
183. Murchison, E.P., et al., *Critical roles for Dicer in the female germline*. *Genes Dev*, 2007. **21**(6): p. 682-93.
184. Tang, F., et al., *Maternal microRNAs are essential for mouse zygotic development*. *Genes Dev*, 2007. **21**(6): p. 644-8.
185. Tam, O.H., et al., *Pseudogene-derived small interfering RNAs regulate gene expression in mouse oocytes*. *Nature*, 2008. **453**(7194): p. 534-8.
186. Watanabe, T., et al., *Endogenous siRNAs from naturally formed dsRNAs regulate transcripts in mouse oocytes*. *Nature*, 2008. **453**(7194): p. 539-43.
187. Watanabe, T., et al., *Identification and characterization of two novel classes of small RNAs in the mouse germline: retrotransposon-derived siRNAs in oocytes and germline small RNAs in testes*. *Genes Dev*, 2006. **20**(13): p. 1732-43.
188. Lu, P., et al., *The apical ectodermal ridge is a timer for generating distal limb progenitors*. *Development*, 2008. **135**(8): p. 1395-405.
189. Wanek, N., et al., *A staging system for mouse limb development*. *J Exp Zool*, 1989. **249**(1): p. 41-9.
190. Bakkers, J., et al., *Zebrafish DeltaNp63 is a direct target of Bmp signaling and encodes a transcriptional repressor blocking neural specification in the ventral ectoderm*. *Dev Cell*, 2002. **2**(5): p. 617-27.
191. Kengaku, M., et al., *Distinct WNT pathways regulating AER formation and dorsoventral polarity in the chick limb bud*. *Science*, 1998. **280**(5367): p. 1274-7.

192. Galceran, J., et al., *Wnt3a^{-/-}-like phenotype and limb deficiency in Lef1^(-/-)Tcf1^(-/-) mice*. Genes Dev, 1999. **13**(6): p. 709-17.
193. Kawakami, Y., et al., *WNT signals control FGF-dependent limb initiation and AER induction in the chick embryo*. Cell, 2001. **104**(6): p. 891-900.
194. Soshnikova, N., et al., *Genetic interaction between Wnt/beta-catenin and BMP receptor signaling during formation of the AER and the dorsal-ventral axis in the limb*. Genes Dev, 2003. **17**(16): p. 1963-8.
195. Wu, M., et al., *Inherited somatic mosaicism caused by an intracisternal A particle insertion in the mouse tyrosinase gene*. Proc Natl Acad Sci U S A, 1997. **94**(3): p. 890-4.
196. Ho, M.S., P.I. Tsai, and C.T. Chien, *F-box proteins: the key to protein degradation*. J Biomed Sci, 2006. **13**(2): p. 181-91.
197. Maniatis, T., *A ubiquitin ligase complex essential for the NF-kappaB, Wnt/Wingless, and Hedgehog signaling pathways*. Genes Dev, 1999. **13**(5): p. 505-10.
198. Watanabe, N., et al., *M-phase kinases induce phospho-dependent ubiquitination of somatic Wee1 by SCFbeta-TrCP*. Proc Natl Acad Sci U S A, 2004. **101**(13): p. 4419-24.
199. Margottin-Goguet, F., et al., *Prophase destruction of Emil by the SCF(betaTrCP/Slimb) ubiquitin ligase activates the anaphase promoting complex to allow progression beyond prometaphase*. Dev Cell, 2003. **4**(6): p. 813-26.
200. Westbrook, T.F., et al., *SCFbeta-TRCP controls oncogenic transformation and neural differentiation through REST degradation*. Nature, 2008. **452**(7185): p. 370-4.
201. Spengler, M.L., L.W. Guo, and M.G. Brattain, *Phosphorylation mediates Sp1 coupled activities of proteolytic processing, desumoylation and degradation*. Cell Cycle, 2008. **7**(5): p. 623-30.
202. Seo, E., et al., *Multiple isoforms of beta-TrCP display differential activities in the regulation of Wnt signaling*. Cell Signal, 2009. **21**(1): p. 43-51.
203. Kimelman, D. and W. Xu, *beta-catenin destruction complex: insights and questions from a structural perspective*. Oncogene, 2006. **25**(57): p. 7482-91.
204. Klopocki, E., et al., *A microduplication of the long range SHH limb regulator (ZRS) is associated with triphalangeal thumb-polysyndactyly syndrome*. J Med Genet, 2008. **45**(6): p. 370-5.
205. Lettice, L.A., et al., *A long-range Shh enhancer regulates expression in the developing limb and fin and is associated with preaxial polydactyly*. Hum Mol Genet, 2003. **12**(14): p. 1725-35.
206. Spilianakis, C.G., et al., *Interchromosomal associations between alternatively expressed loci*. Nature, 2005. **435**(7042): p. 637-45.

8 Indices

8.1 List of Figures

Figure 1: The molecular structure of ROR2.	2
Figure 2: Clinical features of BDB1.	3
Figure 3: Clinical features of RRS.	4
Figure 4: A selection of <i>ROR2</i> mutations leading to RRS and BDB1.	6
Figure 5: A patient homozygous for p.R441fxX15 shows severe brachydactyly in conjunction with RRS features.	7
Figure 6: Clinical variability of ectrodactyly.	9
Figure 7: Localisation of the common duplicated region in SHFM3.	10
Figure 8: The AER contributes to the three dimensional development of the limb.	11
Figure 9: Signalling cascades in AER maintenance.	13
Figure 10: Skeletal phenotype of the dactylaplasia mouse.	14
Figure 11: MusD insertions in the SHFM3 syntenic region.	15
Figure 12 <i>In situ</i> hybridisation of <i>Fgf8</i> and <i>Fgf4</i> in <i>Dac</i> mutant limbs.	16
Figure 13: <i>Mdac</i> causes epigenetic modification of the integrated MusD element.	17
Figure 14: Primer design for site-directed mutagenesis	32
Figure 15: Clinical phenotype associated with the mutation c.1324C>T/p.R441X.	48
Figure 16: Graphical illustration of mutations causing Robinow syndrome (RRS, top) and brachydactyly type B1 (BDB1, bottom) used in this study.	49
Figure 17: Immunocytochemistry for ROR2 (red) and the endoplasmic reticulum (ER) marker BAP31 (green).	50

Figure 18: Co-localisation of wt and mutant ROR2 constructs in transiently transfected Cos-1 cells.	51
Figure 19: Immunocytochemical staining of ROR2 and endogenous BAP31 in stable HEK293 FlpIn T-Rex cells.	53
Figure 20: Relative surface localisation of ROR2 and endogenous pan-cadherin as control in stable HEK293 FlpIn T-Rex cell lines determined by surface biotinylation assay.	54
Figure 21: Absolute quantification of membrane-localized ROR2 in HEK293 FlpIn T-Rex cells.	56
Figure 22: Allelic series of Ror2 mutations in the mouse.	58
Figure 23: Microsatellite mapping reduces <i>mdac</i> interval to ~ 5 Mb.	61
Figure 24: SNP mapping limits <i>mdac</i> interval to ~ 3 Mb.	62
Figure 25: Single nucleotide polymorphisms (SNPs) and strain distribution patterns (SDPs) in the <i>mdac</i> interval.	66
Figure 26: SNP density of strains in respect to C57Bl/6.	66
Figure 27: Overview of the <i>Mdac</i> interval.	67
Figure 28: A MusD element segregates with <i>mdac</i> / <i>Mdac</i> .	69
Figure 29: Apoptosis and proliferation are increased in <i>dac/dac</i> mutants at the 34S stage.	71
Figure 30: Quantitative analysis of apoptosis and proliferation between stages E9.75 and E10.75.	72
Figure 31: <i>In situ</i> hybridisation on longitudinal sections of wild-type and mutant limbs at stage 33S.	73
Figure 32: Immunohistochemistry of activated β -catenin and p63 on longitudinal sections of wild-type and mutant limbs.	74
Figure 33: Schematic of the consequences of ROR2 intracellular distribution.	81
Figure 34: Ping-Pong amplification of piRNA in the mouse.	89

8.2 List of Tables

Table 1: Mutagenesis primer to copy human mutations in ROR2	21
Table 2: qPCR primer for quantification of ROR2 expression in HEK293 cells	22
Table 3: qPCR primer for gene expression analysis in mouse AER	22
Table 4: Primer to amplify specific probes for <i>in situ</i> hybridisation	22
Table 5: Primer for microsatellite profiling of DAC vs, C57Bl/6 genomic information	23
Table 6: Primer for SNP profiling	24
Table 8: List of mouse strains with known allele of <i>mdac</i> [93].	59
Table 9: Summary of F ₁ hybrid backcross	60
Table 10: Summary of genomic features.	68

8.3 Abbreviations

ADULT	Acro-dermato-ungual-lacrima-tooth syndrome	ETn	early transposon
AEC	ankyloblepharon,-ectodermal-defects-cleft lip/palate syndrome	EtOH	ethanol
AER	apical ectodermal ridge	F ₁	first filial generation
approx.	approximately	F ₂	second filial generation
ALP	alkaline phosphatase	FAM	carboxyfluoresceine
BDB	brachydactyly type B	FCS	fetal calf serum
bp	base pairs	FRT	flippase recognition target
BSA	bovine serum albumin	g	gram
°C	degree Celsius	GNF	Genomics Institute of the Novartis Research Foundation
cDNA	coding DNA	GOF	gain of function
<i>C. elegans</i>	<i>Caenorhabditis elegans</i>	GWA	genome-wide association
Chr	chromosome	GWAS	genome-wide association studies
cM	centiMorgan	h	hour(s)
CMV	cytomegalovirus	HISS	heat-inactivated sheep serum
Dac	dactylaplasia	HRP	horse-radish peroxidase
DAPI	4',6-Diamidin-2-phenylindol	Hs	Homo sapiens
ddH ₂ O	double-distilled water	IAP	intracisternal A particle
depc	diethylpyrocarbonate	ICC	immunocytochemistry
DIG	digoxygenin	i.e.	id est (that is)
DMEM	Dulbeccos's modified eagle's medium	IHC	immunohistochemistry
DMSO	dimethylsulfoxide	kb	kilo-bases
DNA	deoxyribonucleic acid	ko	knock-out
dNTP	deoxyribonucleotide	l	liter
DRS	dominant Robinow syndrome	LMS	Limb mammary syndrome
dsRNA	double-stranded RNA	LOF	loss of function
E	embryonic stage	LTR	long terminal repeat
<i>E. coli</i>	<i>Escherichia coli</i>	m	mili (prefix)
EDTA	ethylenediaminetetraacetic acid	M	molar
EEM	Ectodermal dysplasia-ectrodactyly-macular dystrophy	Mb	mega-bases
EEC	Ectrodactyly-ectodermal dysplasia-cleft lip/palate syndrome	Mdac	modifier of dactylaplasia
ER	endoplasmic reticulum	MetOH	methanol
		MGI	Mouse Genome Informatics
		min	minute(s)
		miRNA	micro RNA

Mm	Mus musculus	SSLP	simple sequence length polymorphism
mol	moles	T_m	melting temperature
MPD	Mouse Phenome Database	<i>Taq</i>	<i>Thermus aquaticus</i>
mRNA	messenger RNA	Tet	tetracycline
n	nano (prefix)	TetR	tetracycline resistance
NMD	nonsense mediated decay	μ	micro (prefix)
OMIM	Online Mendelian Inheritance in Man	U	units
p	pico (prefix)	UC	Ultra-Clear
p2	middle phalanx	UCSC	University of California, Santa Cruz
PAGE	polyacrylamide gel electrophoresis	V	Volt
PBS	phosphate-buffered saline	WB	Western blot
PCR	polymerase chain reaction	wt	wild-type
PFA	paraformaldehyde	ZPA	zone of polarizing activity
PFR	phalanx-forming region		
<i>Pfu</i>	<i>Pyrococcus furiosus</i>		
<i>Phu</i>	<i>Phusion</i>		
piRNA	Piwi-interacting RNA		
PNK	polynucleotide kinase		
qPCR	quantitative PCR		
RITS	RNA-induced silencing complex		
RNA	ribonucleic acid		
RNAi	RNA interference		
rpm	revolutions per minute		
rRNA	ribosomal RNA		
RRS	recessive Robinow syndrome		
RT	room temperature		
RTK	receptor tyrosine kinase		
SAP	shrimp alkaline phosphatase		
SDP	strain distribution pattern		
SDS	sodium dodecyl sulfate		
sec	second(s)		
SHFM	split hand and foot malformation		
siRNA	short interfering RNA		
SNP	single nucleotide polymorphism		
SSC	saline sodium citrate buffer		

9 Appendix

9.1 Acknowledgements

I want to thank Prof. Dr. Stefan Mundlos for allowing me to work on these exciting topics in his superbly equipped laboratories. Especially his support on the Ror2-manuscript was very helpful and ensured publication in a high-ranked journal. Furthermore, I want to particularly thank Prof. Dr. Wolfgang Schuster for accepting this work for evaluation and representation at the FU Berlin.

Special thanks go to Dr. Sigmar Stricker - a great supervisor. He has allowed me to work freely and to develop my own ideas, but was always present whenever I needed him. We had many fruitful discussions about hypotheses and techniques, in which he critically assessed my ideas, implanted new ones, and put me back on track. Moreover, he had major impact on my recently gained appreciation for Scottish drinks, introduced me to the best burgers in town and showed unexpected skills when it comes to handling large edible birds (thanks to Andrea, too).

I want to thank all people of AG Mundlos for the great time I had in the lab. Though being so many at times, everyone has been a good sport without exception and always been willing to help whenever asked for. Nevertheless, I have to mention a few for their special contribution: Da chicken and the brain for their genuine interest in my freak hypotheses, all the non-work-related activities and discussions, and for being friends. I had a blast last year! Nicole for making the WM 2006 a very memorable one (I've lost too many brain cells right at the start of this thesis..); Jochen for all his technical knowledge he is willing to share; Boris for introducing the right kind of alcoholic beverages to the lab; and Ulli, Ines, Matti, Anita and Pablo for memorable hours in the coffee room and elsewhere. Again, special thanks to Ulli for all the Schnitzels, snowboarding and fixing lamps on impertinent ceilings.

Outside the lab, I need to thank two very special people: Pampfi for getting me through my studies (though her notes were quite unreadable), being the best dump for pre-doctoral frustration, and for all the great time I had in Freiburg. Secondly, I have to thank LaJo for everything in the last 20 years. She is my favourite travel

mate, the caretaker of my mental sanity, and the best best friend one could possibly have. Berlin is not half as good without you!

Last, but surely not least, all my thanks go to my parents for their everlasting love and support in any situation or whatever I planned. Ich liebe Euch!

9.2 List of publications and congresses

PUBLICATION

Schwarzer W, Witte F, Rajab A, Mundlos S, Stricker S.

A gradient of ROR2 protein stability and membrane localization confers brachydactyly type B or Robinow syndrome phenotypes.

Hum Mol Genet. 2009 Nov 1;18(21):4013-21.

CONGRESSES

Poster 40th Annual Conference of the German Genetics Society,
16.-19.09.2009, Cologne, Germany

9.3 Curriculum vitae

„Der Lebenslauf ist in der Online-Version aus Gründen des Datenschutzes nicht enthalten“